Surface Tension of the Ocean and its Relationship with Environmental Variables

Yousif Assiri

Doctor of Philosophy

University of York

Chemistry

July 2025

Abstract

The sea surface microlayer (SML) is a biologically rich interface that plays a critical role in regulating air–sea exchange, yet its surfactant properties remain under-characterised. This thesis investigates the dynamics of surface-active substances (SAS) through two complementary approaches: (1) evaluating storage protocols and analytical methods to preserve and quantify surfactant signatures, and (2) using surface tension (ST) and surfactant activity (SA) measurements to assess spatial and seasonal variability in SML film coverage ($\Delta\sigma$) across coastal and open-ocean settings. In Chapter 2, this thesis demonstrates that reliable characterisation of SAS depends critically on both the analytical technique and storage method. Tensiometry proved sensitive to total interfacial behaviour, while voltammetry offered specificity for electroactive species, particularly when using a multiple deposition-time calibration. Among storage approaches, deep-freezing at −80 °C using rapid (snap) freezing in large-volume (60 mL), low-adsorption containers most effectively preserved surfactant properties. By contrast, gradual cooling to −80 °C in small-volume vials, as well as refrigeration at 4 °C, resulted in greater variability or loss of surfactant activity. Filtration removed substantial amounts of SAS. Together, these findings confirm that only unaltered, native SML samples enable robust interpretation of interfacial dynamics. In Chapter 3, we addressed the critical lack of seawater surface-tension data by measuring ST in sea surface microlayer samples and calculating $\Delta\sigma$ over two years in the coastal English Channel, and along a 6000 km open-ocean transect. Weekly coastal time series showed strong seasonal cycles, with $\Delta\sigma$ rising during phytoplankton bloom progression. Phytoplankton biomass emerged as the strongest predictor of film coverage ($r = +0.50$), while nitrate drawdown ($r = –0.31$) indicated that surfactant enrichment intensified as inorganic nitrogen became depleted. Sea surface temperature also showed a significant positive correlation with $\Delta\sigma$ ($r = +0.32$), while physical and hydrological variables such as wind, river discharge, chlorophyll-a, and DOC played secondary or non-significant roles. Open-ocean film coverage was weaker and more spatially uniform, consistent with oligotrophic conditions. Taken together, these findings advance our understanding of SML surfactant dynamics and confirm that surfactant enrichment is orchestrated by phytoplankton blooms developing under nitrate-limited, warm, and seasonally stratified conditions, with biomass emerging as the most reliable proxy. This thesis provides a validated framework for sample preservation, a dual-method analytical approach, and new insight into the controls on biologically active surface films—findings that are crucial for improving air–sea exchange modelling and the representation of the SML in future ocean scenarios.

Table of Contents

List of Figures

List of Tables

List of Acronyms

% percentage

°C degree Celsius

°N north

°S south

Ag/AgCl silver/silver chloride

AMT Atlantic Meridional Transect

C carbon

Ca calcium

CCi capacitive current

CDOM chromophoric dissolved organic matter

cells mL^{-1} cells per millilitre

CH_4 methane

cm h^{-1} centimetre per hour

cm^2 square centimetre

cm^3 cubic centimetre

CO_2 carbon dioxide

CONNECT Pan-Atlantic Connectivity of Marine Biogeochemical Processes / Impact of Anthropogenic Pressures

CTD conductivity, temperature, and depth sensor

CVAO Cape Verde Atmospheric Observatory

DMS dimethyl sulfide

CMC critical micelle concentration

DOC dissolved organic carbon

DOM dissolved organic matter

EF enrichment factor

FA fatty acid

GC-MS gas chromatography–mass spectrometry

GFF glass fiber filter

HCl hydrochloric acid

HMDE hanging mercury drop electrode

IQR inter-quartile range

K potassium

KCl potassium chloride

kg L^{-1} kilogram per litre

Km / km kilometre

L litre

MILAN Sea Surface Microlayer at Night

MRC mass flow controller

µg L^{-1} microgram per litre

µL microlitre (1×10^{-6} litres)

µm micrometre

µM micromolar (1×10^{-6} mol)

µmol L^{-1} micromole per litre

NOM natural organic matter

OVOC oxidised volatile organic carbon

PAH polyaromatic hydrocarbon

PFA perfluoroalkoxy alkane plastic

PML Plymouth Marine Laboratory

POC particulate organic carbon

SA surfactant activity / surface area (context-dependent)

SAS surface-active substances

SCCM standard cubic centimetres per minute

SML sea surface microlayer

SLPM standard litres per minute

SPE solid phase extraction

SST sea surface temperature

ST surface tension

TEP transparent exopolymer particles

TOC total organic carbon

ULW underlying water

VOC volatile organic carbon

WCO Western Channel Observatory

Acknowledgments

First and foremost, I am deeply grateful to Professor Lucy Carpenter for her exceptional supervision, unwavering support, and insightful guidance throughout this project. Her mentorship has been instrumental not only in shaping the scientific direction of my research but also in supporting my personal development. I am especially thankful for her understanding and kindness during critical moments and difficult personal circumstances, which made an immeasurable difference in helping me continue and complete this work.

I gratefully acknowledge the Islamic University of Madinah for awarding me a scholarship, without which this work would not have been possible.

I would like to extend my sincere thanks to the entire Carpenter Group, especially Dr. Rosie Chance for her valuable input at every stage of the project, Lucy Brown for her kind assistance during sample collection, and Ieaun Roberts for patiently training me on the instrumentation. I am also thankful to all staff and technicians at the Wolfson Atmospheric Chemistry Laboratories (WACL), whose continuous support over the past four years has been essential to this research.

My appreciation also goes to all staff and technicians at the Plymouth Marine Laboratory (PML) for their effort in collecting extraordinary volumes of sea surface microlayer (SML) samples, which formed the backbone of this work.

To the Saudi student community, thank you for your friendship and the many memorable social gatherings that helped me stay connected to home and culture during my time abroad.

On a more personal note, I would like to express my deepest gratitude to my respected mother, whose prayers and love have always been my source of strength, and to the memory of my late father, whom I dearly miss and wish were here to witness this achievement.

To my brothers and sisters, thank you for your encouragement and support. To my lovely wife, your patience, sacrifice, and steadfast companionship through this journey mean more to me than words can express. I am also blessed by the presence of my children, Mohammad, Ali, and Abdulaziz, who brought light and motivation into every step of this path.

Author's Declaration

I declare that the work presented in this thesis is my own and that it has not been previously submitted to this University or any other institution. I am the sole author of this thesis. All sources of information used in this thesis are properly referenced and can be found in the references section.

Chapter 1: Introduction and Literature Review

1.1 Background and Global Context

The ocean plays an essential role in global climate regulation by absorbing approximately 25–30 % of anthropogenic CO_2 emissions and about 90 % of the excess heat generated by greenhouse gases (IPCC, Pörtner et al., 2019). This immense capacity for heat and carbon sequestration positions marine ecosystems as critical natural regulators of Earth's climate system (Henson et al., 2017). Because both heat and greenhouse gases must cross the air–sea interface to be taken up by the ocean, the properties of the surface microlayer (SML)—the uppermost millimeter of the ocean—are key in modulating these exchanges (Liss et al., 2005). Recent studies have attempted to quantify the magnitude of SML-driven effects on air–sea CO_2 transfer, demonstrating that biologically derived surfactants can suppress gas exchange velocities by up to ~30 % under natural conditions (Pereira et al., 2018). Recent modeling efforts have highlighted the importance of integrating ocean-derived organic aerosols—especially sea spray enriched with surfactants—into Earth system models. For example, the OCEANFILMS parameterization, which includes Langmuir-type behavior of surface-active compounds, indicates that organic surfactants in sea spray can increase cloud condensation nuclei (CCN) concentrations by up to 30 cm^{-3} in the Southern Ocean, leading to a global radiative cooling effect of –0.36 W m^{-2} (Burrows et al., 2022). Since sea spray forms at the air–sea interface, the chemical and physical characteristics of the SML influence the enrichment of surfactants and hence play a direct role in shaping aerosol composition and its climate-relevant properties (Wurl et al., 2011).

Beyond CO_2, the ocean exchanges a wide range of climate- and air-quality-relevant gases—including dimethyl sulfide (DMS), volatile organic compounds (VOCs), and ozone—with the atmosphere. The SML can mediate these fluxes through its enrichment in organic material and surfactants, influencing both exchange rates and chemical speciation (Wurl et al., 2011; Liss et al., 2005). Furthermore, the SML is a site of photochemical processes, such

as reactions between ozone and iodide or photosensitized oxidation, producing volatile species (e.g., isoprene), a highly reactive biogenic hydrocarbon that can influence atmospheric oxidative capacity and can contribute to secondary organic aerosol formation, thereby affecting atmospheric chemistry and aerosol processes (Carpenter & Nightingale, 2015; Ciuraru et al., 2015).

Coastal and open-ocean ecosystems contribute significantly to global biogeochemical cycles, including nutrient cycling and primary production. Perturbations in these systems—driven by warming, acidification, deoxygenation, and eutrophication—can profoundly impact ocean functionality and associated climate feedbacks (IPCC, Pörtner et al., 2019; Doney et al., 2012). Such climate-driven alterations in biological productivity, organic matter cycling, and microbial activity are also expected to influence processes operating at the air–sea interface, particularly within the surface microlayer (SML), where biogeochemical transformations are tightly coupled to exchange processes. These alterations may also affect the composition, structure, and microbial dynamics of the surface microlayer (SML), which in turn modulates air–sea exchange of climate-active gases (including CO_2, dimethyl sulfide, and other trace greenhouse gases) and organic matter (Wurl et al., 2017). Understanding how biogeochemical shifts influence the SML is thus critical for predicting changes in gas fluxes and feedbacks under ongoing global change. The surfactant-enriched layer or “sea surface microlayer (SML)” present on the ocean's surface is a system that remains largely uncharacterized. Surfactants in the SML contribute to a reduction in the air-ocean transfer of CO_2 and other environmental gases, presenting the possibility of decreasing the gas transfer velocity of CO_2 by up to 50 % (Nightingale, 2013; Salter et al., 2011).The concentration of naturally occurring organic molecules, including carbohydrates, proteins, and lipids, alters the chemical and physical characteristics of the sea surface (Gade et al., 2006; Hühnerfuss, 2006) and influences biogeochemical cycles (Wurl et al., 2009; Wurl et al., 2011; Cunliffe et al., 2013; Drozdowska et al., 2017).

In sum, marine ecosystems are not only fundamental to carbon and heat dynamics but also crucial in modulating atmospheric chemistry and cloud formation processes. Understanding the roles and mechanisms of natural surfactant dynamics at the ocean surface is therefore critical for more accurate climate projections and Earth system modeling

1.2 Overview of the Air–Sea Interface

The air–sea interface is governed by a complex boundary layer system, consisting of viscous sublayers on both air and water sides, which control the exchange of heat, momentum, and gases (Liss & Slater, 1974; Turney & Banerjee, 2013). The sea surface microlayer (SML) is a biologically active, gelatinous biofilm at the air–sea interface, fostering unique microbial communities and mediating key ecological processes (Cunliffe et al., 2013; Wurl et al., 2017). This uppermost layer, typically 1–1000 μm thick, hosts specialized microbial assemblages—including bacterioneuston and virioneuston—that are distinct from the underlying water column (Cunliffe et al., 2013). Recent studies indicate that these SML communities can be enriched 10–1000× compared to subsurface waters, depending on environmental conditions (Wurl et al., 2017). These structural components of the SML play an important role in defining its physicochemical identity.

The sea surface microlayer (SML) refers to the boundary region between the ocean and the atmosphere, where the exchange of substances is regulated by intricate physicochemical mechanisms (Liss and Duce, 1997). It contains distinct sublayers, namely the viscous sublayer with a thickness of more than 1000 μm, the thermal sublayer with a thickness of 500 μm, the diffusion sublayer with a thickness of 50 μm, and the surface nanolayer (Figure 1). The viscous sublayer refers to a very small zone inside a fluid flow characterized by laminar behaviour, where the vertical velocity of water is linearly suppressed (McLeish et al., 1975). The thermal sublayer, commonly called the ‘cool skin,’ makes the sea surface cooler than the underlying water by up to 0.4 K under low wind speeds, and by up to 0.2 K under strong wind conditions (Saunders 1967; Horrocks et al. 2003). The presence of the

diffusion sublayer plays a crucial role in facilitating the movement of gases between the atmosphere and the ocean, while simultaneously impeding the transmission of organisms (Azam 1998). The surface nanolayer is the thinnest sublayer at the nanoscale which is rich in surfactants and organic compounds and has a significant impact on air-sea interactions.

Material from the underlying sea surface water (ULW) is transported to the SML via a process of bubble scavenging. Bubbles convey ULW substances to the ocean's surface as they rise through the water column (Tseng et al., 1992). These materials tend to stay in the SML when they reach the surface due to their interactions with the gel layer and surface-active properties. This phenomenon not only facilitates the concentration of substances on the surface of the ocean but also contributes to the rapid reformation of the SML after disruption caused by wave breaking, as the bubbles formed by the breaking waves effectively gather the compounds and transport them back to the ocean's surface. Additional input of material to the SML also comes from the atmosphere via wet or dry deposition, including both anthropogenic pollutants like PAHs and naturally occurring organic molecules (Laha et al., 2009). Surfactants in the SML can increase the solubility of otherwise insoluble organic pollutants (Cincinelli et al., 2001).

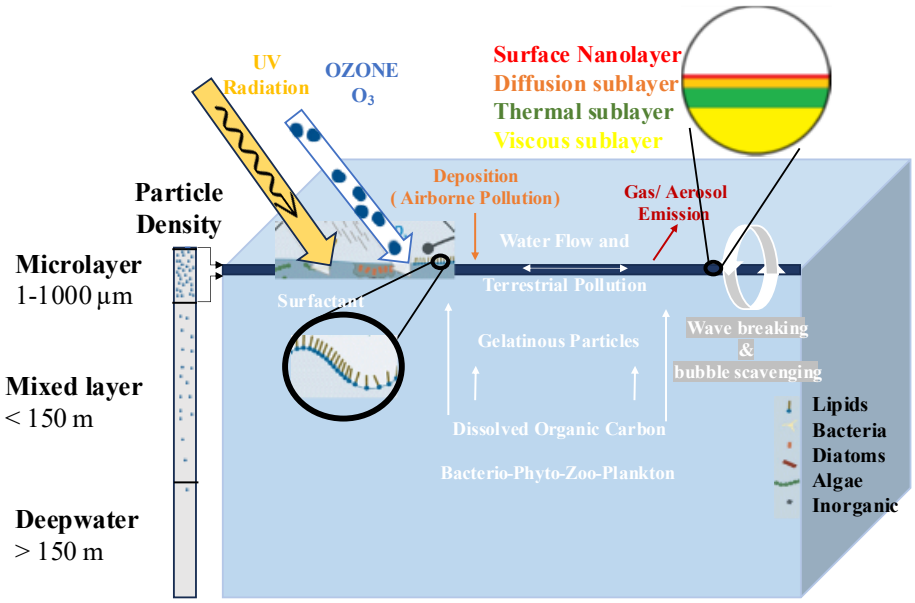

Figure 1: An illustration of the layering and general processes occurring in the SML and its interactions with surrounding systems. Based on Soloviev and Lucas (2014) and Cunliffe et. al. (2013).

The sea surface microlayer (SML) contains surfactants that have the potential to form volatile organic compounds (VOCs) at the ocean surface. The presence of dissolved organic matter (DOM) on the ocean's surface, combined with exposure to solar radiation, stimulates photochemical activity inside the surface microlayer. UV radiation can destroy DOM, resulting in the formation of smaller volatile organic compounds (VOCs), such as isoprene, low-molecular-weight aldehydes, ketones, and short-chain hydrocarbons (Cunliffe et al., 2011). These VOCs play a crucial role in supporting biological activity within the SML, as they can be utilized by microorganisms. Furthermore, the VOCs generated through these photochemical reactions have the potential to form secondary organic aerosols (SOA) when oxidized in the atmosphere and to influence atmospheric oxidative capacity and cloud condensation nuclei formation (Zhou et al., 2014; Brüggemann et al., 2018). SOA affect the radiative properties and lifetime of clouds, which in turn influences the climate system (Shrivastava et al., 2017).

1.3 Significance of Marine Surface Microlayers (SML)

1.3.1 Ecological significance of the SML

By nature of its position and composition, the SML acts both as a sink and source for pollutants such as heavy metals, petroleum hydrocarbons, polycyclic aromatic hydrocarbons (PAHs), and persistent organic pollutants (POPs). These compounds can become enriched in the SML by up to 500× relative to underlying seawater (Wurl & Obbard, 2004). The concentration of pollutants not only affects microbial ecosystems but also has implications for pollutant bioavailability and trophic transfer, as the SML serves as a nursery habitat for fish eggs and larvae (Wurl & Obbard, 2004), magnifying ecotoxicological vulnerability in coastal food webs.

Understanding the SML's role in global carbon cycling has gained traction in recent years. Synthesis studies increasingly highlight the surface microlayer as a highly dynamic interface in which organic carbon is rapidly processed and transformed, with globally integrated fluxes comparable in magnitude to other major oceanic carbon pathways, such as deep-ocean export. This perspective emphasizes the SML not as a long-term carbon reservoir, but as a transient yet biogeochemically significant processing layer at the air–sea interface (Wurl et al., 2017; Engel et al., 2017). The SML's enriched organic matrix—including transparent exopolymer particles (TEP) and labile dissolved organic matter—creates an environment conducive to photochemical reactions, microbial enzyme activity, and rapid organic turnover (Wurl & Holmes, 2008).

1.3.2 Impact of the SML on gas exchange

The sea surface microlayer (SML) acts as a physicochemical barrier at the air–sea interface, enriched with organic particles and surface-active substances that dampen turbulence, suppress bubble bursting, and reduce gas transfer velocities (kw), even under wind speeds up to ~13 m s^{-1} (Sabbaghzadeh et al., 2017; Turney & Banerjee, 2013). The presence of

surface-active substances dampens turbulence, interferes with bubble-mediated transfer of gases (CO_2, DMS), and modifies the production and chemical composition of sea spray aerosols (Pereira et al., 2016). These effects can alter the effective transfer velocity of gases, particularly under low to moderate wind conditions, where interfacial resistance becomes the dominant control on exchange.

Lab and field studies report that natural surfactants, such as phytoplankton exudates, can retard gas exchange by 5–55% under calm conditions (Salter et al., 2011). Models like Liss–Merlivat (1986) and Wanninkhof's (1992) parameterizations estimate gas transfer velocities (kw) based on wind speed, temperature, solubility, and viscosity, yet uncertainties remain—especially at low wind speeds—due to unresolved interfacial mechanisms (Nightingale et al., 2000; Garbe et al., 2014).

Surface tension is a key control on air–sea exchange processes in oceanographic and atmospheric systems. Surfactant films lower surface tension, increasing microlayer viscosity, slowing molecular diffusion, producing smaller and longer-lived bubbles that alter bubble-mediated gas transfer, and damping small-scale waves that drive turbulence and surface renewal. These effects directly influence the exchange of gases such as oxygen and carbon dioxide at the air–sea interface and link surface microlayer dynamics to the global carbon cycle (Nightingale, 2013; Bauer et al., 2013). Surface tension also influences wave behaviour by contributing to the restoring forces that regulate small-scale wave formation and dissipation (Hogan, 1979).

1.4 Fundamental Concepts of Surfactant Science

1.4.1 Surfactant Behaviour at Interfaces

Surfactants are amphiphilic compounds whose hydrophilic head groups and hydrophobic tails preferentially orient at interfaces, significantly reducing surface tension (Abbott, 2020). As their bulk concentration increases to the critical micelle concentration (CMC), additional

molecules aggregate into micelles, and the interface becomes saturated—surface tension plateaus (Abbott, 2020). Surfactants at the air–sea interface may form both insoluble monolayers, which create relatively persistent surface films (e.g. fatty acids), and soluble adsorbed layers that exchange dynamically with the underlying water column (Frew et al., 1990; Turney & Banerjee, 2013). Insoluble films can act as more static interfacial barriers, whereas soluble surfactants primarily influence interfacial rheology and the transfer of energy and momentum across the air–sea interface. Although soluble surfactants do not form rigid films, their presence can still alter interfacial turbulence and renewal processes, with potential consequences for gas exchange, particularly under low to moderate wind conditions (Turney & Banerjee, 2013). Understanding adsorption behaviour is crucial: it is characterized by isotherms (e.g., Gibbs or Langmuir) and surface coverage (Γ), allowing assessment of how surfactant composition affects interfacial properties and SML stability (Abbott, 2020).

1.4.2 Surface Tension Isotherms and Critical Micelle Concentration

The relationship between surface tension and surfactant concentration at the air/water interface can be considered as three separate zones (Figure 2). The divisions correspond to the normal behaviour seen in surface tension isotherms. Surface tension isotherms for surfactants show the connection between surface tension and surfactant concentration at a given temperature. These isotherms are important for understanding surfactant molecules' behaviour at interfaces, such as the air-water interface. At low surfactant concentrations, the first area (A) displays minor changes in surface tension, suggesting a limited surfactant impact. The second area (B) demonstrates a large, generally linear fall in surface tension as surfactant concentration increases, showing surfactant-molecule organisation at the interface. Once the critical micelle concentration (CMC) is reached, where surfactant molecules group together to form micelles, the final area (C) shows that increasing the surfactant concentration does not lower the surface tension any further (Menger, 2011).

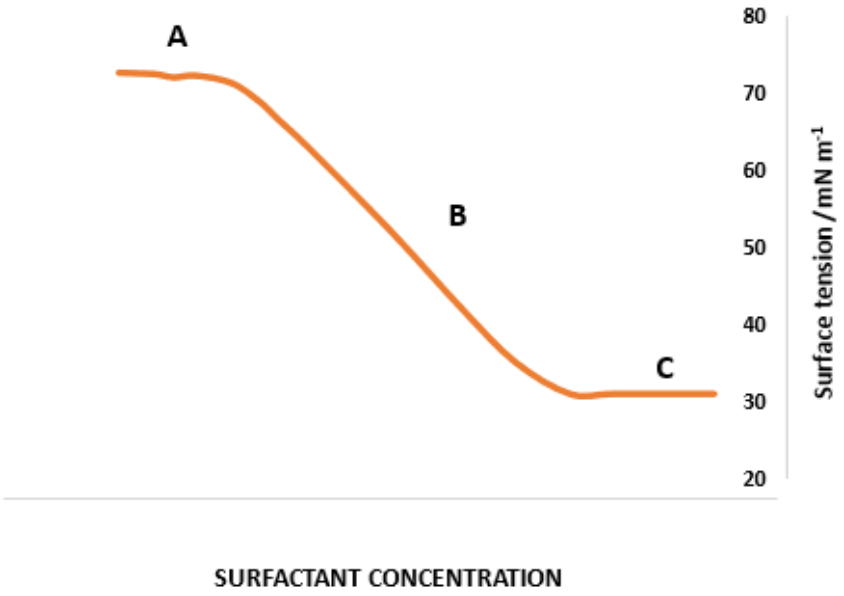

Figure 2: Surface tension as a function of surfactant concentration, showing three distinct regions: (A) initial plateau indicating minimal effect of low surfactant concentration on surface tension, (B) sharp decrease in surface tension as surfactant concentration increases, and (C) second plateau where surface tension stabilises, reflecting the critical micelle concentration (CMC) beyond which additional surfactant does not further reduce surface tension.

1.4.3 Modelling Surface Tension in Complex Systems

When experimental concentration data do not extend into the saturation or plateau region, modelling surface tension behaviour becomes particularly challenging, especially in natural systems containing complex mixtures of surface-active substances. In such cases, empirical sigmoidal models, such as the logistic equation (Equation 1, Prosser and Franses (2001)), offer a practical and robust approach to analysing interfacial behaviour. As shown in Figure 3, the logistic model represents surface tension as a smooth, S-shaped curve based on surfactant concentration, which helps estimate surface tension values even if full saturation isn't seen in experiments.

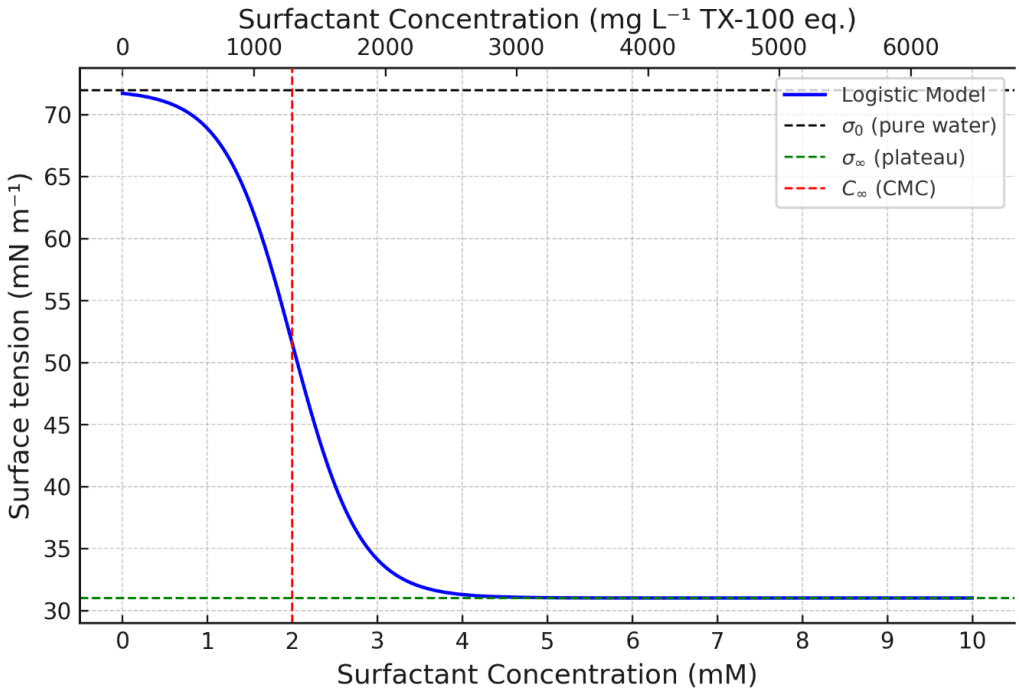

Figure 3: The logistic model describing surface tension as a function of surfactant concentration (Prosser and Franses, 2001). This model captures the gradual transition in surface tension observed in complex, multicomponent systems where experimental data may not reach full saturation.

This model has several key features: the clean-water surface tension (σ_0), a point (C_inf) that usually matches the critical micelle concentration (CMC), and a minimum surface tension (σ_∞) that occurs at high surfactant levels. It also incorporates a slope parameter (k), which controls the sharpness of the transition from low to high surface coverage.

$$\sigma = \sigma\infty + (\sigma_0 - \sigma\infty) / [1 + exp(k(C - C\_inf))] \quad (1)$$

Importantly, the logistic model is not based on mechanistic assumptions about adsorption site geometry or molecular interactions. Instead, it offers a flexible, data-driven approach well suited to heterogeneous natural systems such as seawater and atmospheric surface microlayers, where surface-active components are chemically diverse and naturally variable. Prosser and Franses (2001) highlighted the applicability of this equation in systems where the CMC is poorly defined or not reached within the measured concentration range. More recently, Kleinheins et al. (2023) conducted a comparative study on surface tension

modelling and found that the logistic-based sigmoid model was among the most reliable for fitting both weak and strong surfactants in binary aqueous solutions.

1.4.4 Surface Tension in Multicomponent Seawater Systems

In the case of mixed systems, such as seawater, the surface tension is influenced by the contributions of various individual components such as dissolved salts, gases, organic matter, and microorganisms, each of which has a unique impact on the overall surface tension. Salinity (Na^+, Cl^-, Mg^{2+}, and Ca^{2+} ions) affects cohesive forces at the water-air interface, while natural surfactants and biological factors (phytoplankton, bacteria, and microorganisms) contribute further to the surface tension dynamics.

As shown in Equation 2, the surface tension of a mixed system is calculated using the surface excess (Γ) and chemical potentials (μ) of each component.

$$d\gamma = \Gamma_1 d\mu_1 + \Gamma_2 d\mu_2 \qquad (2)$$

The surface excess *(Γ)* refers to the additional concentration of a substance at the surface compared to what it would be if the concentration throughout the entire volume remained constant up to the interface. If the value of Γ is positive, as is the case for surfactants, the surface tension decreases as the concentration increases. Conversely, if the value of Γ is negative, as is the case for inorganic salts, the surface tension increases with increasing concentration. Schmidt et al. (2011) calculated the surface tension of Baltic Sea and Atlantic Ocean underlying water (ULW) to be 73.2 and 74.0 mN m^{-1}, respectively, compared to 72.8 mN m^{-1} for deionized water. The measurements had an uncertainty range of 0.18-0.37 mN m^{-1}, with an average uncertainty of 0.22 mN m^{-1}. The chemical potential of the salt in the water samples causes this difference, which has a negative surface excess and increases seawater surface tension.

The calculation of the surface excess of a substance can be determined from surface tension using Equation 3, which is derived from the Gibbs isotherm.

$$\Gamma = -\frac{1}{RT}\left(\frac{\partial \gamma}{\delta \ln C}\right)_{T,P} \quad (3)$$

The concentration of the substance in the bulk solution is denoted by C, the gas constant is represented by R, and T refers to the temperature.

1.4.5 Temperature Controls on Surface Tension and SML Processes

Surface tension is a physical feature of liquids that results from cohesive forces between molecules at the surface of the liquid (Kou et al., 2019). As the temperature rises, the kinetic energy of the molecules rises, forcing them to move faster and enhancing their capacity to overcome the cohesive forces at the surface. Temperature also modulates key SML processes—including interfacial photochemical reaction rates, the thermodynamics of surfactant adsorption, microbial biosurfactant production, and circulation-driven nutrient supply—that together shape surfactant film formation and persistence (more details 3.4.3.1).

The study of seawater surface tension has lasted over a century, progressing from simple correlations to advanced experimental examinations. The study of Krümmel (1900) set the foundation for understanding seawater surface tension by establishing an early association between surface tension, temperature, and salinity. This was achieved by Krümmel's observations of seawater with salinities ranging from 10 to 35 g kg^{-1}, within a temperature range of 0 to 40 °C. In 1939, Fleming and Revelle conducted research to modify and improve Krümmel's correlation, which had been widely used as a reference for many years. Around 75 years later, Nayar et al. (2014) performed extensive experiments to measure the surface tension of saltwater using the Wilhelmy plate method over a wide range of temperatures (1 to 92 °C) and salinities (20 - 131 g kg^{-1}) and formulated a parameterisation to determine the surface tension of surfactant-free seawater as a function of these two variables. However, the studies conducted by Krümmel (1900), Guohua et al. (1994), and Nayar et al. (Nayar et al., 2014) did not take into account the possible influence of organic molecules on the surface tension measurements. These measurements demonstrate that, in the absence of surface-

active organic material, the surface tension of seawater is a well-defined and predictable thermophysical property governed primarily by temperature and ionic strength. As a result, σ_0 can be quantified with high confidence across environmentally relevant conditions, providing a robust reference state against which surfactant-induced surface tension depressions can be evaluated. This distinction is fundamental to the interpretation of surface film coverage ($\Delta\sigma$), which reflects deviations from a physically constrained baseline rather than absolute surface tension values. Consequently, observed reductions in surface tension can be directly attributed to the presence and stability of surface-active substances, rather than variability in temperature or salinity alone.

1.4.6 Surface Film Coverage and Biological Controls

The presence of organic surface-active components in natural seawater can significantly reduce the surface tension. Schmidt and Schneider (2011) investigated this phenomenon using the Wilhelmy plate method. They examined coastal samples from the Baltic Sea with a salinity of 11.5 g kg^{-1}, as well as open ocean water samples from the Atlantic Ocean with salinities ranging from 35.5 to 37.2 g kg^{-1}; however, it appears that film pressure data were not reported for the open ocean samples. These samples were transported back to the laboratory for analysis. Schmidt and Schneider (2011) found surface film coverage ($\Delta\sigma$) (Eq 4) of up to 10 mN m^{-1} in the Baltic Sea, which was most elevated during the spring bloom. The surface film coverage defines the alteration in surface tension caused by the addition of a surfactant to the liquid surface. It is calculated as the difference between the surface tension of the sample, σ_{SML}, and the surface tension of water at the same temperature and salinity but without any surface active organic substances, σ_0 (Nayar et al., 2014). The seasonal variation in $\Delta\sigma$, with a maximum in summer, suggested that biological activity was a source of SAS and surface tension reduction in the Baltic Sea (Schmidt & Schneider, 2011).

$$\Delta\sigma = \sigma_0 - \sigma_{SML} \qquad (4)$$

1.5 Historical Development of Marine Surfactant Research

Research on surfactants at the marine air–sea interface began in the early 20th century with surface tension measurements, but significant progress emerged in the mid-1900s with the adoption of tensiometry and early gas exchange studies. Garrett (1967) conducted controlled laboratory experiments demonstrating that organic films can significantly enhance surface film strength compared to clean water. Later studies confirmed that natural surface slicks suppress surface tension and dampen short gravity–capillary waves, affecting air–sea gas exchange and surface dynamics (Alpers and Hühnerfuss, 1989).

In the 1980s and 1990s, the use of laboratory and field tensiometers became more widespread, as researchers such as Frew et al. (1990) quantified the impact of natural surfactants on gas transfer velocities. These studies revealed that phytoplankton exudates can reduce gas-exchange rates by 5–30%, with synthetic analogues suppressing transfer by over 90% under calm conditions (Frew et al., 1990).

The early 2000s saw methodological diversification with the introduction of electrochemical and spectroscopic techniques. AC voltammetry, calibrated against standards like Triton X-100, provided a shipboard-compatible method for rapid surfactant quantification (Ćosović & Vojvodić, 1998; Engel et al., 2017). Meanwhile, a study by Modini et al. (2013) emphasized the ecological significance of surfactants by linking phytoplankton activity with sea spray aerosol (SSA) chemistry in marine environments.

Numerous recent studies have expanded our understanding of sources, dynamics, and implications of marine surfactants. Barthelmeß and Engel (2022) used molecular techniques in the Baltic Sea to demonstrate surfactant production by phytoplankton and their seasonal modulation. Meanwhile, King et al. (2019) refined tensiometric protocols and integrated physicochemical insights into global climate models. Despite these advances, analytical challenges related to sample stability, standardized protocols, and real-time in situ

measurements persist, highlighting the continued need for innovation in this field (Cunliffe et al., 2013; Wurl et al., 2017).

1.6 Surfactant Sources

1.6.1 Biogenic Sources

In this subsection, we review the principal biogenic sources of marine surfactants, focusing on the roles of phytoplankton, bacteria, and grazers. Together, these organisms drive the production and release of surface-active compounds into the sea-surface microlayer (SML).

1.6.1.1 Phytoplankton

Phytoplankton release surface-active substances through direct exudation, cell lysis, and enzymatic processes during growth and bloom events. Žutić et al. (1981) showed that cultured strains release surfactants that accumulate in the SML and reduce surface tension by up to 20 mN m^{-1}. For context, the surface tension of pure water at 20 °C is approximately 72 mN m^{-1}, while natural seawater typically ranges between ~72 and 74 mN m^{-1} depending on temperature and salinity, indicating that such reductions represent a substantial modification of interfacial properties. Species-specific physiology governs the timing of release: Cryptomonas initiates surfactant production during the lag phase, whereas Skeletonema delays release until the stationary phase, reflecting divergent metabolic strategies (Žutić et al., 1981). Laboratory experiments further indicate that extracellular carbohydrate exudates can constitute 27–47% of cellular biomass during stationary growth, underscoring the substantial polymeric contribution to marine surfactant pools (Frew et al., 1990). Field observations from the EIFEX iron-fertilization experiment recorded surfactant concentrations of 0.02–0.03 mg L^{-1} Triton X-100 equivalents in surface waters, values comparable to concentrations previously shown to measurably suppress gas exchange and modify surface tension under natural conditions, directly linking bloom-induced productivity to SML enrichment (Croot et al., 2007).

1.6.1.2 Bacterial Biosurfactant Production

Marine bacteria produce glycolipid and lipopeptide biosurfactants, particularly under hydrocarbon exposure or nutrient stress. Kurata et al. (2016) and Underwood et al. (2022) demonstrated that taxa such as *Pseudomonas*, *Colwellia*, *Alcanivorax*, and *Bacillus* synthesize surface-active compounds, reaching concentrations of 0.5–2.0 mg L^{-1} in enrichment cultures. In near-surface waters beneath natural slicks, DNA sequencing reveals enrichment of surfactant-associated bacteria, indicating in situ production followed by bubble-mediated transport to the SML (Kurata et al., 2016). Biosurfactants released into the water column can be transported to the SML through a combination of buoyant ascent, adsorption onto rising bubbles, and bubble scavenging processes, which efficiently concentrate surface-active material at the air–sea interface. These processes contribute a dynamic biosurfactant source that complements phytoplankton-derived material.

1.6.1.3 Grazers and Protists

Protists and zooplankton influence surfactant dynamics through feeding and sloppy grazing. Kujawinski et al. (2011) showed that dissolved surfactant levels during protist grazing events match those observed in phytoplankton blooms, with measured concentrations of 0.01–0.02 mg L^{-1} TX-100 equivalents. Seasonal field studies report pulsed surfactant production concurrent with bloom-associated grazer peaks. Furthermore, sloppy feeding by copepods and other zooplankton liberates exopolymeric material—rich in surface-active compounds—contributing up to 15% of the total SML surfactant pool (Passow & Alldredge, 1999). These biogenic processes establish a foundation for the molecular mechanisms and environmental pathways examined in 1.6.2.

1.6.2 Mechanisms and Environmental Pathways

Phytoplankton-derived lipids and fatty acids undergo both biotic and abiotic transformations that influence their surface activity. Within phytoplankton cells, photosynthetically derived glucose is converted via glycolysis into acetyl-CoA, which fatty acid synthase transforms

into long-chain fatty acids (Muhlroth et al., 2013). Once released into the water column, extracellular enzymatic hydrolysis cleaves these fatty acids from polar lipid headgroups, making them available for microbial uptake. Coastal bacterial communities can metabolize up to 80% of released fatty acids within 24 hours (Cochran et al., 2016). Abiotic processes such as photooxidation and ozonolysis further modify unsaturated fatty acids, altering chain length and double-bond configuration and thereby affecting their interfacial properties (Heydarizadeh et al., 2013).

Mechanistically, Fogg's two-tier model explains surfactant exudation under varying nutrient regimes without requiring cell disruption. Low-molecular-weight compounds, including amino acids and sugars, passively diffuse across cell membranes, while overflow metabolism releases high-molecular-weight polymers once intracellular concentrations exceed physiological thresholds (Fogg, 1966). This dual process maintains continuous surfactant supply to the SML during nutrient limitation and bloom decay.

Microbial surfactant synthesis and degradation create a dynamic balance in the SML. Genera such as *Pseudomonas*, *Bacillus*, and *Acinetobacter* produce biosurfactants in response to organic enrichment, with production rates reaching 0.5–2.0 mg L^{-1} in culture (Hisatsuka et al., 1971; Rosenberg et al., 1979). Kurata et al. (2016) demonstrate that bubble-mediated transport concentrates surfactant-producing bacteria in near-surface waters beneath slicks, yet degradation pathways—exemplified by *Escherichia*—can mineralize surfactants within hours, highlighting rapid turnover in the SML. These pathways of biosynthesis, exudation, and transformation influence dissolved organic carbon pools at the air–sea interface, as explored in 1.6.3.

1.6.3 Dissolved Organic Carbon and Surfactant Fractions

Dissolved organic carbon (DOC) constitutes a critical pool at the air–sea interface, with an estimated 662 Pg C stored across the global ocean (Hansell et al., 2009). Within this pool,

surfactant-active fractions including glycolipids, lipopeptides, and free fatty acids—play key roles in modulating interfacial processes (Wurl et al., 2011; Cunliffe et al., 2013). DOC enrichment factors (EF_{DOC}) in the SML vary widely: Reinthaler et al. (2008) measured EF_{DOC} up to 2.1 at wind speeds exceeding 7.5 m s^{-1} in the Atlantic and western Mediterranean, while Van Pinxteren et al. (2017) reported EF_{DOC} ranging from 0.2 to 9.1 across multiple Atlantic transects. These surfactant-active DOC fractions influence gas transfer and aerosol dynamics by altering surface viscosity and film stability. High-molecular-weight polymers increase microlayer viscosity, reducing gas exchange rates by up to 50% under calm conditions (Frew et al., 1990). By contrast, low-molecular-weight fractions redistribute rapidly during wave breaking, contributing to sea spray aerosol formation (O'Dowd et al., 2004).

1.6.4 Anthropogenic Sources

The SML also accumulates surfactants of terrestrial and industrial origin. Per- and polyfluoroalkyl substances (PFAS) and persistent organic pollutants (POPs) reach surface waters via riverine discharge, atmospheric deposition, and direct wastewater effluent. Martinez-Varela et al. (2020) measured PFAS concentrations up to 150 ng L^{-1} in SML samples from urbanized estuaries—threefold higher than underlying waters—highlighting strong enrichment of human-derived amphiphiles. These compounds contribute to interfacial activity and can select for surfactant-degrading microbes; for instance, GESAMP (2021) reports increased abundance of *Pseudomonas* spp. in PFAS-contaminated near-surface waters. Anthropogenic surfactants can modify SML viscosity and dampen gas exchange rates comparably to biogenic fractions (Salter et al., 2011), underscoring the importance of incorporating human-derived inputs into models of SML dynamics and climate-relevant processes. With both natural and anthropogenic sources defined, we next examine their combined effects on air–sea interactions and climate-relevant processes.

1.7 Surfactants and Climate-Relevant Processes

1.7.1 Seasonal and Spatial Distribution

Marine surfactant concentrations vary seasonally and geographically in response to biological productivity and environmental forcing (Figure 4). Boreal summer and autumn phytoplankton blooms in the North Atlantic (60°–40°N) generate elevated SML surfactant levels, with concentrations often exceeding 0.1–1.5 mg L^{-1} TX-100 equivalents in bloom centres (Ćosović & Vojvodić, 1987; Wurl et al., 2011b; Sabbaghzadeh et al., 2017). Upwelling zones off West Africa and coastal regions of South America also exhibit enhanced surfactant coverage, driven by nutrient enrichment and high primary productivity (Gašparović et al., 2007; Tsai & Liu, 2003). In contrast, oligotrophic gyres between 30° N and 30° S maintain low surfactant concentrations (<0.3 mg L^{-1}) due to limited biological inputs (Wurl et al., 2011b). These spatial patterns, shaped by productivity and allochthonous organic inputs, underpin current models of SML surfactant distribution under variable climatic regimes.

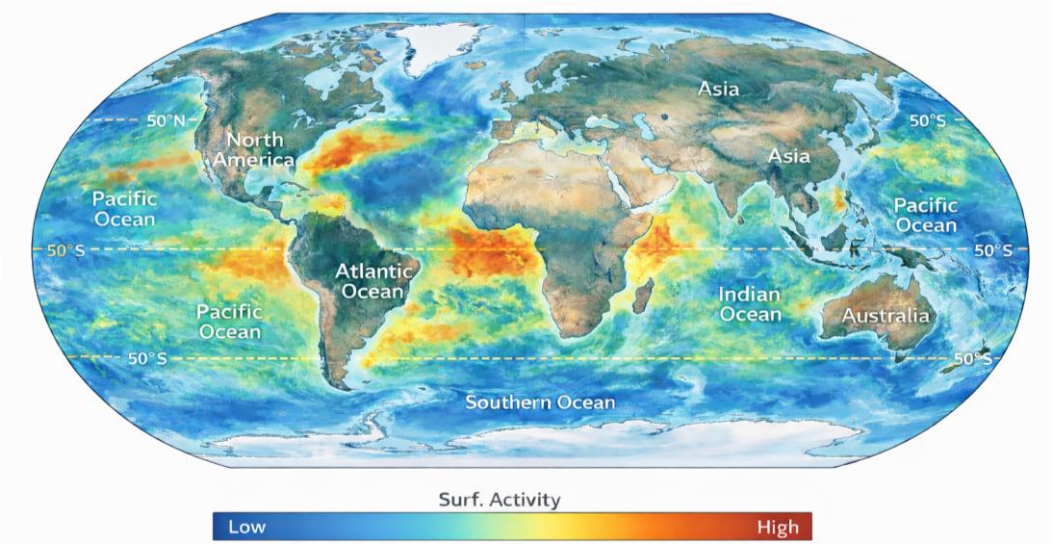

Figure 4: Global distribution of surfactant activity across ocean surface waters (50° N–50° S). The colour scale indicates surfactant activity from low (blue) to high (red). Highest concentrations occur in the Atlantic Ocean, particularly between 40° N and the equator, where surfactants remain enriched even under high wind speeds, influencing air–sea gas exchange processes.

1.7.2 Impact on Air–Sea Gas Exchange

Surfactants suppress gas exchange by altering SML physical properties. Biogenic monolayers reduce gas transfer velocities (k) by up to 55% during bloom conditions (Salter et al., 2011), while synthetic surfactants yield up to 85% suppression in laboratory tests (Broecker et al., 1978; Schneider-Zapp et al., 2014). Soluble surfactants reassemble rapidly following surface disruption, dampening capillary waves and thickening the viscous sublayer, which impedes turbulent renewal (Frew et al., 1990; McKenna & McGillis, 2004). Insoluble films further inhibit molecular diffusion until dispersed by winds above 5 m s^{-1} (Springer & Pigford, 1970; Goldman et al., 1988).

These effects underscore the need to integrate surfactant dynamics into global gas exchange models.

1.7.3 Sea Spray Aerosol Production and Climate Feedbacks

Surfactants modulate bubble-mediated aerosol generation and cloud formation. Enrichment of surfactants in seawater increases film stability, reducing droplet number fluxes by up to

30% under controlled wind conditions (Modini et al., 2013). Surfactant-coated aerosols lower surface tension, enhancing cloud condensation nuclei (CCN) activity by 20–40% relative to seawater devoid of organics (Yli-Juuti et al., 2013). Global model OCEANFILMS predicts that organic surfactant enrichment raises Southern Ocean CCN concentrations by ~30 cm^{-3}, producing a net radiative cooling of –0.36 W m^{-2} (Toner et al., 2022). These interactions illustrate how SML surfactant dynamics influence climate through coupled physical and chemical pathways.

1.7.4 Global Distribution of Marine Surfactants

The use of the SA method has revealed the existence of an active surfactant layer throughout the oceans. Table 1 highlights the wide range of SA concentrations and surfactant enrichment factors (EF) (Equation 5) observed in the surface microlayer (SML) vs the underlying water (ULW).

$$Enrichment\ Factor\ (EF) = \frac{SML\ concentration}{ULW\ concentration} \qquad (5)$$

Table 1: Summary of Surfactant Activity (SA) Measurements in Various Oceanic Regions

Study Region	Time	Oceanic Region	SML SA (mgL^{-1} eq TX-100)	Range (mgL^{-1} eq TX-100)	EF (SA) (Ave ± SD.)	Range (mgL^{-1} eq TX-100)	Reference
Atlantic Ocean	2014	Oceanic	0.34 ± 0.19	0.13 – 1.00	1.8 ± 0.8	1.0 – 4.5	Sabbaghzadeh et al., 2017
Atlantic Ocean	2015	Oceanic	0.47 ± 0.38	0.12 – 1.76	1.6 ± 0.6	1.0 – 3.5	Sabbaghzadeh et al., 2017
North Sea	2013	Offshore	N/A	0.08 – 0.38	N/A	~1.0 – 1.9	Pereira et al., 2016
North Pacific	2009	Oceanic	0.43 ± 0.32	0.19 – 1.48	2.9 ± 1.3	1.1 – 5.3	Wurl et al., 2011b
North Pacific	2009	Offshore	0.26 ± 0.03	0.23 – 0.32	1.7 ± 0.6	1.0 – 2.5	Wurl et al., 2011
River Tyne	2007	Estuary	N/A	0.35 – 1.12	N/A	0.8 – 8.0	Salter., 2010
Southern Ocean	2004	Oceanic		0.005 – 0.03			Croot et al., 2007
Adriatic Sea	2002	Oceanic	0.083	0.042 – 0.145			Gašparović et al., 2011
Sargasso Sea	1994	Coastal		0.05 – 3.00			Frew et al., 2002

These studies indicate that surfactant levels can be influenced by variables such as the distance to coastal regions, anthropogenic activities, and biological productivity. Two cruises between 50 ºN and 50 ºS in the open Atlantic Ocean revealed average SA

concentrations in the SML of 0.34 ± 0.19 mg L^{-1} eq. T-X-100 (range 0.13 - 1.00 mg L^{-1} eq. T-X-100) and 0.47 ± 0.38 mg L^{-1} eq. T-X-100 (range 0.12 - 1.77 mg L^{-1} eq. T-X-100) (Sabbaghzadeh et al., 2017). These results are consistent with those of Wurl et al. (2011b) who reported SA values in the SML ranging from 0.10 to 1.57 mg L^{-1} eq. T-X-100 and of Frew et al. (2002) who reported values of between 0.05 to 3.00 mg L^{-1} eq. T-X-100 in coastal and oceanic SML samples from the Sargasso Sea. Oligotrophic oceanic samples had lower SA values (maximum 0.15 mg L^{-1} eq. T-X-100), whereas more eutrophic coastal samples had higher SA values (up to 3.00 mg L^{-1} eq. T-X-100). This variance might be explained by changes in nutrient inputs, biological activity, and organic matter content as elevated nutrient availability in eutrophic coastal waters promotes higher phytoplankton biomass and microbial activity, leading to increased production and accumulation of surface-active organic matter through exudation, cell lysis, and microbial processing, whereas oligotrophic systems are characterised by lower organic matter production and reduced surfactant availability. Croot et al. (2007) detected an overall enrichment of surfactants in the surface microlayer in the Southern Ocean, which is consistent with earlier research. Salter (2010) found SA levels ranging from 0.35 to 1.12 mg L^{-1} eq. T-X-100, with EFs ranging from 0.8 to 8.0, in the River Tyne estuary. The increased surfactant concentrations detected in the River Tyne estuary compared to open ocean areas might be attributable to inputs of terrestrially produced surfactants in this region, as well as localized pollution from urban and industrial sources. The general enrichment of surfactants in the surface microlayer, as observed by Croot et al. (2007) in the Southern Ocean, is consistent with previous studies. Enrichment factors provide insights into the degree of surfactant accumulation in the surface microlayer compared to the underlying water. Higher EF values indicate greater enrichment, which can have implications for surface tension, gas exchange processes, and the bioavailability of pollutants.

1.7.5 Environmental Controls on Surfactant Distribution

Seasonal and spatial fluctuations in surfactant distributions have been investigated using both direct and indirect approaches. Direct measurements of surfactant activity (SA) and surface tension are commonly used, while indirect approaches often employ primary production (PP) as a proxy for biologically derived surfactants (Frew et al., 2006; Cunliffe et al., 2013; Zhang and Yang, 2013; Pereira et al., 2016). Primary productivity refers to the rate at which phytoplankton, algae, and other marine organisms use photosynthesis to convert sunlight, carbon dioxide, and nutrients into organic matter (Doney et al., 2009).

Wurl et al. (2011) proposed combining primary productivity and wind speed to predict the global distribution of oceanic surfactant coverage. Their approach is based on the biological origin of surfactants, where primary productivity reflects biological surfactant production and wind speed influences their dispersion. Their calculations indicated that the SML can persist at the global average wind speed of 6.6 m s^{-1} and may be more widespread in tropical oceans than at higher latitudes, where stronger winds (>12 m s^{-1}) may inhibit extensive film formation.

Conversely, Sabbaghzadeh et al. (2017) found a weak inverse correlation between measured SML surfactant distributions and wind speed ($r = -0.318$, $p = 0.001$) in the North Atlantic Ocean, indicating that linear regression models based solely on wind speed cannot accurately predict surfactant distributions.

Schmidt and Schneider (2011) further investigated the seasonal dependence of surfactant distributions at a coastal station in the southern Baltic Sea. Their study observed surface tension depressions of up to 10 mN m^{-1}, correlated with seasonal phytoplankton blooms. Film coverage was minimal in winter but increased significantly during the spring bloom, highlighting the close relationship between biological activity and surfactant production. This seasonal correlation with chlorophyll-a supports the use of biological productivity

indicators to assess surfactant concentrations and suggests that phytoplankton blooms play a critical role in regulating surface tension in marine environments.

1.8 Sampling of the Sea Surface Microlayer (SML)

Collecting representative SML samples poses a significant methodological challenge due to its thin, dynamic nature, which requires researchers to evaluate a range of samplers that differ in the thickness and purity of the material they collect. The most commonly used methods include the mesh-screen (Garrett) sampler, rotating-drum devices, membrane filters, and the glass-plate technique (Garrett, 1965; Harvey & Burbell, 1972; Hatcher & Parker, 1974; Franklin et al., 2005; Cunliffe & Murrell, 2009). Other approaches—such as floating trays, freezing probes, and PVC film samplers—are now seldom employed, since they tend to incorporate subsurface water and dilute true SML enrichments to a greater extent and with less reproducibility than more widely adopted techniques (Hamilton & Clifton, 1979; Hatcher & Parker, 1974).

1.8.1 Mesh-Screen (Garrett) Sampler

The mesh-screen (Garrett) sampler is a passive surface microlayer collection technique that isolates surface water based on the adhesion of a thin liquid film to a vertically immersed mesh. During sampling, the screen is dipped through the air–sea interface and withdrawn, allowing surface water retained on the mesh to drain into a collection vessel. First described by Garrett (1965), the Garrett screen collects a relatively large sample volume, with each immersion of a standard-sized screen yielding on the order of several tens of millilitres per dip, corresponding to an effective sampling rate of ~2.5 L h^{-1} under continuous operation (Schneider-Zapp et al., 2014), from depths of approximately 150–400 μm. Its stable sampling rate and ability to collect representative volumes of surface water make it well-suited for multidisciplinary analyses—including labile amino acids (Kuznetsova & Lee, 2001), phytoplankton (diatoms, heterotrophic nanoflagellates), viruses, bacteria, and chlorophyll (Agogué et al., 2004; Momzikoff et al., 2004)—as well as for mapping spatial

and temporal variability in SML composition (Frka et al., 2009; Salter et al., 2011; Pereira et al., 2016). The principal drawback is potential dilution by underlying water—up to six- to eight-fold—which can obscure true surface enrichments (Yang et al., 2001).

1.8.2 Glass-Plate Technique

The glass-plate sampler, introduced by Harvey & Burbell (1972), isolates a thin microlayer (20–150 μm) via adhesion to a hydrophilic or hydrophobic plate. This method efficiently captures low-hydrophilicity compounds such as amino acids and lipids (Momzikoff et al., 2004) and is especially appropriate in oligotrophic regions, where low nutrient and biomass levels require sensitive recovery of trace surface-active compounds (Frka et al., 2009). However, manual deployment is impractical aboard large vessels; throughput is limited (~22 mL min^{-1}), and withdrawal speed—and thus sample thickness—varies with operator technique and wind speed (should be restricted to < 5 m s^{-1}; Guitart et al., 2004; Cunliffe & Wurl, 2014).

1.8.3 Membrane-Filter Collection

Single-use filters—polycarbonate (35–42 μm depth) and PTFE (~6 μm depth)—yield near-pure SML samples with minimal subsurface dilution (Franklin et al., 2005; Cunliffe & Murrell, 2009; Cunliffe & Wurl, 2014). Deployed by floating on the surface and retrieved with forceps, these filters are ideal for bacterioneuston and molecular community analyses but produce very small volumes, require calm conditions, and are not feasible from large vessels (Hamilton et al., 2014).

1.8.4 Other Methods

Rotating-drum samplers, floating trays, freezing probes, and PVC films have been trialed (Cunliffe et al., 2013; Wurl et al., 2017), although their applicability and adoption vary depending on design and deployment. Floating trays collect thicker (and therefore partially subsurface) samples unsuitable for precise enrichment studies (Wurl & Soloviev, 2014),

while probes and PVC films face operational and contamination challenges. In contrast, modern rotating-drum or disk-based systems such as the Sea Surface Scanner (S^3) a remote-controlled catamaran platform designed to automate collection of the sea surface microlayer — have been developed to enable high-resolution sampling of SML properties with reduced subsurface contamination and greater spatial coverage (Ribas-Ribas et al., 2017).

Accurate surface tension measurements require a stable gravitational field; therefore, reliable in situ tensiometry remains challenging on moving platforms such as research vessels. Consequently, SML samples are typically collected for subsequent laboratory analysis under controlled conditions, necessitating storage protocols that preserve the integrity of surfactant-active substances.

1.9 Sample Storage and Preservation

1.9.1 Preservation Challenges in SML Samples

The lack of open ocean surface tension measurements highlights the necessity of developing storage protocols that minimise the degradation and contamination of surfactant-active substances (SAS) over time, ensuring an accurate assessment of surfactant activity in seawater. Current methods for preserving organic matter (OM) in water samples, such as refrigeration at 4°C or freezing at -20°C, exhibit mixed efficacy in terms of SAS preservation within the SML. Chromophoric dissolved organic matter (CDOM) and other organic materials are commonly stored at 4°C, with studies suggesting that this temperature may effectively limit degradation for periods less than 24 hours (Stedmon et al., 2003; Wickland et al., 2007; Hood et al., 2009). Nevertheless, this duration is often impractical on extended open-ocean cruises, whereas it may be feasible for coastal studies in which samples can be returned to shore and analysed within that timeframe. However, research indicates that even with chilled storage, specific components can degrade, leading to reductions in fluorescence and SAS stability, depending on the sample's provenance (Hudson et al., 2009). Filtering

and freezing at -20°C has also been widely utilised for the preservation of CDOM and dissolved organic carbon (DOC); yet, highly coloured samples, particularly those dominated by allochthonous OM, are more susceptible to freeze-thaw degradation compared to autochthonous samples (Gao et al., 2010; Spencer et al., 2010; Yamashita et al., 2010b). Furthermore, pre-treatment of natural water samples—such as filtration, acidification, or preservation with formalin or HgCl—has been shown to significantly alter SAS properties and CDOM characteristics, raising concerns about analytical accuracy (Wurl et al., 2009).

Freezing biological samples is a common way to preserve them, but it comes with problems, especially because of cell bursting and lysis, which can change the original sample and affect the accuracy of the results. When freezing is slow, ice crystals can grow inside the cells and break the cell membrane or wall (Lepesteur et al., 1993; Mazur, 1984). Fast freezing, for example, using liquid nitrogen, helps avoid this damage by reducing the ice formation (Chang & Zhao, 2021; Fowler & Toner, 2006; Jia et al., 2022). Also, during freezing, the concentration of salts around the cells increases, causing water to leave the cells. This makes the cells shrink, and when thawing happens too fast, water comes back in quickly, and the cells can burst due to osmotic shock (Mazur, 1970). During thawing, if the temperature is too high or the process is too fast, cells can break, and substances inside the cells, like proteins, DNA, and enzymes, can leak out and mix with the sample, which can change its chemical composition (Fuhrman et al., 1988; Spencer et al., 2010). In marine samples, this cell lysis can increase the amount of CDOM and surfactant-active substances (SAS), as Rickard et al. (2019) noticed when freeze-thaw cycles led to degradation of SAS in filtered or unfiltered seawater samples.

Some molecules, like lipids and proteins, are very sensitive to freezing and thawing, and even at very low temperatures, some enzyme activity continues, which can lead to further breakdown of sample material (Hudson et al., 2009). Repeating the freeze-thaw process many times can also kill microorganisms, which affects the analysis of microbial

communities (Amann et al., 1995). To reduce this kind of damage, scientists often use cryoprotectants like glycerol or DMSO, which help to protect the cells by lowering ice formation and reducing stress from salt concentrations (Mazur, 1970). It is also better to freeze samples quickly and thaw them slowly and in a controlled way. Another good practice is to divide the sample into smaller portions (aliquots) before freezing so it doesn't need to be thawed and frozen again multiple times.

In environmental and marine research, these problems are very important. Rickard et al. (2019) strongly advised against long-term freezing at -20°C because it can cause SAS degradation. They suggested that samples should be kept unfiltered, in the dark, at 4°C, and analysed within 24–48 hours. Also, Schneider-Zapp et al. (2013) found that freezing unfiltered seawater can cause artificial increases in CDOM, and Spencer et al. (2010) showed that water with a lot of land-derived (allochthonous) organic matter—i.e., organic material imported from outside the aquatic system, such as terrestrial runoff or decaying vegetation—is more likely to degrade during freezing than water containing organic matter produced within the water column (autochthonous), such as algal or microbial exudates. These examples show why it is important to be very careful with how samples are stored and handled, especially when studying labile organic fractions such as surface-active substances (SAS) and chromophoric dissolved organic matter (CDOM).

Because surfactant activity (SA) and chromophoric dissolved organic matter (CDOM) in SML samples are highly labile, storage protocols can profoundly alter analytical outcomes. Below, we integrate detailed findings from key studies to refine our preservation strategy.

1.9.2 Refrigeration at 4 °C

Refrigeration in the dark at approximately 4 °C remains the simplest and most widely applied approach for preserving SML samples, as this temperature is commonly used to suppress microbial metabolism and enzymatic activity while avoiding phase changes associated with

freezing, (Coble et al., 1998; Baker, 2002; Stedmon et al., 2003; Wickland et al., 2007; Fellman et al., 2009; Hood et al., 2009; Lapworth et al., 2009).

- Short-term stability: Mitchell et al. (2000) observed no detectable change in CDOM absorbance over 24 h of dark refrigeration.
- Week-long storage: Hunter & Liss (1981) reported a modest reduction in surfactant activity—around a ten-percent loss—during the first week at 6 °C, followed by a surprising rebound of about twenty percent after 34 days.
- Fluorescence variability: Hudson et al. (2009) found specific fluorophore intensities declined during refrigerated storage, with the magnitude of decline depending on sample provenance.

Together, these studies show that dark refrigeration effectively retards rapid degradation but cannot fully prevent compositional shifts beyond roughly one week.

Schneider-Zapp et al. (2013) conducted the most extensive assessment of preservation protocols to date, testing seven treatments on both freshwater and saline SML samples: simple dark refrigeration at 4 °C, freezing at –20 °C, chemical poisons (silver nitrate, mercuric chloride, formalin), size-fractionation pre-treatments, and combinations thereof.

- Surfactant activity was monitored by alternating-current voltammetry (converted to Triton X-100 equivalents) at multiple time points up to 30 days.
- CDOM was tracked using UV–Vis absorbance ratios (E2:E3), spectral slope, and PARAFAC-derived fluorescence components.

No protocol consistently outperformed simple dark refrigeration: all treatments—including freezing and chemical poisoning—yielded similar or greater drift in both SA and CDOM metrics, typically on the order of 15–20 percent over 30 days. Even the best chemical pre-treatment (silver nitrate filtration) failed to reduce variability below that of dark refrigeration.

1.9.3 Freezing and Freeze–Thaw Effects

Freezing filtered samples at –20 °C is another common preservation method (Coble et al., 1998; Murphy et al., 2008; Conmy et al., 2009; Walker et al., 2009; Gao et al., 2010; Spencer et al., 2010; Yamashita et al., 2010b).

- Provenance-dependent artifacts: Spencer et al. (2007a) and Hudson et al. (2009) documented both increases and decreases in CDOM absorbance and fluorescence after freeze–thaw cycles, with overall CDOM loss and declines in protein-, humic-, and fulvic-like fluorophores. These contrasting responses reflect differences in initial sample composition, with DOM source, molecular complexity, and relative contributions of labile versus refractory components influencing susceptibility to freeze–thaw alteration.
- Minimal optical change in some cases: Yamashita et al. (2010b) reported CDOM absorbance remained largely stable under freezing, though fluorescence signals were compromised; similarly, Gao et al. (2010), Conmy et al. (2009), and Yamashita et al. (2010a) found less than 15 percent change in optical properties, and Spencer et al. (2010) observed under 2 percent variability—all within analytical error.

Freeze–thaw processing therefore introduces unpredictable, sample-specific biases in optical DOM properties. When freezing is unavoidable, studies commonly recommend minimizing freeze–thaw cycles and handling samples consistently, as the extent of alteration appears strongly dependent on initial DOM composition rather than storage temperature alone. Although rapid freezing and storage at lower temperatures (e.g. −80 °C) are often adopted as precautionary measures, their effectiveness in fully preserving optical properties remains insufficiently constrained and may vary among sample types.

1.9.4 Chemical Preservation

Chemical poisons can arrest microbial activity, but they frequently alter DOM and surfactant signals:

- Acidification to pH 2–3 (HCl, H_3PO_4) prevents metal–DOM complexation but shifts CDOM absorbance and causes pH-dependent fluorescence peak shifts (Andersen et al., 2000; Patel-Sorrentino et al., 2002; Mobed et al., 1996; Spencer et al., 2007a).
- Mercuric chloride ($HgCl_2$) quenches fluorescence and perturbs CDOM (Fu et al., 2007; Yamashita & Jaffe, 2008).
- Sodium azide (NaN_3) shows mixed outcomes—no effect in some reports (Ferrari et al., 1996; Astoreca et al., 2009; Patel-Sorrentino et al., 2002) but up to 10 percent absorption increases in others (Tiltstone et al., 2002).
- Chloroform ($CHCl_3$) is volatile and prone to loss from plastic containers (Kremling & Bruggmann, 1999).
- Formalin can preserve surfactants but risks cross-reaction and toxicity (Wurl et al., 2009).

Given these conflicting effects, chemical poisoning is not recommended for SML surfactant or CDOM analyses.

1.10 Research Gap

The sea surface microlayer (SML) is a critical yet boundary at the ocean–atmosphere interface. Its thin, surfactant-rich films regulate biogeochemical cycling, air–sea gas exchange, and sea spray aerosol formation, influencing global climate processes. Despite this significance, major knowledge gaps persist regarding the dynamics of SML surfactants and this hinders their representation in Earth system models.

Two key limitations stand out. First, there is no consensus on storage protocols that preserve the integrity of surface-active substances (SAS) in SML samples for delayed analysis. Previous studies relied on alternating-current voltammetry or optical DOM metrics, which probe only select chemical fractions and may not capture the integrated behaviour of all surfactants at the air–sea interface. Second, direct, long-term field measurements of seawater surface tension ($\Delta\sigma$) are rare, particularly from unfiltered SML samples in natural marine environments. This lack of data constrains our understanding of surfactant film formation, persistence, and their role in climatic feedbacks.

This thesis addresses these challenges by contributing both methodological and scientific novelty:

- To our knowledge, this is the first study to validate SML storage protocols using surface-tension measurements (Wilhelmy-plate tensiometry). Previous work relied on voltammetry or optical DOM metrics; by directly quantifying how ($\Delta\sigma$), defined as the surface-tension depression relative to a clean reference surface at the same temperature and salinity, evolves over time, this study provides an unprecedented perspective on surfactant stability in natural SML samples.
- It also delivers one of the few multi-year, field-based datasets of seawater surface tension, derived from unfiltered SML and underlying water samples across temperate coastal and oligotrophic open-ocean regimes. These data reveal mechanistic controls on surfactant film dynamics and support improved parameterizations of air–sea gas exchange in climate models.

1.11 Objectives of this Thesis

1. Develop and validate storage protocols for sea surface microlayer (SML) samples that preserve surface-active substance (SAS) integrity for delayed analysis, enabling reliable tensiometric and voltammetric measurements.

2. Compare Wilhelmy-plate tensiometry and alternating-current voltammetry to evaluate their sensitivity and representativeness in characterising surfactant activity.

3. Generate novel field datasets of seawater surface tension across coastal and open-ocean regimes, resolving spatial and temporal variability in SML film coverage ($\Delta\sigma$).

4. Quantify key environmental and biogeochemical drivers—including nutrient availability, phytoplankton biomass, temperature, and wind forcing—of surfactant dynamics and assess their implications for air–sea exchange processes.

Together, these objectives integrate methodological innovation with mechanistic analysis to advance understanding of surfactant-mediated processes at the air–sea interface.

Thesis Structure

This thesis comprises three results-based chapters. Chapter 2 develops and validates storage protocols and analytical approaches for surfactant characterisation. Chapters 3 and 4 apply these validated methods to coastal and open-ocean environments, respectively, generating novel surface-tension datasets and examining the physical and biological controls on SML surfactant dynamics. Collectively, these studies provide a framework for improving representation of surfactant films in air–sea exchange and climate-related models.

Chapter2: Evaluating Surfactant Stability in Marine Surface Microlayers: Integrating Tensiometry, Voltammetry, and Storage Protocols

2.1 Preface to the Chapter

This chapter addresses the methodological challenges associated with storing sea surface microlayer (SML) samples for the measurement of surfactant activity (SA) and surface tension (ST). Although SA can be quantified rapidly using alternating current (AC) voltammetry, it reports concentrations as Triton X-100 (TX-100) equivalents and may vary between laboratories. In contrast, surface tension provides a direct measure of cumulative surfactant enrichment at the air–sea interface but cannot be measured reliably on moving platforms, necessitating delayed laboratory analysis.

We therefore developed and evaluated storage protocols designed to preserve surface-active substances (SAS) prior to tensiometric and voltammetric analysis. The effects of refrigeration (4 °C) and deep-freezing (–80 °C) were systematically compared using Wilhelmy plate tensiometry and complementary voltammetric approaches. By assessing the stability of SAS under different storage conditions, this chapter establishes practical preservation strategies to improve the reliability of SML surfactant measurements.

2.2 Objectives

1. Evaluate the stability of SAS under different storage conditions, including refrigeration (4 °C) and deep-freezing (–80 °C).
2. Assess the impact of freezing methodology, container size, and sample pre-treatment on surfactant preservation.

3. Compare voltammetric surfactant activity (SA) measurements with direct surface tension determinations.

4. Examine the performance of a standard 15-second deposition method versus a multi-deposition approach in voltammetric analysis.

By applying surface tension as an integrative measure of total SAS, this chapter establishes a validated storage protocol for reliable SML analysis under delayed laboratory conditions.

2.3 Sampling Protocol

2.3.1 Whitby Sampling (Storage Tests)

To ensure that the sea surface microlayer (SML) samples reflected open-sea conditions and were not highly influenced by coastal contamination, samples were collected from a site approximately 3 km offshore of the coast of Whitby, UK, in the North Sea (Figure 5). All collection equipment and storage vessels were pre-soaked overnight in a 4% HCl acid bath, followed by a thorough rinse with Milli-Q (MQ) water (18.2 MΩ·cm) to eliminate potential contaminants. The mesh-screen (Garrett) sampler was rinsed 3-5 times in seawater prior to sampling, with the collected water used to rinse the plastic bottles. To further minimise potential contamination, the first dip of SML water was vigorously shaken inside the bottle and then discarded.

For sample collection, a Garrett screen was gently immersed in the water and raised through the air–sea interface while keeping the screen parallel to the surface, allowing excess water to drain until only the microlayer film remained within the screen's wire mesh. This retained film was then poured into a 1-litre collection container, and the procedure was repeated until the desired sample volume was achieved. After collection, samples were immediately placed in an ice-filled cork box to maintain the ambient temperature until transport to the WACL laboratories for initial analysis, which was performed the same day.

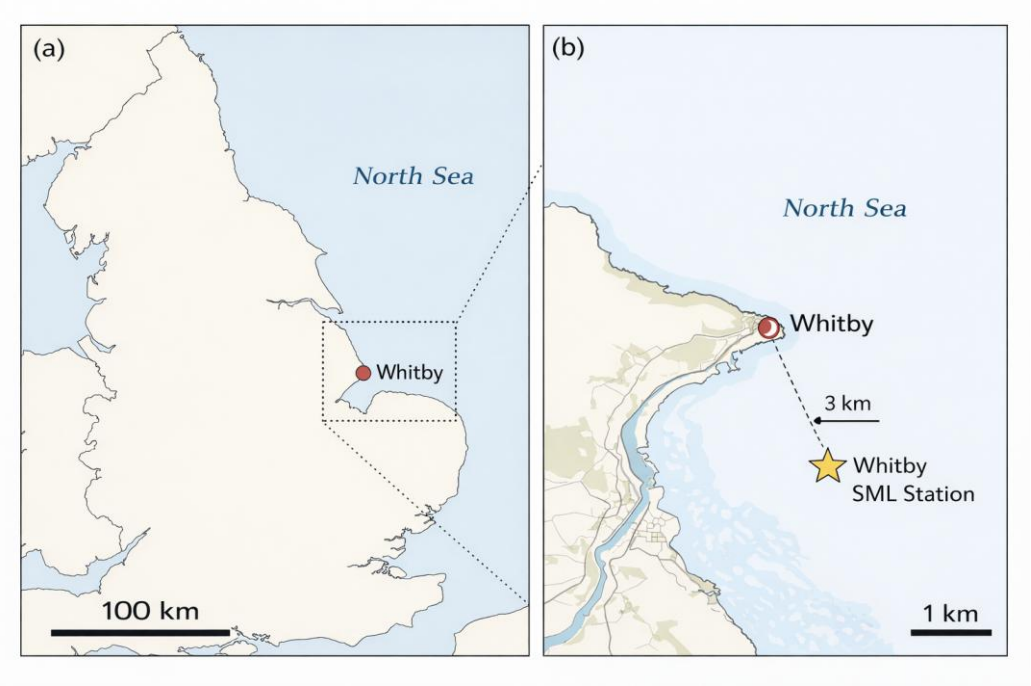

Figure 5: Location of the Whitby SML sampling site in the North Sea: (a) regional overview of the eastern UK coast; (b) zoomed view showing the station ~3 km offshore.

2.3.2 PML Campaign

SML samples were collected by the crew of the Plymouth Marine Laboratory (PML) from the bow of the RV *Plymouth Quest*. The PML is a marine research organisation, situated on the South-East coast of England, who have collaborated extensively with us on work into ozone uptake to seawater. The sampling location was approximately 0.5 km offshore of Rame Head, Cornwall, in the English Channel (Figure 6). The Garrett screen was operated as described above. Samples were stored at 4 °C in the dark. Unfiltered surface tension measurements were conducted at PML using a platinum Wilhelmy plate.

Figure 6: Coordinates of seawater sample collection sites in Plymouth (black dots), taken at locations between 50° 19' 12" N, 4° 10' 12" W and 50° 18’ 32.4” N, 4° 11’ 27.6” W.

2.4 Screen Specifications and SML Thickness

The Garrett screen was chosen primarily because it collects a significantly larger volume of water compared to other types of screens, which is particularly beneficial for ensuring that a sufficient volume of the sea surface microlayer (SML) is collected for subsequent analyses (Cunliffe et al., 2014). We used a relatively large surface area Garrett screen (Table 2) combined with a 16 mesh count per inch and substantial void space, enabling the ability to gather a representative sample of the SML in a small number of dips. This efficiency is crucial in minimising the time the SML is exposed to potential environmental changes, thereby preserving its integrity for accurate surface-active substance (SAS) analysis. The specifications of the Garrett screen, shown in Table 2, directly influence the thickness of the collected microlayer.

Table 2: Specifications of the Garrett screen used for SML sampling, including physical dimensions, mesh count, and average volume collected per dip.

Screen Specifications	Value
Length	78.3 cm
Width	52.5 cm
Area	4111 cm^2
Mesh Count	16 per inch
Void Space	60.8 %
Wire Outer Diameter	0.35 mm
Average Volume per Dip	163 mL

The consistent use of the Garrett screen ensured uniformity in sampling, while variations in handling procedures—such as the location of sampling and immediate treatment post-collection—enabled the differentiation between protocols focusing on real-time analysis versus those designed for storage stability assessments. This distinction is critical for understanding the reliability of SAS preservation in different storage conditions, especially when comparing the influence of storage temperature on SAS stability.

To determine the thickness of the gathered SML, both the volume of liquid collected per dip and the geometry of the screen were considered. The sampling area was derived from the area of the screen, minus the area occupied by mesh wires. The void space (provided by the supplier) reflects the percentage of the area that is empty, so it was used to calculate the sampling area using the following equation:

$$Sampling\ Area = Screen\ Area \times \left(Void\ Space \frac{Percentage}{100} \right) \qquad (6)$$

The gathered sample volume in a single dip was then used to calculate the depth of the theoretical cuboid, which represented the SML thickness, based on the sampling area. The thickness was determined using

$$SML\ thickness = Sample\ volume / Sampling\ area \qquad (7)$$

Our dataset—spanning from Jan 20 to Sept 21—revealed SML thickness values ranging from approximately 600 to 777 μm, with an overall mean of about 653 μm. Most sampling events exhibited low standard deviations of SML thickness relative to their respective means, demonstrating high reproducibility. For example, on 20 Jan 20 the average thickness was 600 μm with a standard deviation of 61 μm (≈10% variability), while on 17 May 20 the average was 777 μm with only 16 μm deviation (≈2% variability). The highest variability was observed on 05 Feb 20, where the standard deviation reached 107 μm (≈17%). The average variability across all events was found to be approximately 8.6%. To visualise this typical sampling uncertainty across the full time series, Figure 7 includes a semi-transparent shaded band corresponding to ±1 standard deviation (±58 μm), calculated as the mean standard deviation from complete sampling events (Table 3). This band represents characteristic sampling variability of the Garrett screen method rather than uncertainty in the mean SML thickness, and provides context for interpreting temporal fluctuations in the dataset. These modest deviations, likely attributable to natural environmental fluctuations and minor operator differences, underscore the reliability of the Garrett screen sampling method. This consistency—supported by both the comprehensive Table 3 and the corresponding plot (Figure 7) with a dashed line indicating the overall mean—provides a robust foundation for further analyses of SAS stability under varied storage conditions.

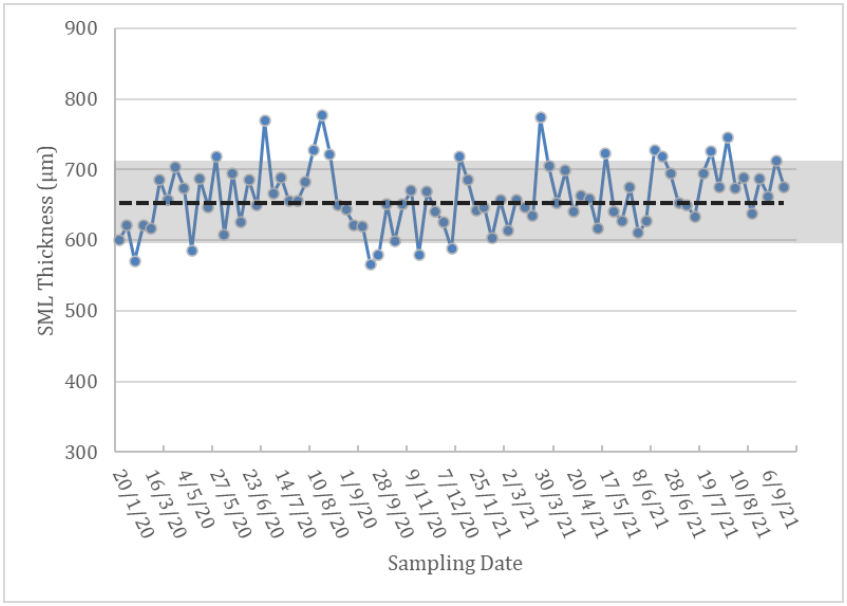

Figure 7: Temporal variation in sea surface microlayer (SML) thickness between January 2020 and September 2021 measured using the Garrett screen sampler. Points show mean SML thickness for individual sampling events, with the dashed line indicating the overall mean (~653 µm). The shaded band represents ±1 standard deviation (±58 µm) derived from complete sampling events (Table 3) and reflects typical sampling variability.

Table 3. Representative subset of SML thickness measurements, standard deviations, and percentage variability for complete sampling events between Jan 20 and Sep 21.

Date	Average volume Sampled/Dip	Thickness Sampled	Stdev	Ratio to Mean Thickness
	mL	µm	µm	
20/01/2020	150	600	61	1.08
05/02/2020	155	621	107	1.04
16/03/2020	154	617	55	1.05
17/08/2020	194	777	16	0.83
05/07/2021	163	652	69	0.99
13/09/2021	169	675	40	0.96

2.5 Surface Tension Measurement Protocol

Surface tension was measured using a Kibron EZ Plus tensiometer, which was equipped with a platinum Wilhelmy plate and a thermocouple. According to the manufacturer, the accuracy of the instrument is ±0.1 mN m^{-1}, while its precision is reported to be within ±0.05 mN m^{-1}. This high level of accuracy and precision made it suitable for detecting subtle variations in surface tension that are indicative of changes in the concentration of surface-active substances (SAS). The setup is illustrated in Figure 8, which shows both the full

instrument and a detailed view of the measurement stage. Additionally, the detailed technical specifications of the instrument are summarised in Table 4, highlighting its operational range, sensitivity, and sample volumes.

Figure 8: Left-hand side: The Kibron EZ Plus tensiometer used for high-precision surface tension measurements. Right-hand side: A close-up of the measurement stage, showing the sample dish beneath the sensor probe and a thermocouple monitoring temperature for accuracy.

Table 4: The detailed specifications of the Kibron EZ Plus tensiometer

Parameter	**Value**
Principle of Operation	Du-Noüy/Wilhelmy
Measuring Range	1-350 mN m^{-1}
Accuracy/Sensitivity	0.01 mN m^{-1}
Sample Cup Material	Polypropylene / Glass / Teflon
Sample Volume	0.5-3 mL
Maximum Viscosity	60,000 cP (Newtonian)
Average Time per Measurement	30 seconds

For each analysis, a small glass tensiometer vessel, with an approximate volume of 3 mL, was prepared through a rigorous cleaning protocol to ensure accuracy in surface tension measurements. The vessel was first rinsed with Milli-Q (MQ) water and ethanol, followed by soaking in 4% HCl for five minutes. After the acid wash, the vessel underwent a final rinse with MQ water and was then dried in an oven at 120°C. Once dried, it was cooled under a stream of compressed nitrogen before being set in the tensiometer. The sample was carefully poured into the vessel until it was completely filled. A thermocouple was then

introduced to measure and equilibrate the sample temperature for at least five minutes before proceeding with the analysis. The platinum Wilhelmy plate, used in the tensiometer, was also thoroughly cleaned before each run by rinsing with MQ water and heating briefly to red-hot in a Bunsen flame to ensure sterilisation. Once cleaned, the plate was mounted in the tensiometer, and surface tension measurements were performed. This meticulous preparation ensured that all containers and instruments were free from any contaminants that might influence the surface-active properties of the sample, thus providing accurate and consistent surface tension readings.

2.5.1 Measurement Procedure

Measurements were conducted only after verifying the proper preparation of both the thermocouple and the Wilhelmy plate. Ensuring the temperature equilibrium of the sample (defined here as a stable temperature reading with fluctuations of less than ±0.1 °C over a period of several minutes, as monitored continuously by the thermocouple) before measurement minimised variability in the surface tension values and contributed to the reliability of the data obtained. Temperature stability was assessed instrumentally rather than visually, and measurements were initiated only once the recorded temperature reached a steady state.

This thorough preparation of both the sample vessel and the Wilhelmy plate was maintained during the study to ensure consistency and reproducibility. Such careful attention to cleaning protocols and measurement conditions was essential to minimise sources of error and ensuring that the surface tension data obtained accurately reflected the effects of different storage conditions on SML samples, as well as the relationship between surface tension and surfactant activity in marine environments.

2.5.2 Tensiometry Calibration

The accuracy of the tensiometer used in this study, the Kibron EZ Plus, was evaluated by measuring the surface tension of Milli-Q (MQ) water at various temperatures and comparing these results to reported literature values. The measurements were conducted to ensure the reliability of surface tension data obtained for subsequent analyses of surface microlayer samples. As shown in Figure 9 and Table 5, the measured surface tension values were closely aligned with literature data (Vargaftik et al., 1983), with minor deviations, particularly at higher temperatures.

The linear fit obtained (gradient = 0.1492, R^2 = 0.9979) aligns well with the literature-reported gradient of 0.1500, and the close clustering of data points around the fitted line indicates a low uncertainty in the regression slope. Given this low scatter and high coefficient of determination, the uncertainty associated with the fitted gradient is small and overlaps with the literature-reported value, demonstrating a strong correspondence. This agreement shows that the tensiometer is very accurate and gives us confidence in using it to check the surfactant stability of SML samples.

Table 5: The average measured surface tensions of pure water at different temperatures, compared to literature values.

Temperature	Measured S. Tension	Literature S. Tension
°C	mN m^{-1}	mN m^{-1}
5	74.97	74.95
10	74.29	74.23
15	73.43	73.50
20	72.64	72.75
30	71.29	71.20

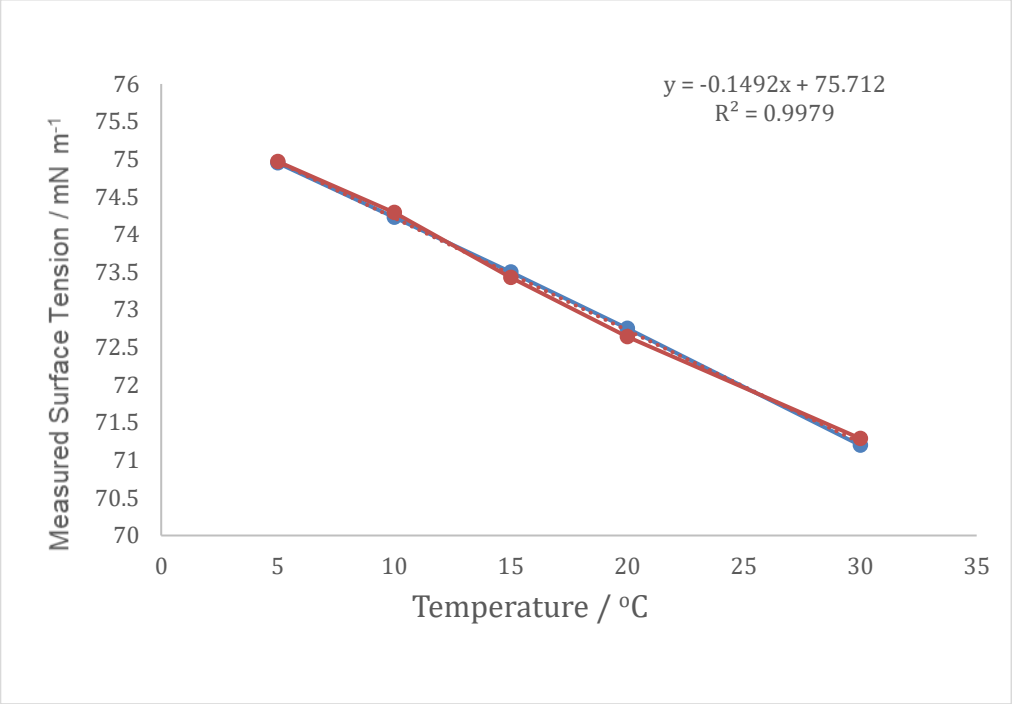

Figure 9: Comparison of measured surface tension of pure water at different temperatures using this study's instrument (orange points; y = -0.1492x + 75.712, R^2 = 0.9979) with literature values (blue points; y = −0.1581x + 75.69, R^2 = 0.9998) reported by Vargaftik et al. (1983). The close agreement between the two data sets demonstrates the instrument's accuracy.

The tensiometer's accuracy was further validated by measuring the surface tension of several reference compounds, including pure water, glycerol, acetonitrile, ethyl acetate, and ethanol, and comparing these measurements to established literature values. As shown in Table 6, the measured surface tensions (with standard deviations) are listed alongside established literature values. For example, pure water was measured at 72.692 ± 0.095 mN m^{-1} compared to a literature value of 72.703 mN m^{-1} (Vargaftik et al., 1983), while ethyl acetate was measured at 24.053 ± 0.113 mN m^{-1} versus 23.95 mN m^{-1} (Mumford and Phillips, 2004). Glycerol (63.914 ± 0.134 mN m^{-1}) and ethanol (22.120 ± 0.070 mN m^{-1}) were slightly lower than the reported values of 64.8 and 22.27 mN m^{-1}, respectively (Vargo et al., 1991; Richards et al., 1915), whereas acetonitrile showed marginally higher values (29.966 ± 0.155 mN m^{-1}) compared to 29.04 mN m^{-1} from the literature (Harkins et al., 1917). The tensiometer calibration performed in this section plays a vital role in establishing the reliability of the surface tension measurements used in our SML sample studies. Accurate calibration is

crucial for the reproducibility and consistency of surface tension data, which forms the basis of surfactant activity and stability assessments throughout this research. This calibration further ensures that the conclusions drawn regarding the storage and handling of SML samples are based on sound and precise analytical results.

Table 6: The average measured surface tensions of known reference compounds

Sample	Surface Tension	Std. Dev.	Lit. Surface Tension	Reference
	mN m^{-1}	mN m^{-1}	mN m^{-1}	
Pure Water	72.69	0.095	72.70	Vargaftik et al., 1983
Glycerol	63.91	0.134	64.80	Vargo et al., 1991
Acetonitrile	29.97	0.155	29.04	Harkins et al., 1917
Ethyl Acetate	24.05	0.113	23.95	Mumford and Phillips, 2004
Ethanol	22.12	0.070	22.27	Richards et al., 1915

2.5.3 Film Pressure Calculation

In the measurements of sea surface microlayer (SML) tension, two key environmental factors—temperature and salinity—are accounted for, since water's interfacial properties are systematically altered by variations in these parameters. First, each reading is normalized to a common thermal baseline to eliminate biases introduced by laboratory temperature fluctuations, using the pure-water model of Nayar et al. (2014). All measured surface tensions were therefore adjusted to 20 °C by applying the following relationship:

$$\sigma_w = 235.8 \times \left(1 - \frac{T + 273.15}{647.096}\right)^{1.256} \times \left(1 - 0.625 + \left(\frac{273.15}{647.096}\right)\right) \qquad (8)$$

In this equation, σ_w represents the reference surface tension (in mN m^{-1}) for pure water at a specific temperature. This relationship accurately models the changes in surface tension as a function of temperature.

Once σ_w had been determined, it was adjusted for the sample's salinity S (g kg^{-1}) following the empirical correction of Sharqawy et al. (2010):

$$\sigma_0 = \sigma_w(1 + 3.766 \times 10^{-4}\, S + 2.347 \times 10^{-6} S\, T) \qquad (9)$$

Where σ_0 represents the reference surface tension corrected for the specific salinity and temperature of the sample. This value serves as the baseline against which the presence of surfactants is measured.

To quantify the influence of surfactants, the actual measured surface tension of the SML (σ_{SML}) was subtracted from the reference surface tension (σ_0), resulting in the film pressure ($\Delta\sigma$), which provides an indication of the reduction in surface tension due to the presence of surfactants as defined by Schmidt & Schneider (2011) in Equation 4. The film pressure ($\Delta\sigma$) effectively represents the degree of surfactant activity within the SML. Higher values of $\Delta\sigma$ correspond to greater reductions in surface tension, which in turn suggest higher concentrations or effectiveness of surfactant materials at the air-water interface.

2.5.4 Data Evaluation and Stability Criteria

Following temperature correction, the surface tension data were further evaluated to assess stability and ensure accuracy. Given the dynamic nature of sea surface microlayer (SML) samples, achieving fully stable measurements can be challenging, particularly when dealing with complex surface-active species (SAS) that are sensitive to subtle environmental changes.

In this study, the stability criterion was set as follows: if the corrected data indicated a change of more than 0.2 mN m^{-1} between consecutive 500-second averages, the values were deemed unstable and filtered out of the final dataset. This threshold was selected based on the instrument performance characteristics of the Kibron EZ Plus (accuracy/sensitivity ~0.01 mN m^{-1}), and published precision for water measurements (CV < 0.1% at 20 °C), such that

a 0.2 mN m^{-1} change represents a conservative deviation that exceeds typical measurement scatter and therefore indicates genuine temporal drift rather than analytical noise.

For some samples, particularly those with low surfactant concentrations, a significantly longer equilibration time was required to achieve stable surface tension values, sometimes extending to as much as 2 hours. Despite these extended equilibration periods, Figure 10 illustrates an instance where the surface tension values continued to stabilise during the course of the measurement run, even after 60 minutes of equilibration prior to the run.

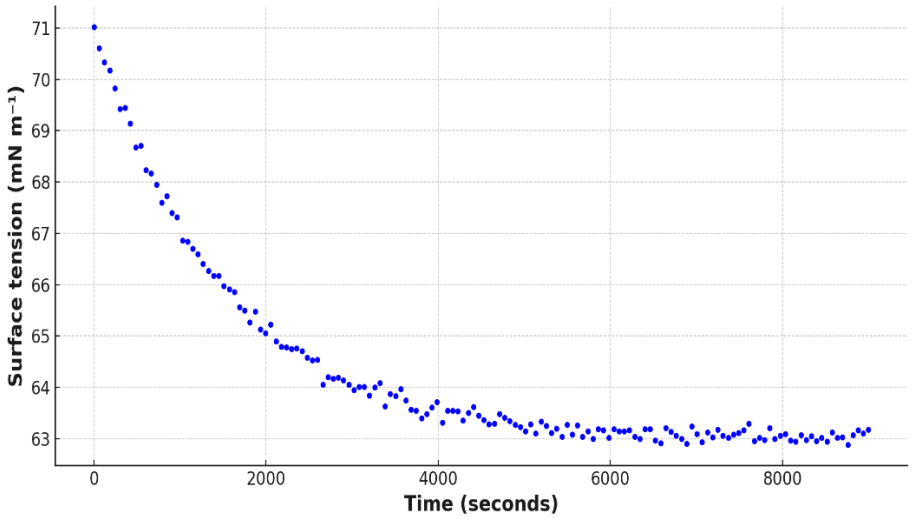

Figure 10: Stabilization of surface tension over time for a low-surfactant sample. Despite 60 minutes of pre-equilibration, values continued to stabilize during the run.

To minimise the influence of these elevated values on the mean surface tension obtained, a strategy was employed where at least 100 repeat dips were conducted per run. If the standard deviation of these runs exceeded 0.2 mN m^{-1}, the first 10% of measurements were excluded from both the mean and the standard deviation calculations, provided that such exclusion led to a reduction of the standard deviation to below 0.2 mN m^{-1}. This method ensured that the reported surface tension values more accurately reflected the equilibrium state of the sample, reducing the impact of transient initial instability.

The occurrence of this initial instability, even after long equilibration times, indicates that factors beyond surfactant adsorption, such as instrument conditions or interactions with container surfaces, may play a role in elevating surface tension values early in the measurement. Such instability in surface tension measurements has also been reported in other tensiometry studies, further highlighting the inherent challenges in obtaining accurate measurements, particularly for samples with low concentrations of surface-active species (Nayar et al., 2014). It is important to note that extended equilibration times were observed only for a small minority of samples (approximately 4–5 out of ~80 measurements), whereas the majority reached the defined stability criterion within substantially shorter time periods. These longer equilibration cases therefore represent exceptional behaviour associated with low-surfactant samples rather than a general characteristic of the dataset, and are documented here to ensure transparency in the interpretation of equilibrium surface tension measurements.

2.6 Gradual freezing using a proprietary freezing container

A freezing container (Mr Frosty, Thermo Scientific™) was employed to facilitate the gradual freezing of surface microlayer (SML) samples, to investigate whether this method was effective for minimising degradation or loss of surface-active substances (SAS). The Mr Frosty system (Figure 11) is an insulated device that allows controlled cooling of samples by surrounding them with isopropanol or ethanol, which acts as a cryoprotectant. By creating a slow and consistent cooling rate of approximately -1°C per minute, the system prevents the formation of large ice crystals that may damage the delicate structures, and surface-active components present in the SML.

SML samples collected for the storage test protocol were aliquoted into 5 mL cryovials, each filled to approximately 80% capacity to allow for expansion during freezing. The cryovials were then placed into the freezing container, which was pre-filled with isopropanol and cooled to -80°C. Once frozen, samples were stored at -80°C until analysis.

This controlled freezing process is especially important because rapid freezing often leads to the formation of large ice crystals, which disrupt cellular and molecular structures. By reducing the rate of ice crystal formation, the Mr Frosty methodology could potentially ensure the stability and consistency of subsequent surface tension measurements used to quantify surfactant activity and maintain the original physicochemical properties of SAS within the SML.

Prior to surface tension measurement, the samples were carefully thawed in a 25°C water bath for approximately 20 minutes, allowing them to reach equilibrium gradually. The slow thawing process is critical to minimise thermal shock, which could otherwise cause further degradation or alterations in the SAS properties of the sample.

Figure 11: The image shows Mr. Frosty Freezing Container, used for freezing samples at a controlled rate of 1°C per minute using isopropanol (IPA).

2.7 Voltammetry Measurement Analysis of Surface Activity

This section discusses the quantification of surfactant activity (SA) in the SML samples using voltammetry analysis with two approaches: a 15-second deposition method and a

multiple deposition time method. The detailed procedures, calibration steps, and key results are presented below.

Surfactant activity was quantified by AC voltammetry using a Metrohm 663 VA Stand (Figure 12) and an IME623 Autolab Type III Potentiostat/Galvanostat. The technique employs three electrodes: (i) a reference electrode consisting of a saturated silver/silver chloride (Ag/AgCl) immersed in a 3 mol L^{-1} KCl solution; (ii) a hanging mercury drop electrode (HMDE) with a renewable, non-polar hydrophobic surface; and (iii) a platinum wire auxiliary electrode. A constant current (E) of -0.6 V is used to create an electrical double layer at the interface between the HMDE and reference electrodes. This is done while stirring the water sample for a certain amount of time to allow the adsorption of surface-active material onto the electrodes, which contrasts with surface tension measurements that probe equilibrium properties of the air–water interface under quiescent conditions. As a result, voltammetry and tensiometry differ fundamentally in their physical treatment of the sample, with voltammetry selectively measuring adsorptive, electroactive surfactant fractions under forced transport, whereas surface tension integrates the cumulative effect of all surface-active substances present at the interface. This methodological distinction must be considered when comparing surfactant activity derived from voltammetry with surface film coverage inferred from tensiometry (Gašparović et al., 2011; Wurl et al., 2011b; Gašparović, 2012; Schneider-Zapp et al., 2014; Pereira et al., 2016). The substances that have been adsorbed then modify the electrical double layer at the interface between mercury and water, with temperature and salinity influencing the measurement indirectly through their effects on solution conductivity, ion mobility, and double-layer structure. However, under the controlled and relatively narrow temperature and salinity ranges used in this study, these effects are secondary compared to variations driven by surfactant concentration and composition. The gradual buildup of surfactant on the HMDE results in changes to both the permittivity and thickness of the double layer, which ultimately leads to a decrease in the

capacitance current (CCi) when a voltage is applied (Cuscov and Muller, 2015). The parameters used in these measurements are summarised in Table 7.

Table 7: Parameters used for voltammetry measurements.

Parameter	Value
Start potential	-0.6 V
Stop potential	-0.7 V
Step	-0.002 V
Modulation amplitude	0.012 V_{RMS}
Modulation time	0.15 s
Frequency	70 Hz
Interval time	0.55 s
Scan rate	0.0036 V s^{-1}
Stirrer speed	3
Drop size	3
Repeats per conc.	5

The voltammeter was linked to a nitrogen gas cylinder (99.99%, supplied by BOC), which was used to purge samples and generate pressure for mercury drop production from the capillary. A 90 mL Teflon cell holds the sample. The cell cleaning procedure was to rinse with hot water three times, then two times with deionised (DI) water, then at least 20 minutes in acid wash (4% HCl). Finally, the cell was rinsed three times with ultrapure water and allowed to air dry. Blanks were performed by filling the cell with MQ (18.2 MΩ cm) water (7.17 mL), sodium chloride (3M, 2 mL) and sodium hydrogen carbonate (10 mM, 1.83 mL). The blank measurements were initiated after two minutes of equilibration.

Figure 12: Metrohm 663 VA Stand used for voltammetric analysis of surfactant activity in sea surface microlayer (SML) samples.

Calibrations were performed immediately after the blank measurements, using 45 µL additions of a 42.4 mg/L solution of TX-100. Measurements were taken for five different deposition times: 5 seconds, 15 seconds, 30 seconds, 45 seconds, and 1 minute. Multiple deposition times improve the precision and accuracy compared to the standard 15-second-only deposition period SA approach (Ćosović and Vojvodić, 1982; Ćosović and Vojvodić, 1998). Each measurement was repeated with 5 scans after each deposition time, with a two-minute equilibration period for each run. After the runs, the electrode was washed with ethanol to remove any residual TX-100 and then rinsed with plenty of DI water. Another blank was measured before analysing the sample, ensuring that the current measured was within the calibration and linear ranges. Once all measurements were completed, the electrodes and cell were cleaned as stated above.

2.7.1 Calibration Procedures for Determining Surfactant Activity

The calibration procedure to determine surfactant activity (SA) in SML samples involved using both the 15-second deposition and the multiple deposition time methods, with Triton X-100 (TX-100) as the reference surfactant.

For the 15-second deposition method, the reduction in current, Δi, was calculated as:

$$\Delta i = CCi_{Blank} - CCi_{Run} \qquad (10)$$

where CCi_{Blank} is the current measured in the blank, and CCi_{Run} is the current measured with a known concentration of TX-100 at the same deposition time. The values of Δi were plotted against the concentration of TX-100, resulting in a linear calibration graph (Figure 13). The slope represented the sensitivity of the current response to changes in TX-100 concentration. Given that the intercept was only very slightly positive ($C_{15s\,cal}$ = 0.0701), it was forced through zero, reducing baseline errors and improving accuracy.

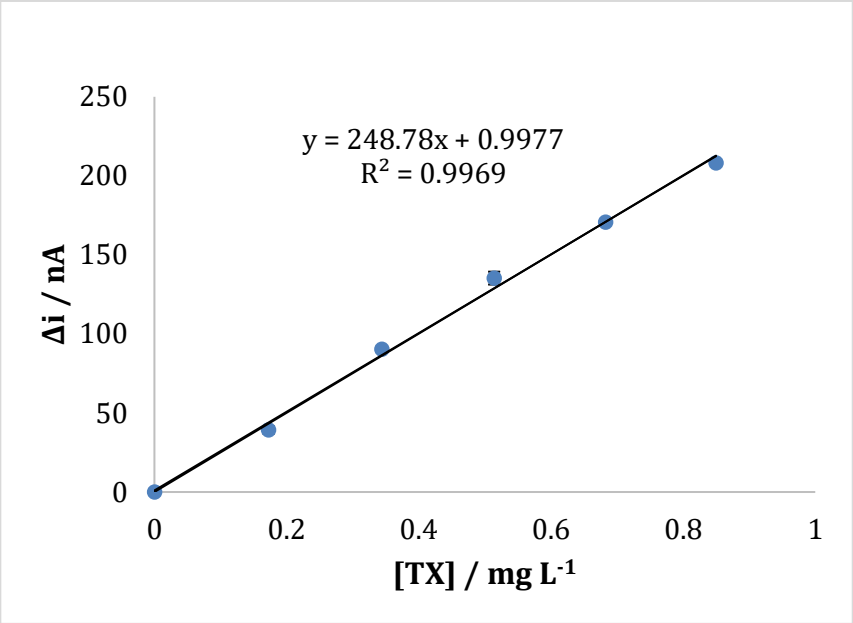

Figure 13: Calibration graph of current reduction (Δi) against TX-100 concentration for the 15-second deposition time.

2.7.1.1 15-second Deposition Method

For surfactant activity determination, first, the sample blank is measured, then a known volume of sample to the blank is added, and then the current at the above-mentioned deposition periods is measured. Only the Δi of the 15s deposition time has to be processed for this calibration, then the SA value for a sample was calculated as:

$$SA_{sample} = \frac{\Delta i_{sample} - c_{15s\ cal}}{m_{15s\ cal}} \quad (11)$$

Where SA_{sample} is the diluted sample's surfactant activity in mg L^{-1} TX-100 eq., Δi_{sample} is the sample current decrease in nA relative to the blank, $c_{15s\ cal}$ is the intercept of the calibration graph in nA, and $m_{15s\ cal}$ is the gradient of the calibration graph nA L mg^{-1}. Further correction for dilution was applied using:

$$SA_{Real} = SA_{Sample} * \frac{V_{Blank}}{V_{Blank} + V_{Sample}} \quad (12)$$

2.7.1.2 Multiple Deposition Times Calibration (Slopes Method)

The multiple deposition times calibration (slopes method) utilised deposition times of 5, 15, 30, 45, and 60 seconds, with each time producing a unique current response (Δi). Calibration graphs for different concentrations of TX-100 were generated by plotting Δi against deposition time, allowing a more comprehensive understanding of adsorption dynamics and yielding more accurate SA values (Figure 14). The R^2 values for these calibration lines were close to 1 (ranging from 0.993 to 0.998), indicating excellent linearity and consistency of the measurements across different concentrations and deposition times.

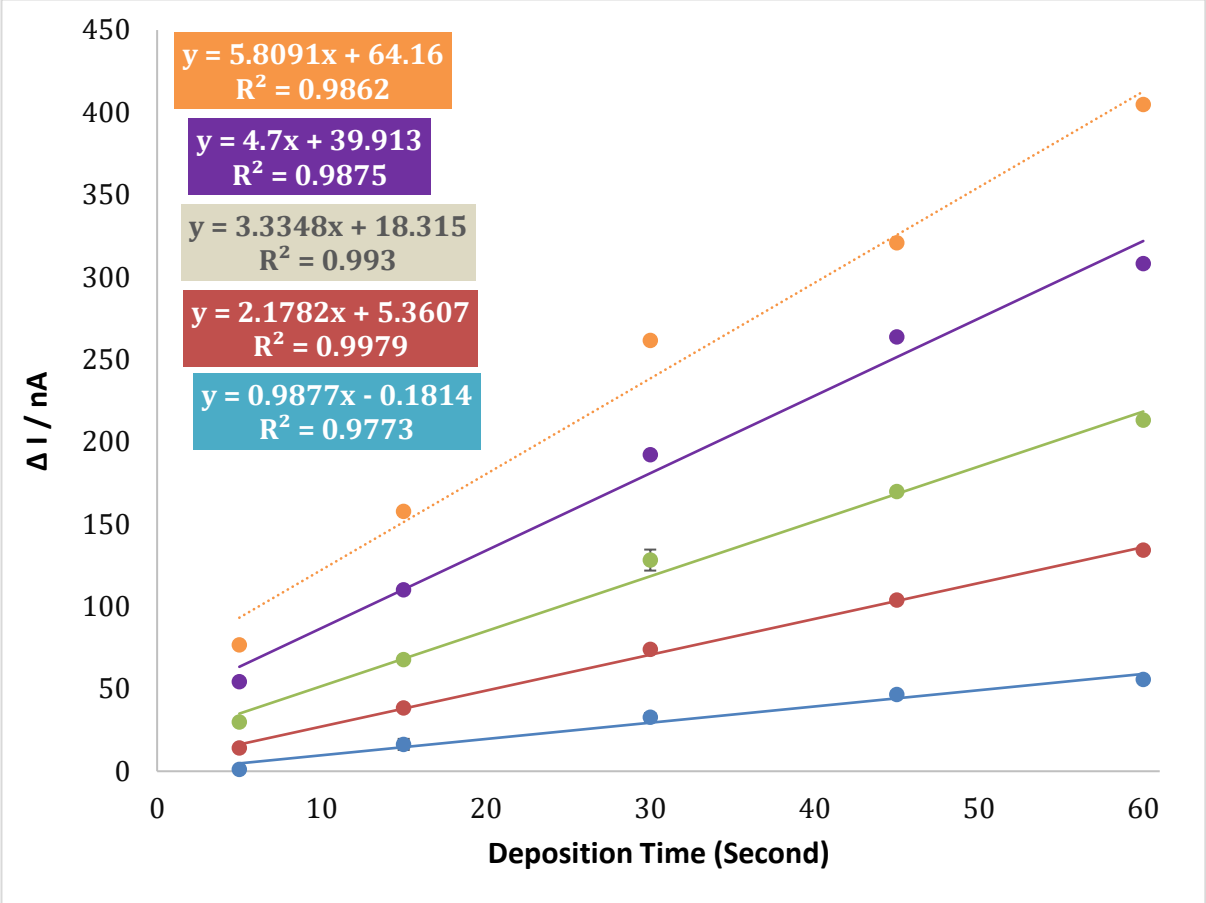

Figure 14: Calibration graph of current reduction (Δi) versus deposition time for different concentrations of TX-100: magenta 0.173 mg L^{-1}, orange 0.344 mg L^{-1}, grey 0.514 mg L^{-1}, purple 0.683 mg L^{-1}, and green 0.850 mg L^{-1}, each showing a linear increase in Δi with deposition time.

To further evaluate the calibration results, Figure 15 shows the relationship between the slopes of Δi versus deposition time and the concentration of TX-100. This calibration graph represents the gradient of each line (from Figure 14) plotted against the respective TX-100 concentrations, providing a more precise assessment of surfactant activity.

To quantify this improvement, the mean and standard deviation of calibration errors were calculated from Table 6: the single-point 15 s method—despite forcing the intercept to zero—yielded percentage errors of 7.4–34.5% (mean ≈ 20.9%, SD ≈ 8.5%), whereas the slopes method produced errors of only 6.7–8.7% without intercept correction (mean ≈ 7.7%, SD ≈ 0.8%) and 10.7–26.5% when the intercept was forced (mean ≈ 18.6%, SD ≈ 6.5%). Thus, even in its best case, the 15 s method is associated with nearly three times the systematic error of the slopes approach, and the tighter error distribution of the slopes

method underscores its superior calibration quality and robustness for SA quantification in SML samples.

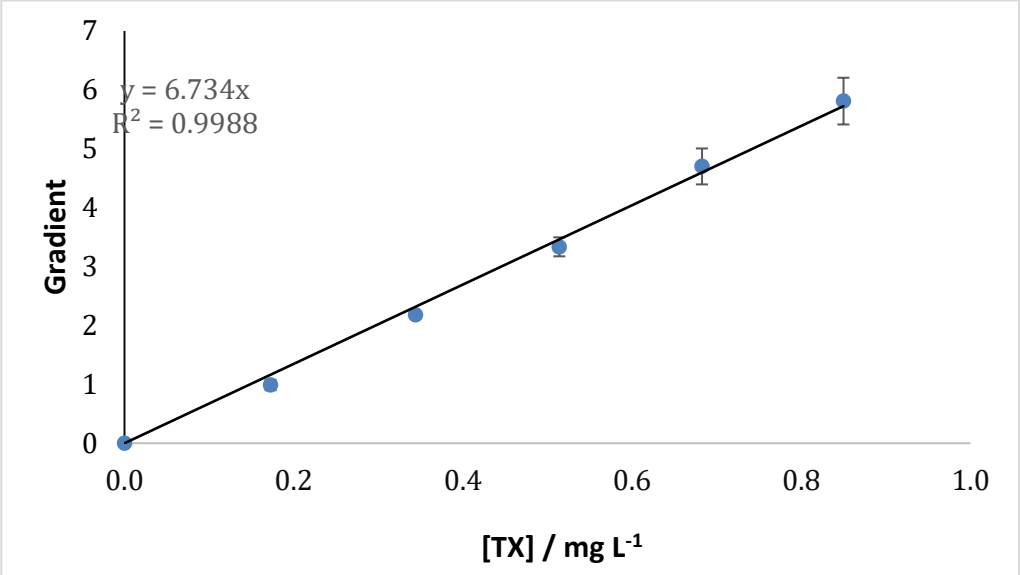

Figure 15: Gradient versus TX-100 concentration from multiple deposition times calibration. The graph shows the linear relationship between the slope of current response (Δi) and concentration of TX-100, with a high R^2 value of 0.9988, indicating excellent linearity and consistency across different concentrations.

Surfactant activity in an unknown SML sample is then determined by the slopes method as follows. Δi is measured at 5, 15, 30, 45, and 60 s; a linear regression of Δi versus time yields the sample slope. Although these deposition times are short compared to the equilibration times observed in surface tension measurements, they reflect the fundamentally different processes probed by AC voltammetry, which quantifies the rapid adsorption kinetics of electroactive surfactants to the mercury electrode under forced transport, rather than the slower establishment of equilibrium at the air–water interface measured by tensiometry. Consequently, the short deposition times are appropriate for voltammetric determination of surfactant activity and do not imply direct equivalence with surface tension equilibration timescales. Using the calibration fit from Figure 14, activity is calculated by

$$SA_{sample} = \frac{m_{sample} - c_{cal}}{m_{cal}} \qquad (13)$$

Finally, the value is corrected for dilution by using Eq. 12 to give the true surfactant activity of the undiluted SML sample.

2.7.2 Comparison Between the Two Voltammetric Methods

The comparison between the two voltammetric methods shows significant variations in reliability and accuracy for determining surfactant activity (SA) in sea surface microlayer (SML) samples, as shown in Table 8. The 15-second deposition approach, although straightforward, showed significant limitations in accuracy, especially when the calibration intercept was not forced through zero, resulting in severe errors, with percentage errors reaching up to 3030%. When the intercept was forced through zero, errors were reduced to a range between 7.4% and 34.5%, but the limitations of depending only on a single-point measurement remained apparent, as any baseline drift, accidental noise, or non-linear adsorption behaviour at that one time point turns into SA error with no additional data for cross-validation. On the other hand, the multiple deposition time (slopes) approach showed better robustness and reliability by taking measurements across numerous deposition times—5s, 15s, 30s, 45s, and 60s. This method consistently yielded lower error rates, even without forcing the intercept, varying between 67.0% and 87.2%. When the calibration intercept was forced through zero, the errors were further reduced to between 10.7% and 26.5%. This method mitigates variability by offering a more nuanced analysis of adsorption dynamics, making it better suited for measuring SA in the SML. However, errors of 10.7 or 26.5 % remain high for trace-level SML analyses, underlining the need for further refinement—such as on-line blank subtraction to correct drift, expanding multi-point calibration series, more replicate scans per deposition, and rigorous HMDE pre-conditioning—to reduce variability and improve SA measurement in the SML.

2.7.3 Importance of Forcing the Intercept to Zero

For both calibration approaches, the importance of forcing the intercept through zero is highlighted by minimising the error. A non-zero intercept shows that baseline factors other

than the analyte are contributing to the determined current. This is specifically problematic for low concentrations, where the baseline can extremely impact the result. By forcing the intercept through zero, these extraneous influences are eliminated, causing improved accuracy, specifically for measurements about the detection limit.

The findings noticeably support the adoption of the multiple deposition time methodology for its greater accuracy and error decline. By combining several data points, this method grants an additional comprehensive understanding of surfactant interactions, indicating more reliable results and a more accurate demonstration of surfactant dynamics in marine environments. This enhancement is critical for improving the consistency and reliability of SML investigations.

Table 8: Comparison of surfactant activity (SA) measured by the 15 s deposition method and the multiple deposition time (slopes) method, showing SA in mg L^{-1} TX-100 eq. and percentage error against calibration standards.

Sample	15s Deposition Time SA (mg L^{-1} TX-100 eq.)		Multiple Deposition Time (Slopes) SA (mg L^{-1} TX-100 eq.)	
	With Intercept	% Error	With Intercept	% Error
	Without Intercept	% Error	Without Intercept	% Error
022_ULW	0.115	3030	0.280	74.6
	0.116	24.6	0.221	10.7
023_ULW	0.231	3030	0.189	78.5
	0.232	24.1	0.123	26.5
023_SML	0.259	3030	0.175	87.2
	0.260	15.8	0.108	46.4
020_SML	0.416	112	0.320	67.0
	0.382	9.58	0.241	20.5
021_SML	0.128	117	0.375	67.0
	0.077	34.5	0.298	19.1
024_SML	0.695	112	0.780	67.0

2.8 Comparative Interpretation of Surface Tension and Surfactant Activity Relationship

Understanding the relationship between surface tension and surfactant activity (SA) in marine environments is complicated by both the diversity of surface-active substances (SAS) and the analytical methods used to detect them. In natural seawater systems, particularly in the sea surface microlayer (SML), this complexity is amplified due to the heterogeneous and dynamic nature of surface-active substances (SAS). Our study investigated this relationship using both tensiometry and alternating current (AC) voltammetry, focusing on the interpretive differences that arise when comparing filtered and unfiltered seawater samples and benchmarking against synthetic and processed standards. Importantly, the comparison between surface tension and surfactant activity presented here is made using equilibrated or near-equilibrated surface tension values obtained under controlled laboratory conditions, and therefore reflects a method-dependent relationship that may vary with equilibration time and SAS composition rather than an instantaneous in situ response of the SML

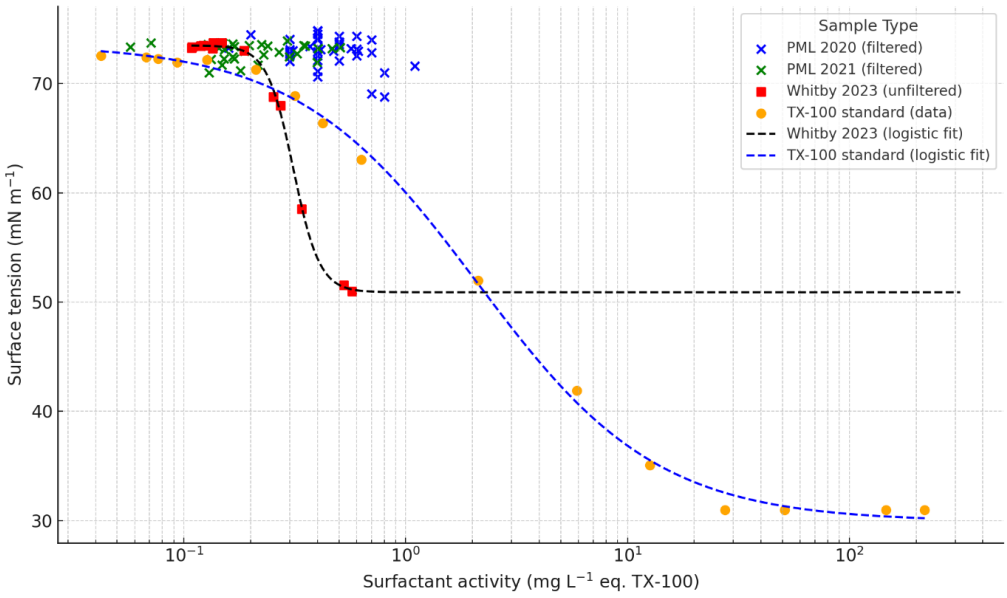

Figure 16. Surface tension versus surfactant activity (SA) in marine and reference samples, including filtered Plymouth SML (2020–2021), unfiltered Whitby SML (2023), and a TX-100 standard. Logistic fits illustrate sigmoidal trends for the Whitby and TX-100 datasets. Surface tension values represent equilibrated or near-equilibrated measurements meeting the defined stability criterion, and SA is expressed as mg L^{-1} TX-100 equivalents on a logarithmic x-axis.

Unfiltered SML samples collected from Whitby in spring 2023 exhibited a well-defined sigmoidal decrease in surface tension with increasing SA—from ~73.7 to 51.0 mN m^{-1}—over a concentration range of 0.11 to 0.57 mg L^{-1} TX-100 equivalents (Figure 16). These values are consistent with prior field measurements of marine SMLs: Cosović et al. (1982) reported 0.32–0.64 mg L^{-1} in the Adriatic Sea, Sabbaghzadeh et al. (2017) found 0.34–0.47 mg L^{-1} in the Atlantic Ocean, and Wurl et al. (2011) observed means of ~0.62 mg L^{-1} in nearshore waters. The sigmoidal shape of the surface tension response is characteristic of increasing interfacial saturation and reflects the progressive accumulation of amphiphiles at the air–water boundary.

For contextual comparison, we evaluated TX-100, a synthetic nonionic surfactant, which produced a comparable sigmoidal isotherm but at higher concentrations, with surface tension decreasing from ~72.5 to 31.0 mN m^{-1} across 0.04 to 220 mg L^{-1}. Notably, the onset of surface tension suppression occurred earlier in Whitby samples (~0.31 mg L^{-1}) than in TX-100 standards (~1–2 mg L^{-1}), suggesting that natural SML surfactants are more efficient at reducing surface tension on a per-mass basis. This enhanced efficiency likely stems from the structural diversity of natural SAS—such as fatty acids, glycolipids, and microbial exudates—which may interact synergistically and possess stronger interfacial affinities than TX-100.

This variance, shown clearly by the logistic fits in Figure 16, highlights the influence of sample composition and underscores limitations in interpreting voltammetric SA as a proxy for interfacial behaviour. While voltammetric SA is expressed in TX-100 equivalents, this equivalency reflects adsorption at the electrode, not at the air–water interface. Natural surfactants such as fatty acids, glycolipids, and microbial exudates may differ from TX-100 in structure and interfacial affinity, and mixtures may exhibit synergistic effects that enhance surface tension suppression. These effects likely account for the earlier and steeper decline observed in the Whitby data. Importantly, when plotted against $\log_{10}$-transformed SA, the

unfiltered Whitby surface-tension data align along a straight line (Figure 17). This transformation is justified by our logistic model (Eqn 2), which enters concentration through an exponential term (where C is the surfactant concentration and C_inf is the inflection concentration at the midpoint of the sigmoidal transition). Over the intermediate concentration range around C_inf, the logistic curve behaves approximately linearly with $\log_{10}$ C, such that taking $\log_{10}$(SA) both stabilises variance and facilitates comparison with a linear approximation. Accordingly, linear regression is used here as a descriptive tool to quantify the strength of association rather than as a mechanistic model. The resulting Pearson correlation of –0.943 ($p = 1.3 \times 10^{-6}$) confirms that voltammetric SA and tensiometric σ track each other closely when native, interfacially active compounds dominate.

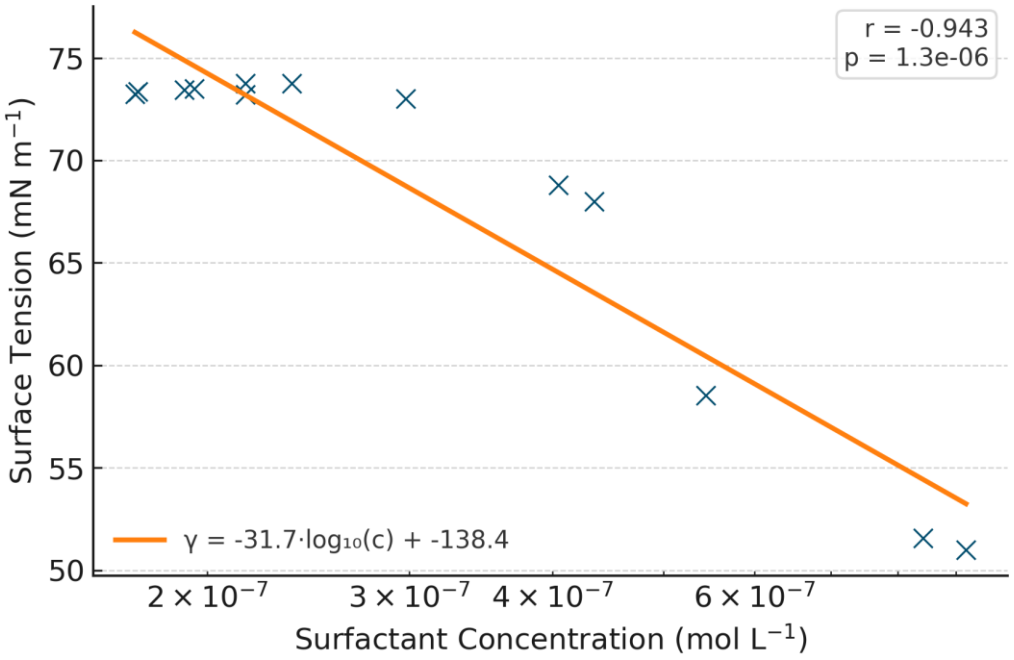

Figure 17: Scatter plot of natural SML surface tension versus surfactant concentration on a $\log_{10}$ scale. Blue crosses show experimental data; the orange line represents a linear regression used to illustrate the strength of the correlation, while the underlying relationship is better described by a sigmoidal (logistic) response.

In contrast, filtered SML samples collected from Plymouth between 2020 and 2021 demonstrated a pronounced disconnect between SA and surface tension. As shown in Figure 16, surface tension remained consistently above 72 mN m^{-1} despite SA values reaching up

to 1.1 mg L^{-1} (see also Figure 18). This discrepancy highlights the limitation of voltammetry as a proxy for interfacial behaviour in filtered or nearshore samples, where electroactive but non-amphiphilic compounds—often introduced through wastewater or urban runoff—may be over-represented in nearshore environments like Plymouth. Filtration likely removed larger biogenic surfactants, including exopolymeric substances (EPS), proteinaceous gels, and colloidal surfactants—components known to strongly reduce surface tension but often weakly detected electrochemically. Their absence in the Plymouth samples helps explain the flat surface tension response, despite high SA values. It is important to note that these Plymouth samples are not directly comparable to the unfiltered North Sea (Whitby) SML dataset or the processed samples analysed by Frossard et al. (2019). These results provide a strictly technical comparison of tensiometric and voltammetric responses on filtered SML samples and are not intended for environmental interpretation. Further supporting this interpretation, over a 20-month time series, the surface tension of filtered Plymouth samples remained steady at 73.07 ± 0.53 mN m^{-1}, with brief dips to ~71.0 mN m^{-1} in mid-2020 and summer 2021. In contrast, surfactant activity (again of filtered seawater) averaged 0.31 ± 0.17 mg L^{-1} eq. TX-100 but showed episodic spikes, particularly in spring as shown in Figure 18.

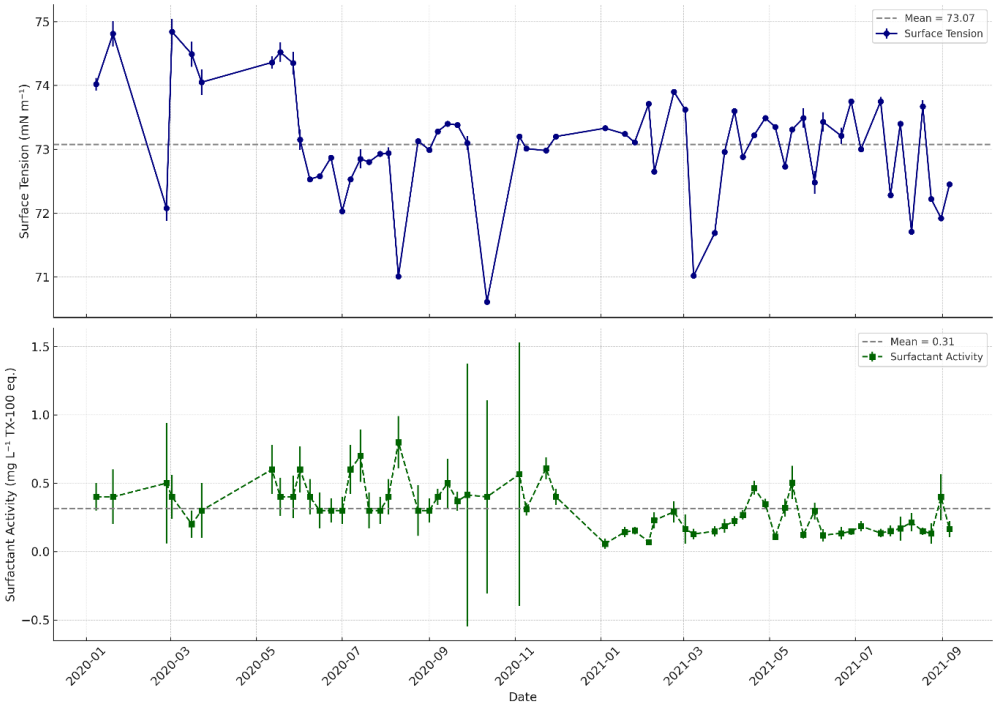

Figure 18: Time series of surface tension and surfactant activity (SA) in filtered SML samples from Plymouth (January 2020–September 2021). Surface tension (top) and surfactant activity (bottom) are shown with mean values indicated by dashed lines (73.07 mN m^{-1} and 0.31 mg L^{-1} TX-100 equivalents, respectively). Error bars represent standard deviations. The data highlight modest fluctuations in surface tension and episodic increases in surfactant activity over the study period.

Regression analysis further emphasised this difference: Figure 19 illustrates the relationship between voltammetric surfactant activity (SA, in mg L^{-1} TX-100 equivalents) and tensiometric surface tension for filtered SML samples in 2020 and 2021. In the 2020 panel, the linear fit ($y = -0.88\ x + 73.43$) yields $R^2 \approx 0.00$ ($p = 0.761$), indicating no significant trend: surface tension remains clustered around 72–74 mN m^{-1} regardless of SA within this range. Similarly, the 2021 data show a nearly flat regression ($y = 0.04\ x + 72.97$; $R^2 \approx 0.00$, $p = 0.975$) with overlapping tension values across SA. The absence of any meaningful slope in both years confirms that, under filtered conditions where colloidal and high-molecular-weight surfactants are removed, voltammetric SA does not scale linearly with interfacial tension within the typical concentration window. These results underscore that voltammetric SA reflects adsorption at a mercury electrode rather than at the air–water interface. Therefore, it cannot be assumed to scale linearly with interfacial activity—particularly in filtered samples lacking natural colloidal surfactants.

Furthermore, the low concentrations of dissolved surfactants in these filtered SML samples and the limited sensitivity of tensiometric methods likely contribute to the observed decoupling since, at such low SA levels, the expected decrease in surface tension may be smaller than the instrument's resolution. Consequently, even when voltammetry detects measurable electroactive species, tensiometry may not register a significant change in interfacial tension if the surfactant loading is near or below its detection threshold. This limitation underscores the importance of considering both analytical sensitivity and sample concentration when interpreting the absence of a linear relationship between SA and surface tension in filtered samples.

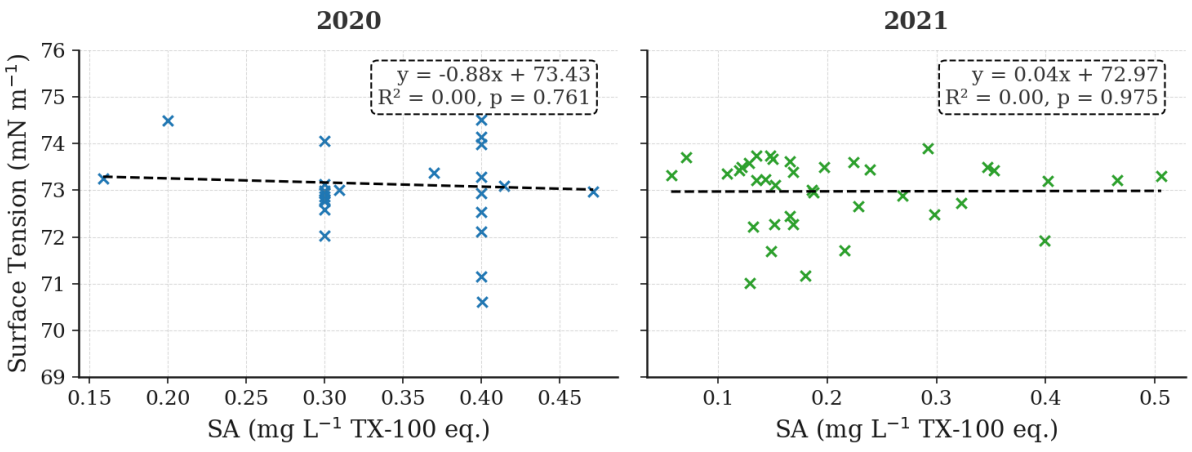

Figure 19: Surface tension vs. voltammetric SA (mg L^{-1} TX-100 eq.) for filtered SML samples: 2020 (left) 2020 data: y = –0.88x + 73.43 (R^2 = 0.00, p = 0.761), indicating no significant linear trend. Also 2021 (right) shows no meaningful relationship y = 0.04x + 72.97 (R^2 = 0.00, p = 0.975). Dashed boxes display the regression equation and coefficient of determination for each panel.

Taken together, these results emphasise that tensiometry and voltammetry assess complementary but non-identical facets of surfactant behaviour. Tensiometric measurements reflect the compounds' interfacial accumulation and disruption of water cohesion, whereas AC voltammetry probes electrochemical interactions at the mercury electrode. The absence of a detectable SA–tension relationship in both years under filtered conditions likely arises from the limited sensitivity of tensiometry at low surfactant levels

and the reduced surfactant concentrations observed. Importantly, when contrasted with the untreated natural SML samples, this analysis highlights how filtration removes key surface-active macromolecules that are critical to interfacial behaviour—underscoring that only native SML samples faithfully represent real marine conditions. These findings highlight the importance of refining protocols for SML sampling and filtration. They also provide a framework for interpreting SML surfactant dynamics in large-scale monitoring or process studies, especially when correlating chemical properties with oceanographic or meteorological variables.

To enable direct comparison with the processed datasets reported by Frossard et al. (2019), the concentrations of both natural SML and TX-100 surfactants were converted from mg L^{-1} TX-100 equivalents to mol L^{-1}. This standardisation was necessary because Frossard's data were reported exclusively in molar units. All processed seawater samples (Stations 4, 1, and 4B) came from biologically productive water masses and were 0.45 μm-filtered and subjected to C18 SPE (500 mg/3 mL) with acetonitrile elution, N_2 drying, and reconstitution in 40 μL Milli-Q water; surfactants were quantified by class-specific ionic-dye UV–Vis assays. Surface-tension isotherms—measured by pendant-drop tensiometry at 20.2 ± 1.0°C over 1–10 min (equilibrium assured, no evaporation), with each bulk seawater sample replicated 3 times.

The comparison of surface tension isotherms is shown in Figure 20. Natural SML exhibits an exceptionally low CMC (4.4×10^{-7} mol L^{-1}) and high plateau tension (50.9 mN m^{-1}), indicative of a densely packed monolayer of high-molecular-weight amphiphiles that resist further compression. In contrast, processed seawater extracts show CMCs of 3.2×10^{-5} to 1.6×10^{-4} mol L^{-1} and plateau tensions of 30–37 mN m^{-1}, reflecting the selective loss or dilution of trace, highly surface-active constituents during 0.45 μm filtration and C18 SPE. The steep pre-CMC slope in natural SML implies that only nanomolar concentrations suffice for interfacial saturation, whereas processed samples require concentrations two to three

orders of magnitude higher. Spatial trends among Stations 4, 1 and 4B further underscore the influence of water-mass age: Station 4B's highest CMC corresponds to freshly upwelled organics, while Station 1's lower CMC suggests accumulation of more surface-active degradation products. These contrasts demonstrate that filtration and SPE bias against the very macromolecules that dominate interfacial behaviour in untreated SML (Figures 20, Table 9). Consequently, laboratory proxies based on processed extracts risk underestimating the role of native amphiphiles in modulating surface tension and bubble-burst dynamics. Incorporating unprocessed SML—or synthetic mixtures that replicate its steep isotherm characteristics—is therefore essential for accurate modelling of air–sea exchange.

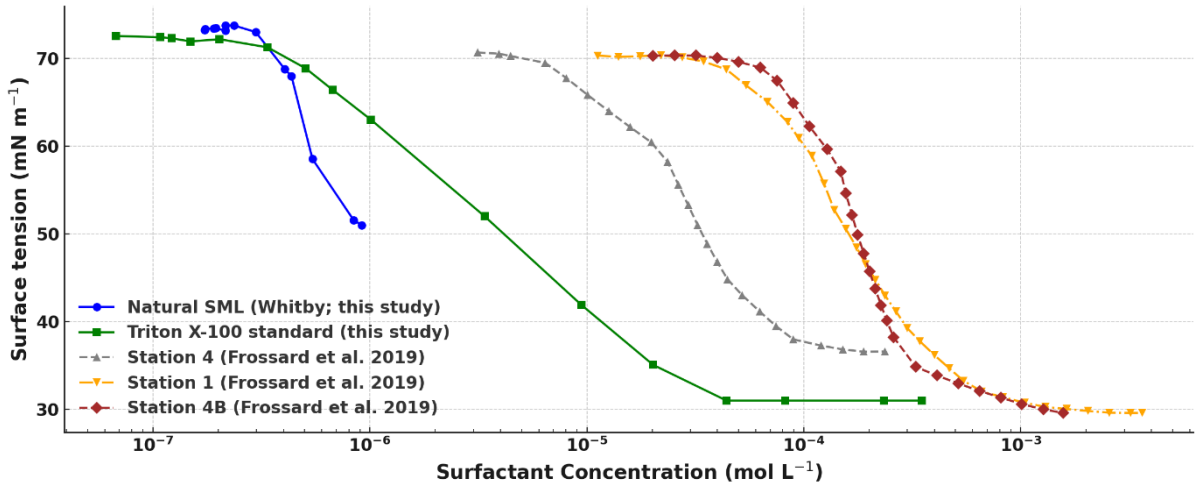

Figure 20: Surface-tension isotherms for natural SML (solid blue circles), Triton X-100 standard (solid green squares), and processed seawater extracts from Stations 4 (grey dotted triangles), 1 (orange dash-dot triangles) and 4B (brown diamonds; Frossard et al. 2019). Natural SML exhibits the lowest CMC (4.4×10^{-7} M) and the highest residual tension ($\sigma\infty \approx 50.9$ mN m^{-1}), whereas the processed samples and TX-100 require two to three orders of magnitude higher concentrations to reach their plateau tensions (30–37 mN m^{-1}), reflecting the selective loss or dilution of highly surface-active components during filtration and SPE. All isotherms represent equilibrium surface tension behaviour measured under controlled laboratory conditions.

Table 9: CMC and plateau surface tension (σ∞) for natural SML, processed seawater samples, and TX-100. Natural SML shows the lowest CMC and highest σ∞, indicating superior surface activity.

Series	CMC (mol L^{-1})	Plateau (mN m^{-1})
Natural SML	4.4×10^{-7}	51
Station-4	3.2×10^{-5}	37
Station-1	5.0×10^{-5}	30
Station-4B	1.6×10^{-4}	30
TX-100	3.7×10^{-5}	31

In conclusion, these findings confirm that tensiometry and voltammetry assess related but non-identical properties of the surfactant pool. This study demonstrates the utility of combining tensiometric and voltammetric techniques to characterise surfactant activity in the sea surface microlayer. Tensiometry provides a comprehensive measure of interfacial behaviour, while voltammetry offers specificity for electroactive components. The alignment observed in unfiltered samples confirms that both methods are complementary when surface-active substances are present in their native state. Conversely, the lack of correlation in filtered samples underscores the limitations of relying solely on electrochemical detection, particularly where high-molecular-weight or colloidal surfactants have been removed. These findings emphasise the importance of preserving native SML composition and adopting integrated analytical approaches in future studies of ocean–atmosphere exchange and marine biogeochemistry. It is also important to recognise that the surface tension values discussed here reflect equilibrium or near-equilibrium conditions achieved under controlled laboratory settings. While such conditions enhance the detectability and comparability of surfactant signals, they do not fully capture the continuously forced nature of the in situ sea surface. Accordingly, the relationships identified in this study should be interpreted as defining the potential influence of native surfactants on

interfacial properties, rather than their instantaneous expression under dynamic marine conditions.

2.9. Developing a Storage Test Protocol

2.9.1 Comparative Analysis of Storage Techniques

Initially, the SML samples were collected and preserved in an ice-filled cork box to maintain ambient temperatures until the first surface tension analyses (T0) could be conducted. Subsequently, two distinct methodologies were employed for freezing the samples: a controlled cooling method using gradual freezing containers before storage at −80°C and a rapid freezing method without any controlled cooling mechanism. These were selected to evaluate how freezing conditions influence the stability of SAS and to determine the optimal protocol for maintaining sample integrity over time.

The controlled cooling process (at approximately −1°C per minute) was designed to minimise ice crystal formation and structural damage to surfactants, potentially preserving the original characteristics of the samples. This approach, commonly used in biological preservation, may benefit SML studies by reducing surfactant alteration during freezing and thawing (Chang & Kendrick, 1996; Matsubara et al., 2024). In contrast, the rapid freezing method involved placing SML samples directly into a −80°C freezer without using a gradual cooling device. This offered a practical, resource-efficient approach but raised concerns over uncontrolled ice formation and potential degradation of surfactants (Esmaeili et al., 2021; Kim et al., 2007). A rapid temperature drop can facilitate the growth of large ice crystals, which may physically disrupt surfactant assemblies. This risk is particularly relevant for nonionic surfactants, which are prone to phase separation or aggregation under certain freezing conditions (Garti et al., 1996; Chen and Wang, 2007; Pot et al., 2015). A third condition—storage at 4°C—was included to assess stability under refrigeration, commonly used for short-term storage but potentially problematic due to microbial activity and

chemical degradation (Tokiwa et al., 2018). This comparative design aimed to identify the most reliable method for preserving SML samples and SAS stability, with a focus on surface tension as the primary metric. The results below explore how each condition affects interfacial behaviour, including the role of container size. These findings have important implications for developing standardised protocols that ensure reliable and consistent analysis of the SML, particularly in the context of long-term marine research expeditions.

2.9.2 Gradual Freezing: Performance and Limitations

The controlled freezing process, using specially designed 5 mL vials, aimed to minimise intracellular ice formation, reduce potential structural damage to surfactants and maintain molecular integrity in biological systems, thereby preserving the original characteristics of the samples (Whaley et al., 2021; Hunt, 2017). However, surface-tension measurements showed notable variability, likely due to surfactant adsorption onto the container walls: two vials tested on the same day produced markedly different results. Although this method is commonly employed in biological contexts (Chang & Kendrick, 1996; Matsubara et al., 2024), these findings suggest it may not reliably preserve interfacial properties in small-volume SML samples. As shown in Figure 21, it became clear that Replicate 1 (R1) and Replicate 2 (R2) do not track identically, deviating from the same-day T_0 baseline (~ 67.47 mN m^{-1}) at multiple time points. By Day 1, R2 has risen sharply to 70.88 mN m^{-1} while R1 remains at 67.44 mN m^{-1}. Subsequent time points show R1 sometimes above and sometimes below R2, e.g., Day 2 (R1 = 72.10 vs R2 = 67.33) and Day 3 (R1 = 69.98 vs R2 = 67.33). By Day 25, R1 is 67.53 mN m^{-1} while R2 sits at 72.01 mN m^{-1}—a full 4 mN m^{-1} divergence. These consistent deviations suggest initial surfactant loss followed by limited interfacial re-equilibration. While controlled freezing effectively pauses biochemical degradation, physical interactions with container surfaces can significantly influence SAS retention.

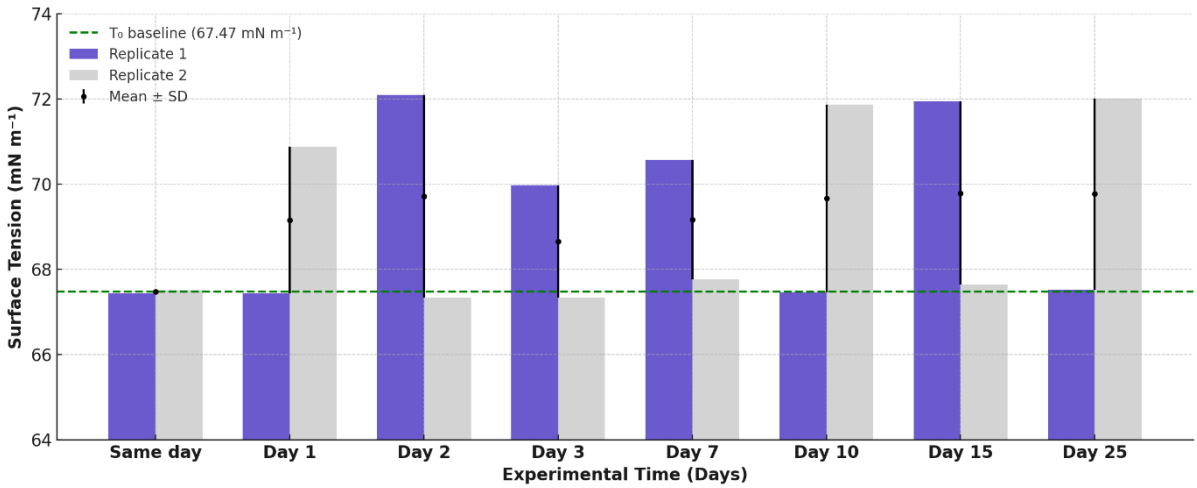

Figure 21: Surface tension in two replicate 5 mL vials over 25 days under Mr. Frosty gradual freezing. Slate-blue bars (Replicate 1) and light-grey bars (Replicate 2) show individual measurements; black markers ± whiskers indicate the mean ± SD; the dashed green line marks the T_0 baseline (67.47 mN m^{-1}). The y-axis spans 64–74 mN m^{-1}. Divergence between replicates at Day 1, Day 7, Day 15 and Day 25 reveals vial-specific surfactant adsorption and interfacial instability.

The pronounced divergence between replicates on the same day cannot be attributed to heterogeneity in sample composition or cooling rate—both vials underwent identical freezing conditions—but rather to adsorption of amphiphilic molecules onto the high surface-area vial walls. Similar behaviour has been reported in pharmaceutical formulations, where small-volume containers promote significant protein and surfactant adsorption (Rathore & Rajan, 2008; Kiran et al., 2011), removing amphiphilic material from the interface, reducing interfacial coverage and elevating surface tension.

These observations underscore that, although controlled freezing may halt chemical degradation, it does not inherently preserve interfacial SAS in small volumes. Container geometry, material and surface chemistry must therefore be treated as critical design parameters in SML sample storage—larger, low-adsorption vessels or surface-passivation treatments may be required to maintain interfacial stability. Future storage protocols should explicitly optimise both the freezing regime and container characteristics to ensure reproducible surface-tension measurements in SML studies.

2.9.3 Rapid Freezing: Interfacial Stability and Preservation

The rapid freezing protocol used 60 mL containers placed directly into a −80°C freezer. Surface tension measurements remained stable around 62 mN m^{-1} over 60 days, with <2% fluctuation—indicating strong preservation of interfacial activity (Figure 22).

This stability may be partly attributed to the use of larger containers, which presented a lower surface-area-to-volume ratio compared to smaller vials, thereby reducing surfactant loss through wall adsorption. Additionally, larger containers may help buffer thermal gradients during freezing and reduce localised concentration effects that can destabilise surfactant assemblies, contributing to overall interfacial stability (Cheng et al., 2004; Franks, 1985). Although rapid freezing is typically associated with the risk of ice crystal formation, which can disrupt surfactant assemblies, no evidence of such degradation was observed in this study. Prior work suggests that systems with structured surfactant matrices can tolerate sudden freezing when protected from thawing and physical agitation (Morales et al., 2022; Minatovicz et al., 2023).

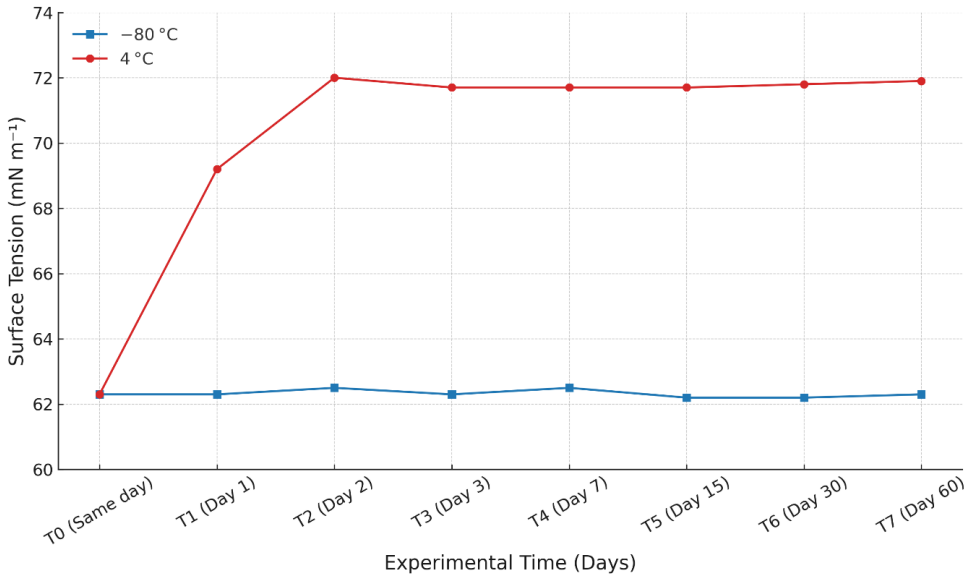

Figure 22: Surface tension of SML samples over 60 days stored at 4°C and -80°C. Samples at 4°C show an initial rise, stabilizing around 72 mN m^{-1}, while samples at -80°C remain stable near (within 2% of) the starting value of 62 mN m^{-1}.

This stability may be partly attributed to the use of larger containers, which presented a lower surface-area-to-volume ratio compared to smaller vials, thereby reducing surfactant loss through wall adsorption. Additionally, larger containers may help buffer thermal gradients during freezing and reduce localised concentration effects that can destabilise surfactant assemblies, contributing to overall interfacial stability (Cheng et al., 2004; Franks, 1985). Although rapid freezing is typically associated with the risk of ice crystal formation, which can disrupt surfactant assemblies, no evidence of such degradation was observed in this study. Prior work suggests that systems with structured surfactant matrices can tolerate sudden freezing when protected from thawing and physical agitation (Morales et al., 2022; Minatovicz et al., 2023).

When compared with refrigeration at 4°C, the advantage of rapid freezing becomes even clearer. Surface tension measurements diverged significantly between the two conditions. Initially identical (~62 mN m^{-1}), 4°C samples increased to ~71 mN m^{-1} by Day 2, stabilising at values characteristic of clean seawater as illustrated in Figure 22. This shift reflects degradation of surface-active substances and loss of interfacial activity.

2.9.4 Integrating Findings from Surface Tension and Voltammetric Analyses: Current Work vs. Salter (2010)

These findings were qualitatively compared with the results of Salter (2010), who investigated surfactant degradation under several storage conditions using voltammetric analysis of SML samples from the River Tyne estuary. Salter observed that, at 5 °C, filtered samples exhibited a moderate decline in surfactant activity, whereas unfiltered, untreated samples suffered a severe loss. Filtration provided only partial protection, and $HgCl_2$ preservation afforded some improvement, yet neither approach matched the stabilisation achieved by –80 °C storage. Despite using different analytical approaches (voltammetry versus surface tension), both studies reveal the same pattern: refrigeration degrades interfacial-active compounds, while deep freezing preserves them, as shown in Figure 23.

An alternative representation would be to plot the change in surface tension relative to the −80 °C samples, which act as a stable baseline; however, the absolute presentation retained here allows direct comparison with published datasets and highlights both the magnitude and direction of storage-induced drift.

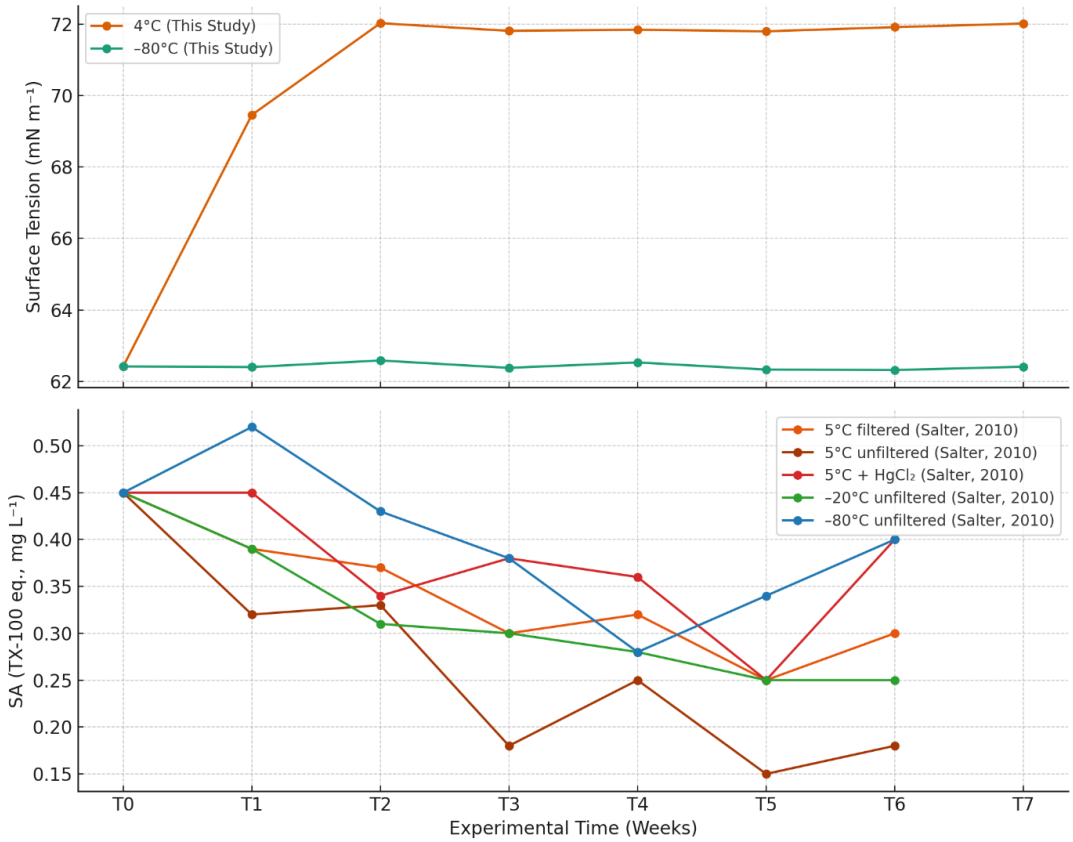

Figure 23: Temporal evolution of surfactant-related properties in sea surface microlayer (SML) samples stored under various conditions. (A) Surface tension (mN m^{-1}) of unfiltered samples from this study. (B) Surfactant activity (TX-100 eq., mg L^{-1}) from Salter (2010).

It is important to recognise that the two analytical methods used capture different fractions of the surfactant pool. Voltammetry selectively detects electroactive surfactants, such as Triton X-100 analogues, that adsorb to a mercury electrode surface. In contrast, surface tension provides a holistic measure of interfacial activity, encompassing all surface-active substances, including non-electroactive biogenic colloids and high-molecular-weight polymers (Zhou et al., 1998). In addition, the two sampling sites differ substantially in their environmental context. The Whitby samples originated from a biologically productive shelf region, whereas Salter's estuarine samples from the River Tyne are more likely to reflect

terrestrial and anthropogenic inputs. These differences in location and matrix likely influence the molecular composition, degradation pathways, and overall reactivity of the SAS assemblages observed (Cunliffe et al., 2013). Although direct numerical comparison between voltammetry and surface tension is not appropriate due to their differing sensitivities and detection scales, the alignment of qualitative trends across both datasets underscores storage temperature as the critical factor in preserving surfactant activity in natural marine samples. This consistency not only reinforces the validity of our surface-tension–based protocol for long-term SML stability assessments but also supports its broader adoption—particularly when −80 °C storage is employed—to ensure the integrity of surface-active material in future research.

In conclusion, this study demonstrated that −80 °C deep freezing, particularly in large, low-adsorption containers, offers the most reliable strategy for preserving surface-active substances (SAS) in sea surface microlayer (SML) samples. While voltammetry provides higher sensitivity for specific electroactive compounds, surface tension proved to be a robust and integrative indicator of overall interfacial activity in unfiltered marine samples. This protocol addresses a critical gap in marine surface research by offering a validated, practical solution for long-term storage in field-based or time-delayed analytical contexts. The consistent trends observed across methods confirm storage temperature as the principal determinant of SAS integrity.

2.10 Conclusion

This study demonstrated that reliable characterisation of surface-active substances (SAS) in the sea surface microlayer (SML) depends critically on both analytical method and storage protocol. Using a combined approach—tensiometry to assess total interfacial behaviour, and voltammetry to quantify electroactive components—we evaluated how SAS integrity is preserved or degraded under different conditions.

Surface tension measurements proved highly sensitive to cumulative interfacial effects, while voltammetric analysis offered specificity for electroactive species, particularly when employing the multiple deposition-time calibration method. This approach significantly improved analytical precision and reduced systematic error relative to the conventional 15-second method, enabling a more robust quantification of surfactant activity (SA).

Among storage conditions tested, deep-freezing at −80 °C in large-volume, low-adsorption containers most effectively preserved surface-active properties. In contrast, refrigeration at 4 °C resulted in rapid degradation, reflected by elevated surface tension values. The use of Mr Frosty for gradual freezing, though effective in biological systems, exhibited increased variability in small vials likely due to surfactant adsorption to container walls.

Critically, the study showed that filtration and chemical preservatives failed to match the preservation performance of freezing. Unfiltered, untreated SML samples frozen at −80 °C maintained interfacial properties over time, reinforcing the importance of maintaining native sample composition.

Together, these findings confirm that tensiometry and voltammetry probe complementary but non-identical facets of the surfactant pool, and that only unaltered, native SML samples enable reliable interpretation of air–sea interfacial dynamics. They also offer a validated protocol for sample preservation and a framework for interpreting SML surfactant variability across environmental gradients. Overall, this work advances our understanding of the physical and chemical dynamics at the air–sea interface and affirms the importance of integrated approaches in SML research.

Chapter 3: Surface tension of the ocean and its relationship with environmental variables

3.1 Preface to the Chapter

This chapter investigates seasonal variability in sea surface microlayer (SML) film coverage (Δσ) within a temperate coastal system in the western English Channel. Weekly measurements of unfiltered SML and underlying waters (November 2019–September 2021) are used to quantify surface-tension dynamics and evaluate their relationship with temperature, phytoplankton biomass, and nutrient variability.

By integrating surface-tension data with biogeochemical observations, this chapter examines the biological and physical controls governing surfactant film formation in a productive coastal environment and establishes a baseline for comparison with open-ocean conditions.

3.2 Objectives

1. Derive a high-resolution two-year time series of Δσ from paired SML and underlying water tensiometry.

2. Characterise the seasonal and temporal variability of Δσ in a temperate coastal environment.

3. Evaluate the relationship between Δσ and potential physical, chemical, and biological drivers, including sea surface temperature, phytoplankton biomass, chlorophyll-a, dissolved inorganic nitrogen (nitrate and ammonium), dissolved organic carbon, selected fatty acids, wind speed, and river discharge.

4. Apply correlation and multivariate regression analyses to determine the relative importance of these variables in regulating surfactant film formation.

Through these objectives, the chapter examines the integrated controls governing SML surfactant films in temperate coastal waters.

3.3. Methods

3.3.1 Sample locations

Sampling followed the detailed protocol described in Chapter 2, Section 2.3.2, with campaign-specific variations as noted below:

Plymouth Marine Laboratory (PML) Campaign

The English Channel samples were collected between November 2019 and September 2021 onboard the RV Plymouth Quest, at locations plotted in Figure 6 (50° 19′ 12″ N, 4° 10′ 12″ W to 50° 18′ 32.4″ N, 4° 11′ 27.6″ W). Collections occurred approximately once per week for 76 weeks, primarily ~0.5 km offshore of Rame Head, Cornwall. Samples were collected by the PML team, and either analysed at the PMl laboratories (unfiltered ST analysis) of filtered (0.7 um GF/F), frozen at -20^{o}C and retruned to the University of York for analysis.

3.3.2 Surface Tension Measurements

Surface tension measurements were carried out using the Kibron EZ Plus tensiometer equipped with a platinum Wilhelmy plate and a thermocouple, following the cleaning, equilibration, and calibration procedures described in Chapter 2, Section 2.5. Instrument accuracy (±0.1 mN m^{-1}) and precision (±0.05 mN m^{-1}) are as specified by the manufacturer. Screen specifications, rinsing procedures, and microlayer-thickness calculations are as detailed in Chapter 2, Sections 2.4. Analysis of unfiltered samples collected during the PPAO campaign were analsyed within 4 hours of collection in the PML Laboratories; analysis was conducted by R. May, PML technician. CONNECT samples were defrosted and analysed at the University of York within 2 months of collection.

Brief Procedure

The small glass sample vessel (~3 mL) was rinsed with Milli-Q water and ethanol, soaked in 4% HCl for 5 minutes, then rinsed again with Milli-Q and oven-dried at 120 °C. After cooling under compressed nitrogen, samples were poured into the vessel and equilibrated for at least 5 minutes with a thermocouple. Before each run, the platinum Wilhelmy plate was rinsed with Milli-Q water, flame-sterilised for a few seconds, and mounted in the tensiometer. All cleaning, rinsing, and Garrett-screen handling steps follow Chapter 2, Section 2.5.1.

3.3.3 Surfactant Activity Measurements

Surfactant activity was quantified using AC voltammetry with a Metrohm 663 VA Stand and an IME623 Autolab potentiostat/galvanostat. The system employed a hanging mercury drop electrode (HMDE), a saturated Ag/AgCl reference electrode, and a platinum auxiliary electrode. A deposition potential of –0.6 V was applied while stirring the sample, allowing surface-active material to adsorb onto the HMDE. The resulting change in capacitance current (CCi) was used to assess surfactant concentrations. Measurements used both a standard 15-second deposition and a multiple deposition time approach (5–60 s) for improved precision. Calibration was performed with TX-100, and blanks were run with Milli-Q water. Full procedural details are described in Chapter 2, Section 2.7.

3.3.4 Ancillary Biogeochemical Measurements

3.3.4.1 Dissolved Organic Carbon Analysis

Throughout both the coastal and open ocean campaigns, small portions of filtered (GF/F) samples were preserved by freezing them at a temperature of -20 ºC. These samples were then analysed by Katherine Weddell at the University of York to determine the dissolved organic carbon (DOC) amount. In this analysis, 9 mL of the sample, ultrapure water blank, or standard was put into a 12 mL glass vial that had been washed with acid. The vial was then covered with tin foil. Each vial was treated with a 10% HCl solution to remove any

inorganic carbon and then assessed using an Elementar Vario TOC cube instrument. The standards were made by diluting a commercial TOC standard (TOC standard 50 mg L^{-1}, 76319 – 250ML – F, Supelco) with ultrapure water (MQ). For the CONNECT campaign, DOC analyses were conducted by Anja Engel

3.3.4.2 Chlorophyll-a Analysis and Phytoplankton Biomass Estimation

During the coastal time-series campaign, water samples were collected and filtered using a 47 mm diameter GF/F filter paper to determine the concentration of chlorophyll-a. The volume of water filtered ranged from 0.1 to 1 L. The remaining substance was obtained by employing 90% acetone for extraction, and the concentration of chlorophyll-a was determined by fluorescence measurement using a Turner Trilogy fluorometer. Chlorophyll-a measurements were conducted by R. May and O. Jones at PML. Phytoplankton biomass was estimated by Matthew Jones (University of York) using data from L4 provided by Claire Widdicombe (PML). For the CONNECT campaign, chlorophyll-a concentrations, including measurements were determined by Rüdiger Röttgers (Hereon Institute). Total phytoplankton cell counts (cells/mL) were collected onboard by Sandra Golde and Tania Klüver, analysed by Klüver, and provided by Anja Engel.

3.3.4.3 Fatty Acid and Nutrient Analysis

Fatty acid analysis was carried out by Katherine Weddell. Throughout both the coastal (PML) and CONNECT campaigns, seawater samples were filtered through an inline 0.7 µm GF/F filter and either processed immediately or defrosted (where previously frozen at –20 °C). In this analysis, 2 L of each filtered sample—acidified to pH 2 with 37 % HCl—was percolated through Agilent Bond Elut PPL cartridges (500 mg sorbent, 6 mL) at ≤ 10 mL min^{-1} under gentle vacuum. Cartridges were pre-conditioned with three headspaces of Optima LC/MS-grade methanol, then rinsed with three headspaces of 0.01 M HCl, dried under vacuum for 5 min, and eluted with 8 mL methanol into ashed glass vials. Eluates were capped, sealed with Parafilm, and stored at –20 °C until derivatisation.

For GC-MS analysis, each 8 mL methanol extract received 50 µL methyl nonadecanoate internal standard (0.1 mg mL^{-1}), 0.103 mL concentrated H_2SO_4 (95–97 %), and 4 mL hexane. Vials were flushed with N_2, sealed, and heated gently until solvent reflux persisted for 2 h. After cooling, acidity was neutralized by sequential additions of 1 mL hexane and 2 mL distilled water, with aqueous phases removed by pipette (three times). The combined hexane layers were centrifuged, dried under N_2, and re-dissolved in 100 µL hexane.

Samples were analysed on an Agilent 6850 GC coupled to a 5975C MSD (EI mode): 1 µL injections (5:1 split) at 250 °C inlet temperature; He carrier flow of 1 mL min^{-1}; oven held at 50 °C for 2 min, ramped to 140 °C at 10 °C min^{-1}, to 220 °C at 3 °C min^{-1}, then to 260 °C at 30 °C min^{-1} (6 min hold). A full mass scan (m/z 50–500) was followed by SIM at m/z 55, 67, 69, 74, 79, 81, 87, and 93 (50 ms dwell). Data were processed using Agilent MassHunter and the NIST spectral library, with external calibration against authentic standards where available.; Full details and method development are described in Weddell (2023). Nutrient concentrations were determined by Malcolm Woodward at PML. Nitrate (NO_3^-) and phosphate (PO_4^{3-}) concentrations during the CONNECT campaign were measured and provided by Hermann Bange (GEOMAR).

3.4 Results and Discussion

3.4.1 Seasonal and Spatial Dynamics of Surface Microlayer Properties

This section investigates the variability of surface tension (ST) and surfactant activity (SA) in the surface microlayer (SML) and underlying water (ULW) across temporal (seasonal) and spatial (coastal vs. open ocean) gradients. Enrichment factors (EFs) were calculated to quantify the relative concentration of surface-active substances at the air-sea interface.

Surface tension measurements reveal marked spatial contrasts between the coastal English Channel (Nov 2019–Sep 2021) and the open ocean (CONNECT campaign, Dec 2021–Jan 2022). The open ocean exhibited higher and more stable SML surface tension (mean: 72.34

mN m^{-1}; range: 68.53–73.3 mN m^{-1}). In contrast, English Channel SML values were lower and more variable (mean: 70.09 mN m^{-1}; range: 59.4–73.99 mN m^{-1}), indicating greater influence from surfactant-active substances. Similarly, film coverage variability (Δσ) was broader in the coastal zone (0.46–15.14 mN m^{-1}) than in the open ocean (0.09–4.78 mN m^{-1}), reinforcing the idea of a more variable and surfactant-rich environment nearshore (Figure 24, upper panels, Table 11).

This spatial distinction is further corroborated by surface tension observations along the RV SONNE transect (Las Palmas to Guayaquil). During the initial stages, sampling in the oligotrophic North Atlantic Tropical Gyral Province (WATR) revealed reduced SML surface tension (mean: 68.73 mN m^{-1}) despite the region's remoteness and very low productivity. These lower values are unlikely to result from terrestrial inputs or anthropogenic influence and may instead reflect the accumulation of surfactant-active material within the gyre. In contrast, subsequent stations in the Caribbean, Chile-Peru Current, and Central American Coastal provinces exhibited higher and more stable SML surface tension (mean: 73.3 mN m^{-1}), closely aligned with the reference value for pure water (72.8 mN m^{-1}). This pattern suggests that microlayers in these regions were relatively depleted in surfactant material and influenced by lower biological activity.

Previous studies agree with results. Schmidt and Schneider (2011) observed tension depressions of up to 10 mN m^{-1} in coastal Baltic waters, particularly during spring phytoplankton blooms. Similarly, Burdette et al. (2022) reported SML ST depressions of 3.36–4.11 mN m^{-1} due to surfactant-active substances. Such reductions align with the magnitude of ST differences found in the English Channel, reinforcing the biogenic origin of coastal surfactants.

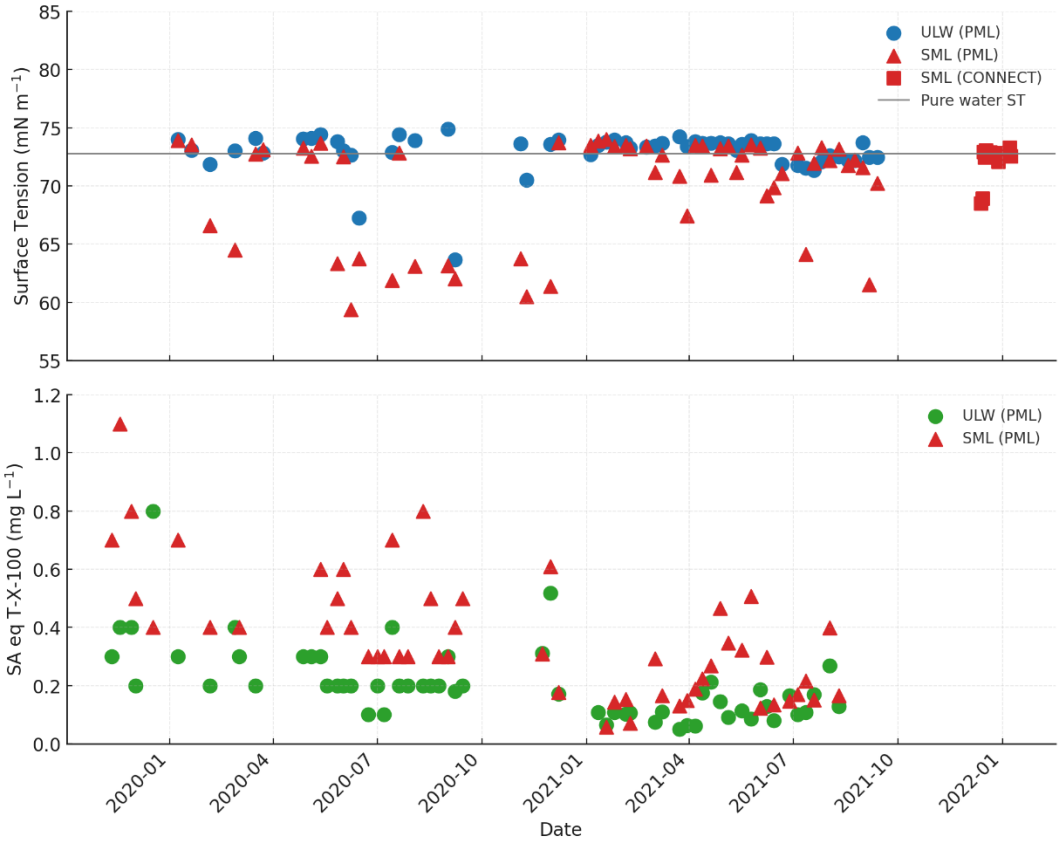

Figure 24: Time series of surface tension and surfactant activity in the surface microlayer (SML) and underlying water (ULW) from the English Channel (Jan 2020–Sep 2021), with SML data from CONNECT added for comparison. Top: Surface tension (mN m^{-1}) with red triangles (SML), blue circles (ULW), and red squares (CONNECT SML); the grey line marks pure water tension (72.8 mN m^{-1}). Bottom: Surfactant activity (mg L^{-1} eq. T-X-100), showing elevated SML values during spring–summer.

The stacked plots (Figure 24) provide a comparative view of surface tension and surfactant activity in the ULW and SML. The upper panel illustrates the variability of surface tension values, highlighting consistently lower, more variable surface tensions in the SML compared to the ULW, reflecting enrichment with surfactant-active substances (SAS). Notably, fluctuations in SML surface tension indicate stronger and more surfactant enrichment, particularly in late spring and summer, compared to the relatively stable ULW values, which cluster near the pure water reference (72.8 mN m^{-1}).

Complementing surface tension measurements, surfactant activity was assessed voltammetrically and expressed in Triton X-100 equivalents (mg L^{-1}) (Figure 24, lower panel). Surfactant activity in the SML regularly exceeded that of underlying water (ULW),

displaying pronounced seasonal peaks during late spring and summer months (May–July). Such peaks indicate periods of increased biogenic production are associated with accumulation of surfactants at the sea-air interface. This observation underscores the ability of voltammetry to detect subtle variations in surfactant concentrations, highlighting differences not readily captured through surface tension measurements alone. SA values observed in this study (SML: 0.057–1.10 mg L^{-1} eq. T-X-100; ULW: 0.050–0.80 mg L^{-1} eq. T-X-100) are consistent with prior work. Frew et al. (2002) reported 0.05–3.00 mg L^{-1} in the Sargasso Sea and coastal areas, Wurl et al. (2011b) found 0.10–1.57 mg L^{-1} across the Atlantic, and Sabbaghzadeh et al. (2017) reported up to 1.77 mg L^{-1} during trans-Atlantic cruises. Lower values are typically linked to oligotrophic offshore waters, while elevated concentrations signal biologically productive coastal regimes.

Surface tension measurements in the temperate coastal ocean exhibit strong seasonal cycles (Figure 24, upper panel). Winter (Dec–Feb) SML values were relatively high and stable (~73.5–73.9 mN m^{-1}), indicative of reduced biological activity. Spring (Mar–May) introduced substantial fluctuation, from 73.6 mN m^{-1} in March to 63.4 mN m^{-1} in May, consistent with the expected timing of the spring phytoplankton bloom in temperate coastal waters. Summer (Jun–Aug) showed continued variability, with pronounced tension depression (63.1–66.1 mN m^{-1}), while Autumn (Sep–Nov) reflected a rebound toward higher values (63.9–73.7mN m^{-1}).

Comparing 2020 and 2021, seasonal trends were present in both years, but the 2021 dataset was characterised by slightly higher average SML ST and reduced variability. In contrast, 2020 displayed sharper seasonal transitions, particularly a substantial summer drop. These results suggest interannual variability modulates but does not override the dominant seasonal pattern.

Enrichment Factors (EF)

To further quantify microlayer dynamics, enrichment factors were calculated. The surface tension enrichment factor ranged from 0.84 to 1.38 (mean: 1.05; add median) in the English Channel, peaking during midsummer and converging to unity during winter. CONNECT open-ocean ST EF values were tightly clustered near unity (0.94–0.99, mean: 0.98; median), underscoring lack of SML enrichment (Figure 25, upper panel and Table 10).

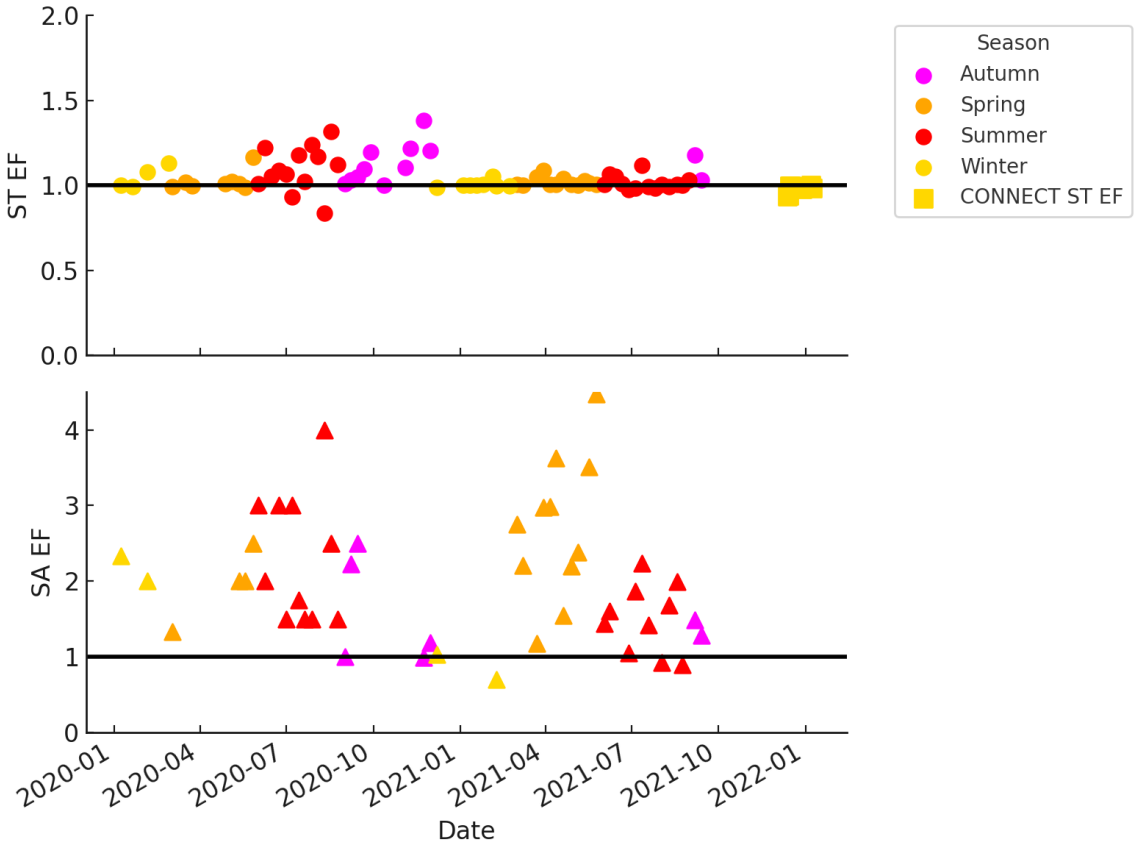

Figure 25: Seasonal time series of enrichment factors (EFs) for the surface microlayer (SML) in the English Channel and open ocean. Top: Surface tension-derived enrichment factor (ST EF), colour-coded by season, with CONNECT open-ocean values shown as yellow squares. Bottom: Surfactant-activity enrichment factor (SA EF), derived voltammetrically. The black line at EF = 1 denotes no enrichment. SA EF shows greater variability and higher peaks than ST EF, particularly during spring and summer, highlighting strong biogenic surfactant enrichment in the SML.

Voltammetrically measured surfactant activity enrichment during the PML campaign ranged from 0.50 to 3.00 (mean: ~1.80), with winter values near unity and peak enrichments (~3.0) in late spring and summer (Figure 25, lower panel). While both ST EF and SA EF exhibited

seasonal trends, SA EF showed higher variability and amplitude, suggesting it is more sensitive to episodic, possibly biological events. This divergence reflects methodological differences. ST EF responds to overall film coverage affecting interfacial tension, while SA EF detects specific electroactive surfactants that may occur in transient concentrations. Winter minima in both metrics likely reflect either reduced biological surfactant production and/or increased mixing and dispersion. Increased surfactant consumption by microbes is another possible factor; however, microbial degradation rates generally decline at low temperatures—making higher winter consumption unlikely to be the dominant cause (Bagi et al., 2013, Gillooly et al., 2001).

Together, ST EF and SA EF capture both broad-scale and transient SML variability: in the English Channel, ST EF (0.84–1.38) peaks with spring blooms and SA EF (0.50–3.00) spikes during rapid phytoplankton growth; along SO287–CONNECT both metrics (ST EF 0.94–0.99; SA EF 0.70–1.20) remain near unity, reflecting oligotrophic stability. These patterns mirror bloom-driven SAS increases (< 0.005 to ~ 0.02–0.03 mg L^{-1}; Croot et al., 2007) and EF ranges of 1.7–2.7 across trophic regimes (Wurl et al., 2011) , providing a robust framework that underscores stronger biogenic heterogeneity in coastal microlayers.

Table 10: Summary of surface microlayer (SML) statistics in the English Channel and open ocean, including surface tension (ST), surfactant activity (SA), enrichment factors (EF), and film coverage (Δσ) over specified date ranges.

Region	Date Range	Sample Type	Film Coverage Δσ	ST Mean	ST Range	ST EF Mean	ST EF Range	SA Mean	SA Range	SA EF Mean	SA EF Range
			mN m^{-1}					mg L^{-1} eq. T-X-100			
English Channel	Nov 2019–Sep 2021	SML	0.46 – 15.14	70.09	59.4 – 73.99	1.05	0.84 – 1.38	0.36	0.057 – 1.10	1.80	0.50 – 3.00
CONNECT (Open Ocean)	Dec 2021–Jan 2022	SML	0.09 – 4.78	72.34	68.53 –73.30	0.98	0.94 – 0.99	n/a	n/a	n/a	n/a

n/a: surfactant activity not measured for CONNECT (open-ocean) campaign

3.4.2 Environmental and Biogeochemical Controls on Surfactant Film Coverage in the Coastal SML

Building on the seasonal and spatial variability in surface tension and surfactant activity observed across English Channel and open-ocean waters, we examined the potential environmental and biological drivers of surfactant film coverage ($\Delta\sigma$) in the sea surface microlayer (SML), defined here as the reduction in surface tension relative to surfactant-free seawater and representing the cumulative effect of surface-active substances at the air–sea interface. While enrichment factors provided a quantitative measure of microlayer enhancement, they did not resolve the underlying mechanisms driving temporal and spatial heterogeneity. To address this, we examined seasonal patterns and pairwise relationships between $\Delta\sigma$ and key environmental variables—including *SST*, wind speed, *Chl-a*, nutrient concentrations, *DOC*, riverine discharge, and phytoplankton biomass—and integrated fatty-acid composition to provide a comprehensive, mechanistic interpretation of surfactant enrichment dynamics in the coastal SML.

3.4.2.1 Seasonal Dynamics of Film Coverage, Temperature, and Phytoplankton Biomass

Throughout January 2020 to September 2021, film coverage ($\Delta\sigma$), sea-surface temperature (*SST*), and phytoplankton biomass exhibited similar seasonal cycles (Figure 26), reflecting a tightly coupled biophysical system in the English Channel.

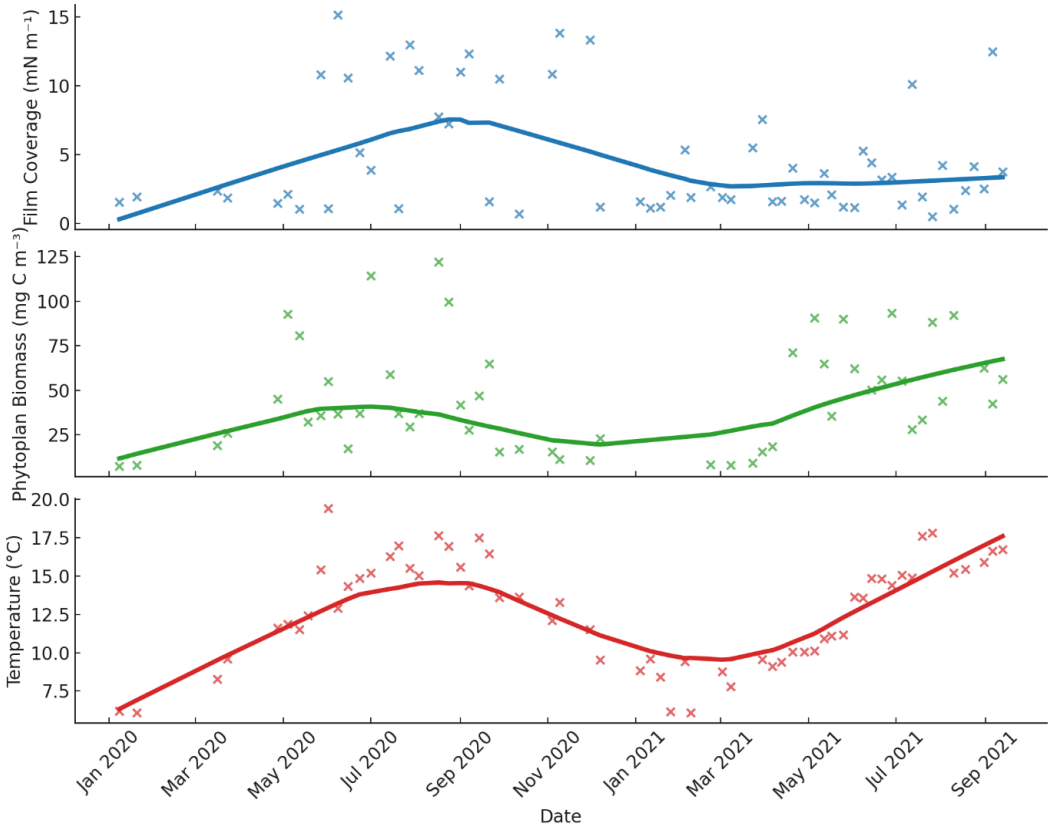

Figure 26**:** Seasonal time series of surfactant film coverage (Δσ, mN m⁻¹; blue crosses and LOESS best fit line) alongside phytoplankton biomass (mg C m⁻³; green crosses and LOESS best fit line) and sea-surface temperature (°C; red crosses and LOESS best fit line) from January 2020 to September 2021. All three variables rise in late spring, peak in midsummer, and decline through autumn–winter, highlighting their tightly coupled biophysical cycle in the coastal SML.

At the beginning of 2020, $\Delta\sigma$ values remained very low (~1–2 mN m⁻¹) from January through May, concurrent with cool water temperatures and modest biological activity. As *SST* rose in late spring—from ~6 °C in January to ~12 °C by May—phytoplankton biomass began its characteristic spring bloom (≈ 10 mg C m⁻³ in April to 40–60 mg C m⁻³ by June 2020). Concomitant with this warming and biomass surge, $\Delta\sigma$ rapidly increased to a peak near 10 mN m⁻¹ in mid-July to August 2020. After this summer maximum, all three variables declined into autumn: by November 2020, $\Delta\sigma$ fell to ~2–3 mN m⁻¹, *SST* cooled to ~10–12 °C, and biomass decreased to 20–30 mg C m⁻³. During winter (December 2020–February 2021), *SST* bottomed out at ~6–8 °C, biomass remained low (10–20 mg C m⁻³), and $\Delta\sigma$ hovered around 1–3 mN m⁻¹. In late spring and early summer 2021, *SST* rose above 10 °C by April, biomass rebounded, and $\Delta\sigma$ peaked near 4–5 mN m⁻¹ in July–August 2021.

Although the 2021 peak was smaller than mid-2020, the pattern remained consistent: $\Delta\sigma$ tracks closely with the combination of rising *SST* and enhanced phytoplankton biomass, suggesting that biogenic surfactant production under warm, productive conditions is the primary driver of surface film formation.

3.4.2.2 Seasonal Variability in Chlorophyll-a, Wind Speed, DOC, and River Discharge

The seasonal dynamics of chlorophyll-a (Chl-a), wind speed, dissolved organic carbon (DOC), and river flow further illuminate how biological, physical, and hydrological processes interact to influence surface conditions in the English Channel (Figure 27).

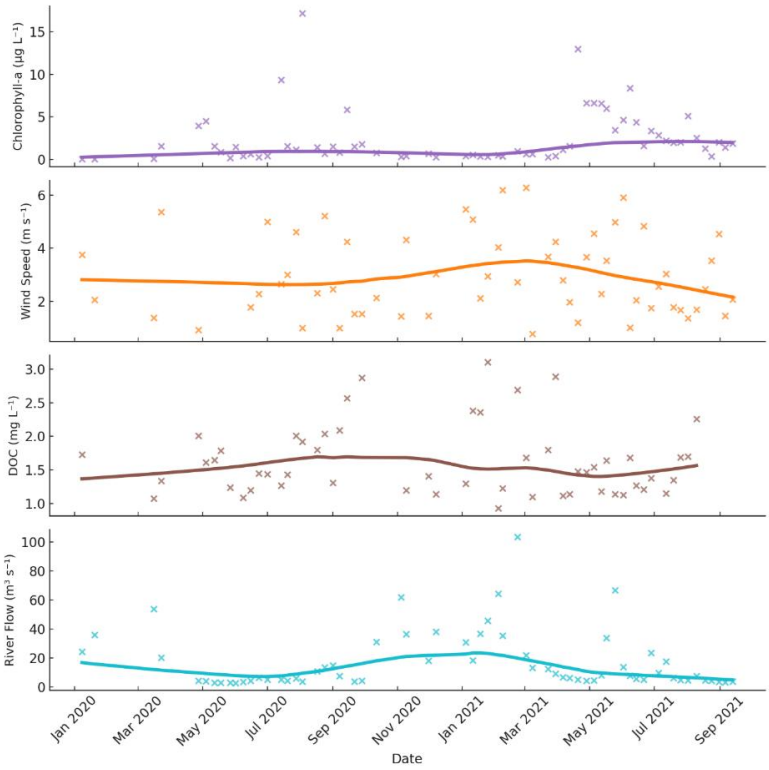

Figure 27: Seasonal dynamics of chlorophyll-a (µg L^{-1}; purple), wind speed (m s^{-1}; orange), dissolved organic carbon (mg L^{-1}; brown), and combined river discharge (m^3 s^{-1}; teal) over the same period. Chlorophyll-a and DOC increase during blooms, wind speed peaks in high-mixing months, and river flow spikes in winter—together modulating the timing and magnitude of surfactant film formation.

Chl-a rose from near zero µg L^{-1} in February–March 2020 to ~1–2 µg L^{-1} by July 2020, peaking around 4.5 µg L^{-1} in mid-August. This summer *Chl-a* maximum coincided with peaks in $\Delta\sigma$, *SST*, reinforcing suggestion that dense phytoplankton populations drive elevated

surfactant coverage. After August 2020, *Chl-a* declined to ~0.5 µg L^{-1} by October and remained low through early 2021 before surging again to ~4–5 µg L^{-1} in June–July 2021.

DOC started around 1.5 mg L^{-1} in January 2020, rose to ~2.0 mg L^{-1} by July 2020, and dipped to ~1.3 mg L^{-1} by October. A November 2020 rise to ~1.7 mg L^{-1} likely reflected increased river discharge; similarly, a spring 2021 *DOC* jump to ~2.2 mg L^{-1} in March coincided with a river-flow spike.

Wind speed trended from ~3 m s^{-1} in January 2020 down into early spring, then rose to ~3–3.5 m s^{-1} by June–July 2020 and peaked near 5 m s^{-1} in August. Higher wind speeds during late summer likely partially disrupted the SML, keeping $\Delta\sigma$ from rising further. In autumn 2020, wind stabilized around 2–3 m s^{-1} before climbing above 5 m s^{-1} in December 2020–January 2021, a period when $\Delta\sigma$ remained low despite moderately elevated *DOC* and residual biomass. By early 2021, wind dipped to ~1 m s^{-1} in February, then rose to ~3–4 m s^{-1} by March, facilitating the modest spring–summer 2021 film resurgence under calmer conditions.

River flow remained < 10 m^3 s^{-1} through early 2020, surged to ~60 m^3 s^{-1} in November 2020, peaked above 100 m^3 s^{-1} in January 2021, then declined into late 2021. A smaller peak (~30 m^3 s^{-1}) in June 2021 corresponded with slight late-summer increases in *DOC* and *Chl-a*, illustrating that while runoff can augment coastal organic and nutrient stocks, it only bolsters film formation when temperatures and biological activity are favourable.

3.4.2.3 Integrated Biophysical Interpretation

Taken together, these time-series emphasize that surfactant film coverage in the English Channel is governed by a combination of biological production, thermal forcing, wind-driven mixing, and terrestrial inputs. The strongest film coverage occurs in mid-summer when *SST* are highest (~17–18 °C), phytoplankton biomass and *Chl-a* peak, *DOC* is elevated, and winds are moderate enough (3–4 m s^{-1}) to allow stable surface films. In contrast, during

winter months, (high winds > 5 m s^{-1} and low temperatures ~6–8 °C) suppress film formation despite occasional spikes in *DOC* from river discharge. Late-autumn and winter river-flow events deliver terrestrial *DOM* and nutrients, but these do not fully manifest as elevated Δσ until waters warm and phytoplankton production resumes. Therefore, while *DOC* and river flow can modulate the availability of organic material, the ultimate formation and persistence of surface films depend on warm, biologically active conditions and relatively calm winds. This multifactor synergy—whereby temperature, phytoplankton biomass, and moderate winds act together to generate robust SML films, while riverine inputs and high winds modulate their timing and magnitude—provides a comprehensive framework for understanding seasonal surfactant dynamics in temperate coastal waters.

3.4.3 Film Coverage Correlation analysis

Having synthesized how seasonality, biological production, physical mixing, and terrestrial inputs together shape surfactant films, we now turn to assess each environmental variable quantitatively in isolation. First, we examine the relationship between sea-surface temperature and film coverage.

Table 11: Pearson correlations (r) and p-values for weekly SML film coverage versus environmental parameters (Nov 2019–Sep 2021). Significant relationships ($p < 0.05$) are listed first.

Variable	r	p-value	Relationship
phytoplankton biomass (mg C m^{-3})	+0.50	0.001	Significant positive
Sea-surface temperature (°C)	+0.41	0.009	Significant positive
Nitrate (NO_3^-, µM)	–0.31	0.013	Significant negative
River discharge (m^3 s^{-1})	–0.26	0.105	Weak negative, not significant
Ammonium (NH_4^+, µM)	–0.14	0.292	Weak, not significant
Wind speed (m s^{-1})	–0.23	0.157	Weak negative, not significant
Chlorophyll-a (µg L^{-1})	+0.19	0.251	No correlation
Dissolved organic carbon (µM C)	+0.03	0.855	No correlation

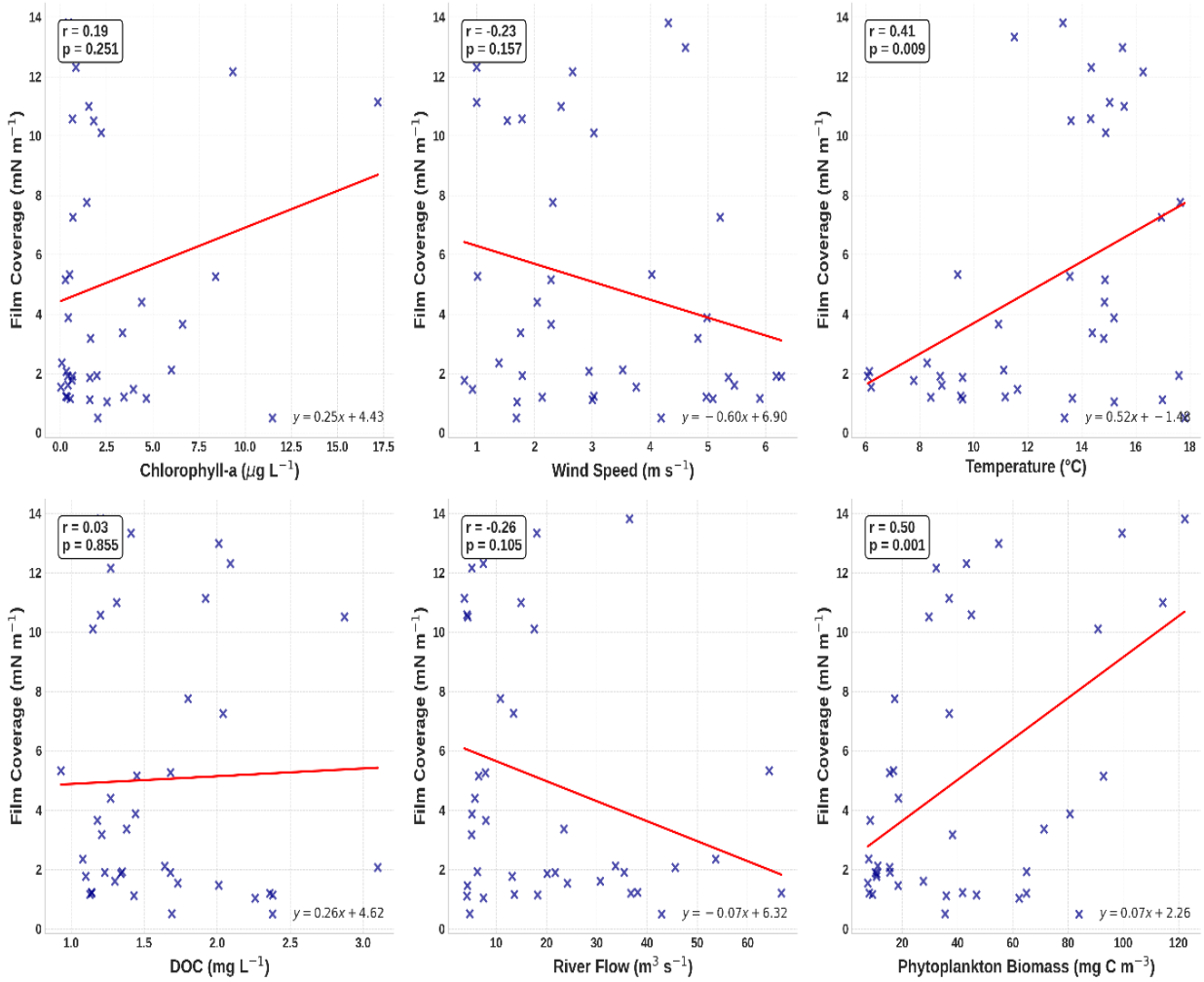

Figure 28: Scatterplots of surfactant film coverage (Δσ) against six environmental drivers (blue crosses) with linear fits (red) and Pearson's r/p values: top-left shows chlorophyll-a (r = 0.19, p = 0.25), top-middle shows wind speed (r = –0.23, p = 0.16), top-right shows temperature (r = 0.41, p = 0.009); bottom-left shows DOC (r = 0.03, p = 0.86), bottom-middle shows river flow (r = –0.26, p = 0.11), and bottom-right shows phytoplankton biomass (r = 0.50, p = 0.001). Of these, only temperature and biomass exhibit significant positive correlations with film coverage.

3.4.3.1 Film Coverage and Temperature

Temporal changes in surface film coverage appear to be broadly linked to sea surface temperature across the time series (Figure 26). Figure 28 (top-right) shows that the Pearson correlation coefficient between film coverage and sea surface temperature was 0.41, with a p-value of 0.009, indicating a statistically significant positive correlation between the two variables. To our knowledge, this is among the first studies to report a statistically significant positive correlation between surfactant film coverage and sea surface temperature based on long-term, in situ observations. While previous work has proposed that higher temperatures

may facilitate microlayer formation through reduced surface tension (Otremba, 2000) and enhanced biological activity (Wurl et al., 2011; Sabbaghzadeh et al., 2017), no natural marine study to date has directly quantified the Δσ–SST relationship.

Film coverage can be influenced by temperature *via* a number of direct and indirect physical, chemical, and biological mechanisms (Otremba, 2000). Surface tension is a physical feature of liquids that results from cohesive forces between molecules at the surface of the liquid (Kou et al., 2019, reference added to bibliography). As the temperature rises, the kinetic energy of the molecules rises, forcing them to move faster and enhancing their capacity to overcome the cohesive forces at the surface, thereby reducing the surface tension (Atkins, 2014).

Temperature influences several key SML processes—including photochemical reaction rates at the interface, the thermodynamics of surfactant adsorption, microbial biosurfactant production, and circulation-driven nutrient supply. Photochemical reactions at the air–sea interface follow Arrhenius kinetics, whereby reaction rates increase exponentially with temperature (Laidler, 1987). As a result, a 10 °C rise can roughly double reaction rates, accelerating the breakdown and transformation of surfactant precursors in the SML. Adsorption of surface-active molecules to the air–water interface is generally exothermic ($\Delta H^\circ < 0$) and governed by the Gibbs adsorption equation. Langmuir isotherm experiments demonstrate that, over the 10–30 °C range, increasing temperature reduces interfacial tension and enhances surfactant surface excess (Rosen & Kunjappu, 2004), leading to thicker, more cohesive films under warmer conditions. Moreover, microbial biosynthesis of surface-active substances is also temperature-dependent: enzyme-mediated metabolic processes follow Arrhenius behaviour with a Q_{10} of approximately 2, implying that production at 25 °C is roughly twice that at 15 °C (Gillooly et al., 2001). Finally, warming-induced stratification and circulation changes regulate vertical nutrient fluxes, often limiting nutrient supply to the surface and thereby modulating phytoplankton growth—and surfactant

precursor availability in the SML (Behrenfeld et al., 2006). Together, these temperature dependent processes help explain the seasonal increase in Δσ and SA EF we observe during spring and summer blooms.

3.4.3.2 Film Coverage and Phytoplankton Biomass

As discussed above, film coverage is expected to be related to primary production (phytoplankton biomass) through the production of organic compounds by algal cells. Furthermore, the phytoplankton closer to the sea surface could be light-damaged and may therefore overproduce anti-oxidants, or potentially die and release all their cell compounds, which can increase organic materials in the SML (Wurl et al., 2011).

Chlorophyll-a is a convenient phytoplankton biomass proxy because it is easily measured, although the relationship is not necessarily linear since the chlorophyll content per unit phytoplankton biomass can vary by species. Previous studies have reported conflicting results regarding the relationship between chlorophyll-a and surfactants. Sabbaghzadeh et al. (2017), who studied the open Atlantic Ocean, found no significant association between chlorophyll-a and surfactant activity ($r = 0.117$, $p = 0.226$), with chlorophyll concentrations averaging only ~0.05 $\mu g\, L^{-1}$ (range: 0.00–1.08 $\mu g\, L^{-1}$). In contrast, Salter (2010) reported a strong positive relationship ($r = 0.87$) between surfactant activity and chlorophyll-a in a mesocosm bloom experiment and along a North Sea transect, with chlorophyll-a concentrations ranging between ~0.5–6.0 $\mu g\, L^{-1}$.

In the present study, chlorophyll-a concentrations were markedly higher overall, with values ranging from 0.03 to 17.19 $\mu g\, L^{-1}$ and a mean of 3.17 $\mu g\, L^{-1}$. These levels are far more comparable to, and even exceed, those reported by Salter (2010), and differ substantially from the open ocean levels reported by Sabbaghzadeh et al. (2017). This reflects the coastal, productive nature of our study site, and therefore our results are more likely to reflect the dynamics of phytoplankton-driven surfactant production under nutrient-rich conditions

similar to those described by Salter, rather than the oligotrophic to mesotrophic oceanic settings examined by Sabbaghzadeh.

Despite this, our data revealed no significant association between film coverage and chlorophyll-a (Figure 28, top-left; $r = 0.19$, $p = 0.25$) despite the association with biomass. This apparent disconnect may be because factors beyond total pigment content—such as phytoplankton species composition, physiological condition, or extracellular release mechanisms— modulate the relationship between chl-a as a biomass proxies and surfactant presence. One explanation is that specific phytoplankton taxa or trophic interactions, rather than bulk chlorophyll levels, may be more directly linked to surfactant production. For instance, grazing by zooplankton can introduce additional organic material through sloppy feeding and excretion, decoupling surfactant dynamics from Chl-a concentration. The complexity of these processes makes it difficult to use chlorophyll alone to predict surfactant presence.

In contrast, we found a strong significant positive link between film coverage and phytoplankton biomass throughout the course of the study period (Figure 28, bottom-right; $r = 0.50$, $p = 0.001$). Phytoplankton biomass was estimated from microscopy counts, biovolume conversions, and carbon estimates (mg C m^{-3}) following the method of Menden-Deuer and Lessard (2000), applied to samples collected and analysed according to BS EN 15204:2006 standards. This biomass metric includes a broad range of phytoplankton taxa (diatoms, dinoflagellates, coccolithophores, flagellates, *Phaeocystis*, ciliates), with observed values ranging from approximately 5 to 122 mg C m^{-3}.

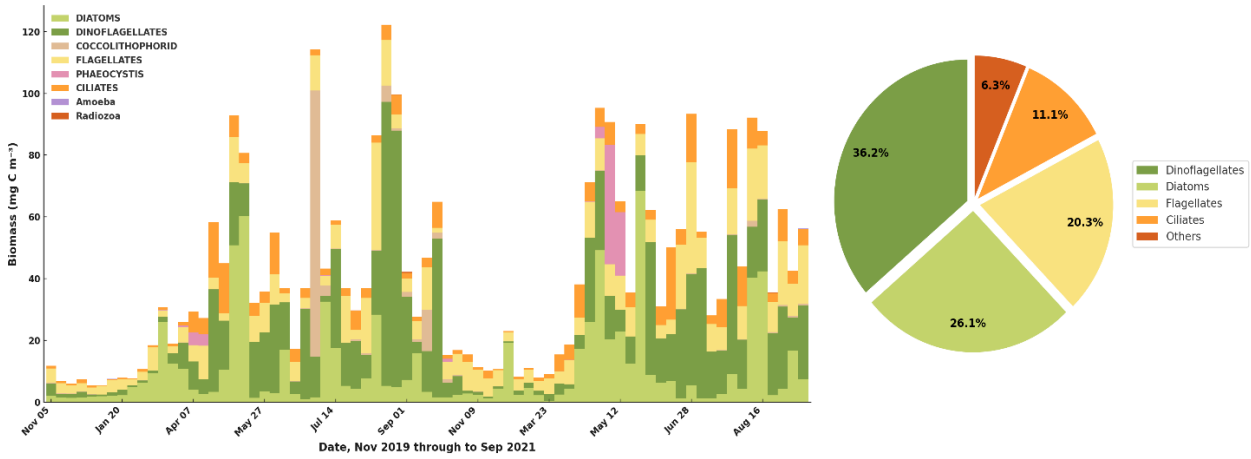

Figure 29: Phytoplankton community structure at Station L4 (50.25°N, 4.217°W) from November 2019 to September 2021. (a) Stacked bar chart showing day-by-day biomass (mg C m^{-3}) contributions from eight major phytoplankton groups, highlighting seasonal and interannual variability. Data from the Plymouth Station L4 phytoplankton time-series (1992–2020; Widdicombe & Harbour 2021; BODC 10.5285/C9386B5C-B459- 782F-E053-6C86ABC0D129 (b) Pie chart summarizing cumulative biomass proportions across the entire dataset. Dinoflagellates (36.2%), Diatoms (26.1%), Flagellates (20.3%), and Ciliates (11.1%) collectively represented over 93% of total phytoplankton biomass. Biomass was estimated from Utermöhl microscopy and Menden-Deuer and Lessard (2000) biovolume-to-carbon conversions.

In our study, phytoplankton biomass was overwhelmingly dominated by large eukaryotic taxa, particularly dinoflagellates (36.2%) and diatoms (26.1%), followed by notable contributions from flagellates (20.3%) and ciliates (11.1%). Together, these four groups accounted for more than 93% of total biomass (Figure 29). Diatoms were most prominent in the spring, while dinoflagellates showed strong peaks in late summer. These groups not only contribute substantially to total carbon biomass but are also known producers of a broad array of surface-active substances (SAS), such as exopolymeric substances and cell-derived lipids, especially during bloom senescence or lysis. Although the present work did not include a formal correlation analysis between film coverage and individual phytoplankton groups—a worthwhile endeavor for future research—the coincident seasonal maxima in diatom biomass and elevated film coverage in spring suggest a potentially strong linkage. This community composition reflects a coastal mesotrophic environment with relatively high productivity and pronounced seasonal succession, underscoring the need for targeted statistical assessment of SAS producers in subsequent studies.

Compared to Atlantic Ocean transects (AMT24 and AMT25) reported by Sabbaghzadeh et al. (2017), where phytoplankton communities were dominated by the picoplankton *Prochlorococcus* and *Synechococcus* in oligotrophic gyres, our coastal dataset is markedly distinct. Picophytoplankton, while numerically dominant in oligotrophic open-ocean environments, contribute relatively little to total phytoplankton carbon biomass and are generally considered minor sources of surface-active organic material compared to larger phytoplankton taxa (Li, 2002; Marañón et al., 2001; Passow, 2002). In contrast, our PPAO dataset shows elevated biomass with substantial representation of surfactant-producing phytoplankton groups. This difference in community composition likely explains the absence of a clear correlation between chlorophyll-a and film coverage in our study. While chlorophyll-a indicates phototrophic biomass, it does not differentiate taxa actively producing surfactants from those that do not. Given the variable SAS production among different phytoplankton, taxonomic resolution is essential—future investigations should therefore focus on how specific groups (e.g., diatoms, dinoflagellates) contribute to surface-film formation. Surfactant enrichment in our data appears more tightly linked to total biomass as evidenced by the strong and statistically significant positive relationship observed between surface film coverage and phytoplankton biomass over the study period (Figure 28, bottom-right; $r = 0.50$, $p = 0.001$). Thus, taxonomic resolution and functional-group contributions are critical when interpreting chlorophyll–film coverage relationships.

This observation aligns with the seasonal pattern reported by Schmidt and Schneider (2011), who studied surfactant production and phytoplankton dynamics in the Baltic Sea. They identified distinct variations, with peak surfactant levels coinciding with phytoplankton bloom periods from January through March, particularly during spring blooms. They demonstrated that surfactant production closely tracks phytoplankton bloom dynamics, emphasizing a strong biological origin for these surfactants. Schmidt and Schneider's (2011)

findings thus provide robust external validation for our observed seasonal trends, supporting the concept of a direct, biologically driven linkage between phytoplankton biomass and surfactant production.

3.4.3.3 Nutrient–Surfactant Relationships in the Sea Surface Microlayer

Building on our fatty-acid and DOC analyses, we next investigated how dissolved inorganic nitrogen (DIN) dynamics relate to surfactant film formation. We focused on two key DIN species—nitrate (NO_3^-) and ammonium (NH_4^+)—whose seasonal cycles reflect phytoplankton uptake and microbial recycling, respectively.

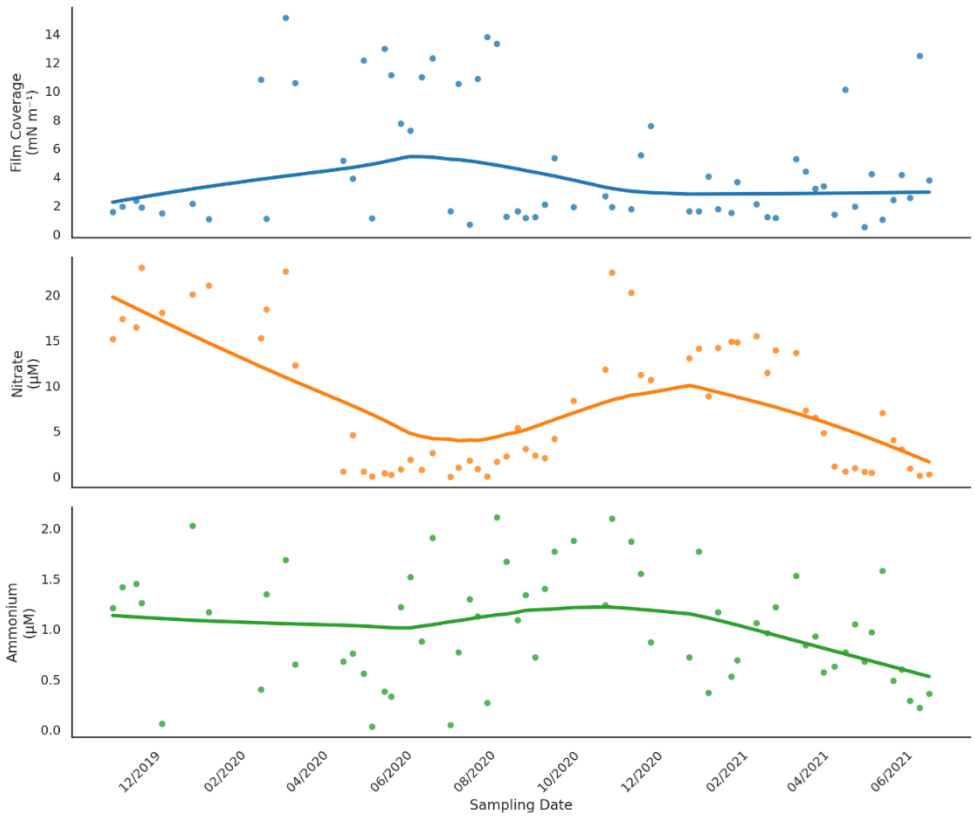

Figure 30: Seasonal co-variability of surfactant films and dissolved inorganic nitrogen Top: Weekly surfactant film coverage (Δσ, mN m^{-1}; blue symbols and LOESS curve), nitrate (NO_3^-, µM; orange symbols and LOESS), and ammonium (NH_4^+, µM; green symbols and LOESS) from November 2019 through June 2021. Film coverage increases from winter minima to a mid-summer maximum (~8 mN m^{-1}) in 2020, then declines into winter before stabilizing at modest levels in 2021. Nitrate exhibits a classic draw-down—from >20 µM in winter to <2 µM in summer—followed by autumn rebound, while ammonium remains relatively constant (0.8–1.5 µM) year-round.

Figure 30 presents weekly time series of Δσ, NO_3^-, and NH_4^+ from November 2019 through September 2021. Surfactant film coverage rose from winter lows to peak in mid-summer

(June–July), coinciding with the spring bloom. Nitrate displayed a complementary draw-down pattern: high winter concentrations (>15 µM) declined to near zero during summer stratification before rebounding in autumn. In contrast, ammonium remained low and relatively stable (0.8–1.5 µM), with only subtle mid-year increases.

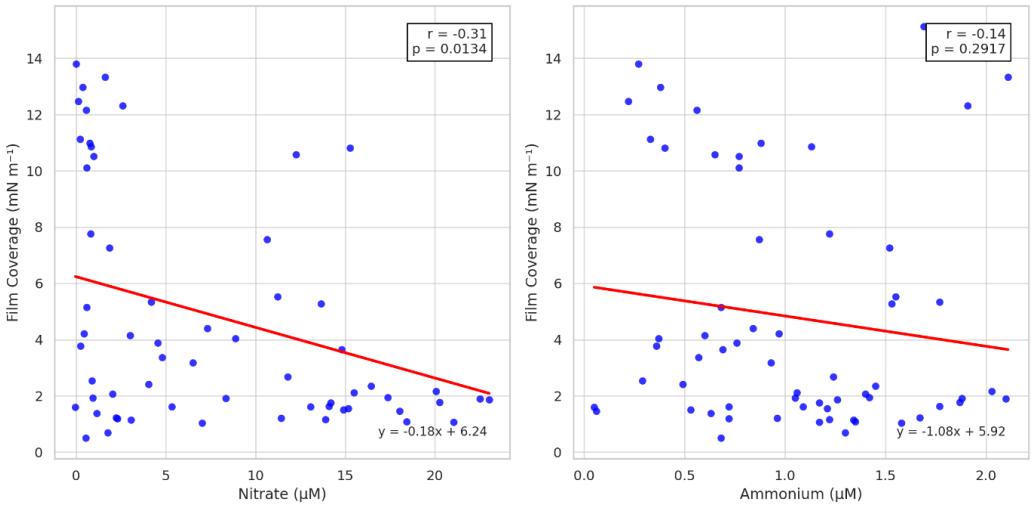

Figure 31: Nutrient–surfactant scatterplots (Lift) Surfactant film coverage (Δσ, mN m^{-1}) versus nitrate concentration (NO_3^-, µM). A significant inverse Pearson correlation (r = –0.31, p = 0.0134) indicates that peak film coverage coincides with nitrate-depleted, bloom-stage conditions. (Right) Surfactant film coverage (Δσ, mN m^{-1}) versus ammonium concentration (NH_4^+, µM). A weak, non-significant correlation (r = –0.14, p = 0.2917) suggests that regenerated nitrogen does not directly control film strength.

Scatterplots of Δσ versus DIN (Figure 31) reveal a significant inverse relationship with nitrate (r = –0.31, p = 0.013), indicating that elevated surfactant films occur under nitrate-depleted, bloom-stage conditions in mid-summer. By contrast, Δσ showed a weak, non-significant correlation with ammonium (r = –0.14, p = 0.292), suggesting that regenerated nitrogen does not directly drive film strength. Here, linear regression is applied as a descriptive tool to assess the direction and strength of association rather than to imply a mechanistic or predictive relationship. Given the scatter and potential non-linearity in the data, the regression line should be interpreted as indicative of an overall tendency rather than a functional dependence.

Phytoplankton rely on dissolved inorganic nitrogen—especially NO_3^- for growth, consuming it rapidly during bloom events. The observed inverse relationship between NO_3^-

and Δσ therefore reflects the coupling of surfactant production to periods of heightened primary production and organic exudation in the SML. NH_4^+, produced through microbial remineralisation and recycled within the microbial loop, lacks a clear seasonal draw-down and accordingly shows no consistent link to Δσ

While instantaneous DIN concentrations alone cannot predict film coverage, the inverse NO_3^-–Δσ relationship suggests that surfactant enrichment is associated with periods of nutrient depletion and physiological stress, when phytoplankton biomass is high and nitrogen becomes limiting. Under such conditions, enhanced exudation and cell lysis are expected, promoting the accumulation of surface-active material in the SML. These findings reinforce that biogenic activity—rather than bulk nutrient levels—governs the seasonal development of surfactant films in the coastal SML.

3.4.3.4 Film Coverage and DOC

We assessed whether total DOC concentration could predict film coverage in the SML. DOC may originate from a range of sources, such as terrestrial sources, aquatic primary production, atmospheric deposition, and anthropogenic inputs including wastewater discharge and agricultural runoff (Kaiser and Benner, 2008). While the concentration of total DOC in the SML could be related to surface tension, it is important to note that the relationship can be complex and dependent on several factors, including the composition and concentration of organic compounds present in the SML (Holmes et al. 2008). This complexity underscores the limitation of bulk-DOC measurements and highlights the need for targeted analyses of DOC molecular composition—such as amphiphilic lipids, proteinaceous fractions, and polysaccharides—to identify which specific classes of dissolved organics govern surfactant film formation and stability in the microlayer.

However, we found no significant relationship between total DOC and surfactant film coverage (Figure 28, bottom-left; $r = 0.03$, $p = 0.86$), indicating that DOC concentration alone did not predict film formation. In the Baltic Sea SML, both Ćosović & Vojvodić (1998)

and Frew et al. (2001) similarly reported no direct correlation between bulk DOC and surfactant abundance, underscoring that total DOC fails to capture the surfactant-active fraction of dissolved organic carbon. Frew et al. (2001) further demonstrated that positive DOC–surface-activity correlations in coastal waters vary seasonally, reflecting shifts in DOC quality between autochthonous and allochthonous sources. Wurl and Holmes (2008) observed rapid in situ production of gel matrices, often achieving enrichment factors exceeding 10×. Yet despite this extreme enrichment, they reported only weak co-variation with bulk biomass proxies, indicating that total DOC concentration fails to capture the surfactant-active fraction of surface organic carbon. Croot et al. (2007) found that only a fraction of dissolved organic carbon (DOC) has surfactant characteristics, which can be attributed to variables such as molecule structure and concentration. Thus, while DOC set the upper bound of organic-carbon availability in the microlayer, it was the molecular composition enrichment processes, and source quality of specific gel particles—and the environmental conditions that stabilized them—that ultimately governed surfactant film coverage in the coastal SML.

3.4.3.5 Fatty Acid Composition and Its Link to Surfactant Film Coverage

Building on the dominant role of phytoplankton-derived surfactants, we tracked six fatty acids—four biogenic (C12:0, C14:0, C16:2, C16:4) and two anthropogenic (C11:0, C13:0)—to explore their seasonal dynamics and potential contributions to SML film coverage (Figures 32–33). Fatty acids are widely recognised as key contributors to the pool of surface-active organic matter within the sea surface microlayer (SML) (Wurl et al., 2009; Gašparović et al., 2014). These compounds can originate from diverse sources, with saturated and unsaturated long-chain fatty acids typically associated with biogenic production, while mid-chain saturated fatty acids may also arise from anthropogenic inputs (Guitart et al., 2007; Marty et al., 1979).

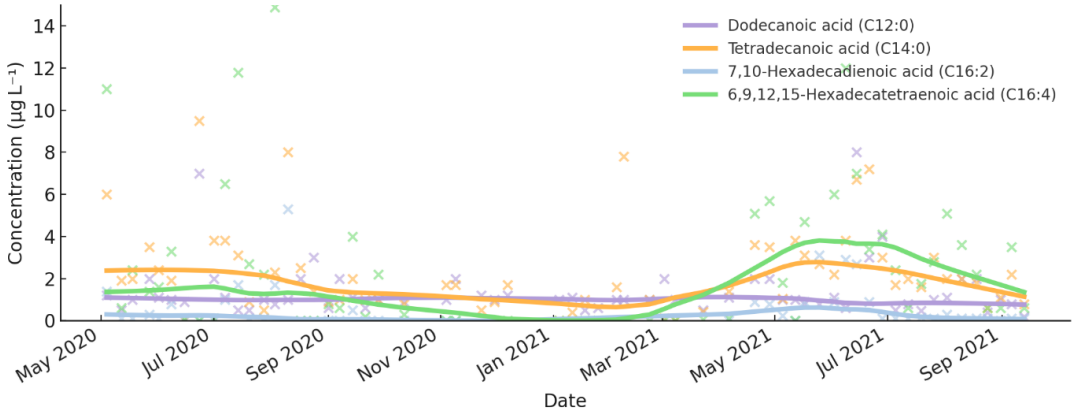

Figure 32: Time series of biogenic fatty acid concentrations (µg L^{-1}) for Dodecanoic acid (C12:0), Tetradecanoic acid (C14:0), 7,10-Hexadecadienoic acid (C16:2) and 6,9,12,15-Hexadecatetraenoic acid (C16:4), with LOESS trend lines

3.4.3.5.1 Biogenic Fatty Acids: Dodecanoic acid (C12:0), tetradecanoic acid (C14:0), and 7,10-hexadecadienoic acid (C16:2) all displayed pronounced spring–summer peaks: C12:0 rose from background levels of <0.5 µg L^{-1} in March 2020 to ~3.2 µg L^{-1} by mid-June; C14:0 followed from ~1.0 to 4.0 µg L^{-1} over the same interval; and C16:2 surged from ~0.3 to 2.8 µg L^{-1} (Figure 32). A second, smaller pulse occurred in May–June 2021, coinciding again with a biomass-driven Δσ maximum (~8–10 mN m^{-1}). 6,9,12,15-hexadecatetraenoic acid (C16:4) showed similar but more muted peaks, rising to ~1.5 µg L^{-1}. These episodic enrichments occur during the spring bloom period—when phytoplankton release exudates enriched in amphiphilic lipids—and coincide temporally with periods of elevated film coverage; however, correlation analysis indicates that no individual fatty acid alone explains the observed variability in Δσ (Figure 34).

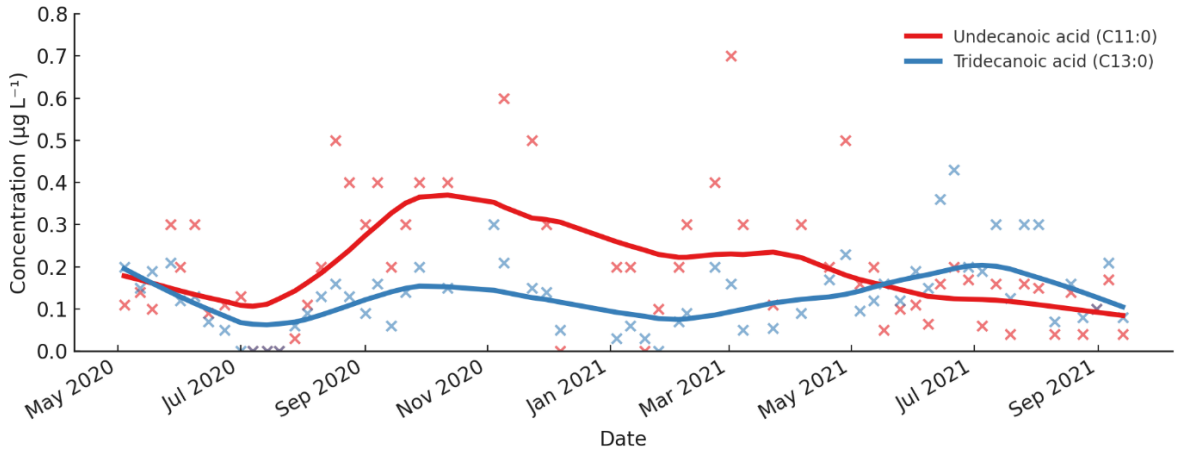

Figure 33: Time series of anthropogenic fatty acid concentrations (µg L^{-1}) for Undecanoic acid (C11:0) and Tridecanoic acid (C13:0), with LOESS trend lines.

3.4.3.5.2 Anthropogenic Fatty Acids: By contrast, markers of terrestrial or anthropogenic origin—undecanoic acid (C11:0) and tridecanoic acid (C13:0)—remained low (<0.8 µg L^{-1}) and sporadic (Figure 33), with no consistent seasonal pattern. Occasional brief elevations (e.g. C11:0 to ~1.0 µg L^{-1} in August 2020) did not correspond to Δσ changes, underscoring their minor role in film formation.

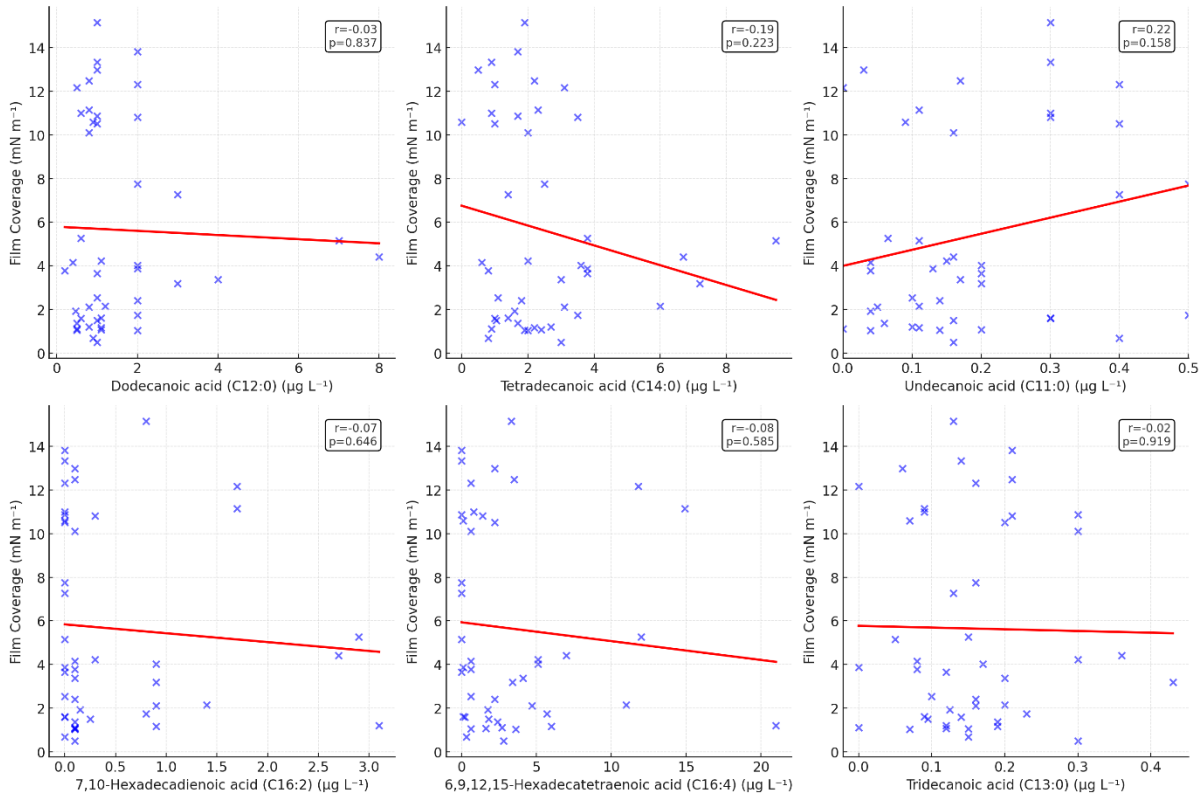

Figure 34: Film coverage (Δσ) versus individual fatty acids in the SML: (top-left) C12:0 (r = –0.03, p = 0.84), (top-middle) C14:0 (r = –0.19, p = 0.22), (top-right) C11:0 (r = 0.22, p = 0.16), (bottom-left) C16:2 (r = –0.07, p = 0.65), (bottom-middle) C16:4 (r = –0.08, p = 0.59), (bottom-right) C13:0 (r = –0.02, p = 0.92). No individual fatty acid correlates significantly with film coverage.

To further examine the potential role of fatty acids in regulating film coverage, we performed a correlation analysis between individual fatty acid concentrations and film coverage values (Figure 34, Table 12). Pearson correlations between each fatty acid and Δσ were uniformly weak ($-0.19 \leq r \leq +0.22$) and non-significant (all $p > 0.15$), confirming that no individual compound serves as a reliable predictor of film coverage. By contrast, total phytoplankton biomass correlated strongly with Δσ and SST correlated moderately, highlighting that integrated biological production under warmer conditions is the principal driver of surfactant films.

Table 12: Pearson correlations between individual fatty-acid concentrations and SML film coverage (mN m^{-1}).

Fatty acid	R	p-value	Relationship
Dodecanoic acid (C12:0)	–0.03	0.837	No correlation
Tetradecanoic acid (C14:0)	–0.19	0.223	No correlation
Undecanoic acid (C11:0)	+0.22	0.158	No correlation
7,10-Hexadecadienoic acid (C16:2)	–0.07	0.646	No correlation
6,9,12,15-Hexadecatetraenoic acid (C16:4)	–0.08	0.585	No correlation
Tridecanoic acid (C13:0)	–0.02	0.919	No correlation

These results suggest that while individual fatty acids can be presumed to contribute to the SML's amphiphilic matrix, they are not the dominant component. This is consistent with the view that film coverage emerges from a synergistic blend of multiple lipid and non-lipid surfactants produced during bloom events. Phytoplankton exudates release a spectrum of long-chain fatty acids, pigments, and exopolymeric substances that coalesce into stable films, with temperature and wind conditions modulating their persistence.

In summary, while fatty acids are enriched in the SML during productive periods and are presumed to support film formation, yet their weak individual correlations with $\Delta\sigma$ underscore that aggregate biological processes—rather than any single lipid class—govern the timing and magnitude of surfactant film coverage at our coastal site.

3.4.3.6 River Flow/Discharge Influences

We next evaluated whether terrestrial inputs from the Tamar, Plym, and Yealm rivers modulate surfactant films in the coastal SML. These rivers—whose catchments drain agricultural land, urban centres, and former mining areas—enter the English Channel within 5–10 km of our sampling station (Figure 6). Agricultural runoff, sewage, and industrial activity are the main polluting factors affecting these rivers (Cornish Mining World Heritage,

2020). Studies have shown that river discharge has an impact on the characteristics and behaviour of the surface microlayer in coastal and estuarine waters. Sutherland et al. (2009) found that, compared to the underlying water, the surface microlayer of an estuary impacted by a river had more particulate organic matter and less dissolved organic matter. Engel et al. (2016) have shown that the microbial community composition, nutrient availability, and pollutant concentrations of the surface microlayer alter in response to river flow.

To investigate the impact that river discharge has on film coverage, Daily mean discharge data ($m^3\ s^{-1}$) were obtained from the UK National River Flow Archive for gauges 47001 (Tamar at Gunnislake), 35001 (Plym at Marsh Mills), and 36003 (Yealm at Ermington) spanning January 2020 to September 2021 (Figure 27). Over this period, flow remained below 5 $m^3\ s^{-1}$ through spring–summer 2020, rose to ~60 $m^3\ s^{-1}$ in November 2020, peaked at ~105 $m^3\ s^{-1}$ in March 2021, and then declined into late 2021. We correlated mean daily river flow with surfactant film coverage ($\Delta\sigma$) at the adjacent coastal station. We observed a weak inverse relationship (Figure 28, bottom-middle; $r = -0.26,\ p = 0.11$), indicating no statistically significant control of river discharge on $\Delta\sigma$. It is noted, however, that discharge from the River Tamar is strongly tidally modulated, such that daily mean flow values may not capture short-term variability in freshwater input or estuarine mixing that could influence near-surface surfactant distributions (Sims et al., 2022).

The lack of a clear link may reflect dilution and transport, as the river mouths lie several kilometers from our station, discharge signals disperse rapidly as a result of hydrodynamic mixing by wind, tides, and waves. These processes are continually eroding and redistributing the SML (Upstill-Goddard et al., 2002). In addition, the authochthonous biological production may override allochthonous signals, i.e.local phytoplankton exudation and gel-particle enrichment exert a stronger control on $\Delta\sigma$ than distant terrestrial inputs. Together, these observations indicate that, in our study area, river discharge does not exert a primary

control on surfactant film coverage; instead, in situ biological and physical processes dominate.

3.4.3.7 Wind and Wave-Driven Controls on SML Film Coverage

Under the sample conditions encountered in this study, the film coverage displayed a weak inverse association with prior 6-hour averaged wind speed, which was not statistically significant (Figure 28, top-middle; $r = –0.23,\ p = 0.16$). However, this analysis is likely restricted by the low range of wind speeds experienced (interquartile range of 2.0 to 4.0 ms^{-1}), which substantially limits the ability to resolve wind-driven effects on SML film coverage within this dataset. It should be noted that wind speed is used here as a proxy for surface forcing, while wave breaking and sea state represent the more direct physical mechanisms controlling surface microlayer disruption and renewal. This result is largely consistent with previous studies. In both the North Pacific and the Arctic Ocean, Wurl et al. (2011) discovered that there was no significant link between the distribution of surfactants (and their enrichment factors EF in the SML) and wind speed. Similarly, Sabbaghzadeh et al. (2017) reported a consistent enrichment of surfactants in the SML at all wind speeds measured (up to 13 m s^{-1}) during two cruises in the open Atlantic Ocean between 50 ^{o}N and 50 ^{o}S. The correlation between SA EFs and wind speed was not statistically significant on either cruise.

The link between wind speed and surface microlayer film coverage is complex and could vary depending on local climatic and biological circumstances. Very high wind speeds can disturb and break up the surface microlayer, primarily through enhanced wave breaking and turbulence, reducing film coverage (Reinthaler et al., 2008). Frew et al. (2004) proposed that surfactant enrichment in the SML decreases at wind speeds higher than 6 - 8 m s^{-1}. Carlson (1983) identified dissolved organic carbon (DOC) enrichment in the SML at wind speeds as high as 8 m s^{-1}, but no obvious effect of wind speed or wave condition was noted on the DOC enrichment factors. However, moderate wind speeds increase surface

microlayer production by encouraging organic matter and surfactant accumulation at the air-water interface (Sabbaghzadeh et al., 2017). Wind speed history (at least 6 hours of reported wind speeds before observations) has been proposed to be more essential for SML enrichment than immediate winds because it impacts the accumulation and distribution of organic matter along the air-water interface (Obernosterer et al. (2008)). In contrast, short-lived wind or wave events may transiently disturb only the uppermost layer of the SML without fully eroding the underlying surfactant reservoir. As a result, the wind speed history approach was chosen for the study presented in this research.

3.4.4 Multivariate Analysis

In previous correlation analyses, we identified a statistically significant, although moderate, positive correlation between film coverage and sea surface temperature (Figure 28, top right; $r = 0.41$, $p = 0.009$). This association indicates that higher temperatures generally coincide with increased film coverage; however, correlation alone cannot determine whether temperature exerts a direct physical control on film formation or whether the relationship is indirect, arising from the co-variation of temperature with biological productivity in temperate waters.

To disentangle these effects, a multiple linear regression was conducted with film coverage as the dependent variable and phytoplankton biomass and temperature as explanatory variables. This approach allows the independent contribution of each factor to be assessed while statistically accounting for their covariance, thereby testing whether temperature explains additional variance in film coverage once biological effects are considered.

The regression analysis shows that phytoplankton biomass is a statistically significant predictor of film coverage ($p = 0.002$), demonstrating a strong and independent link between biological abundance and surfactant film formation. In contrast, the temperature coefficient

is not statistically significant ($p = 0.351$), indicating that temperature does not exert a direct control on film coverage when phytoplankton biomass is held constant.

From a mechanistic perspective, sea surface temperatures typically increase during spring and summer, coinciding with periods of elevated biological productivity. However, this seasonal co-occurrence does not imply a causal role for temperature in driving film formation. Instead, warmer conditions promote phytoplankton growth indirectly by enhancing light availability and stratification. Conversely, colder conditions are often associated with deeper vertical mixing, which increases nutrient supply to the surface mixed layer (Large et al., 1994; Alexander et al., 2000; Wiggert et al., 2000).

Taken together, these results indicate that phytoplankton biomass is the primary driver of enhanced film coverage, while temperature influences surfactant enrichment indirectly through its role in regulating biological growth and seasonal ecosystem dynamics

3.4.5 Integrated Controls on Surfactant Film Coverage

Having examined each driver in isolation, we now synthesize these findings (Table 11) to demonstrate how nutrient draw-down, thermal forcing, biological production, river discharge, and physical agitation collectively regulate surfactant films in the coastal SML.

3.4.5.1 Biogenic Supply & Uptake

Biological production during spring–summer, when seasonal stratification typically develops in temperate shelf waters, nutrient-limited conditions emerged as the principal driver of surfactant films. Total phytoplankton biomass exhibited the strongest correlation with $\Delta\sigma$ ($r = +0.50$, $p = 0.001$), indicating that higher biomass coincides with enhanced surfactant activity. Nitrate concentrations declined sharply during spring–summer blooms and were inversely correlated with film coverage ($r = -0.31$, $p = 0.013$), suggesting that surfactant production intensifies as inorganic nitrogen is depleted by phytoplankton uptake. In contrast, ammonium—a regenerated nitrogen species—showed no significant

relationship with Δσ ($r = -0.14$, $p = 0.292$), underscoring that recycled nitrogen turnover does not directly modulate film strength. Although exuded compounds such as lipids, proteins, and polysaccharides were not directly quantified in this study, fatty acid markers provided episodic confirmation of biogenic input: C12:0, C14:0, C16:2, and C16:4 peaked during blooms but exhibited only weak correlations with Δσ, while anthropogenic markers (C11:0, C13:0) remained at trace levels. These findings underscore that the SML surfactant film is an emergent property of a complex blend of amphiphilic compounds rather than the product of any single dominant lipid class.

3.4.5.2 Thermal Modulation

Sea-surface temperature also showed a significant positive association with Δσ ($r = +0.41$, $p = 0.009$), reflecting seasonal patterns of enhanced metabolic and exudation rates in warmer waters. However, multivariate analysis indicates that temperature's effect is indirect and mediated through its role in promoting phytoplankton growth, thus timing and intensifying bloom-linked surfactant release.

3.4.5.3 Physical Disruption & Dilution

Physical forces and bulk proxies showed limited influence. Wind speed displayed a modest, non-significant negative correlation with Δσ ($r = -0.23$, $p = 0.157$), consistent with episodic film disruption under high wind conditions. River discharge also exerted a limited influence, with a weak inverse correlation ($r = -0.26$, $p = 0.105$), likely reflecting rapid offshore dilution of terrestrial inputs and the dominance of local biological and physical processes in regulating SML properties. Neither chlorophyll-a ($r = +0.19$, $p = 0.251$) nor dissolved organic carbon ($r = +0.03$, $p = 0.855$) predicted surfactant film coverage, suggesting that pigment concentrations and bulk organic matter pools may not reliably reflect Δσ variability at fine temporal and spatial scales.

In summary, surfactant film formation in the coastal SML is primarily orchestrated by nitrate-limited phytoplankton blooms under warm, stratified conditions, while riverine

inputs, physical disturbance, recycled nutrients, pigment concentrations, and individual lipid classes act as supporting, secondary factors. These results highlight the central role of integrated biogenic activity in shaping air–sea interface chemistry in dynamic coastal systems.

3.5 Conclusion

In this chapter, we addressed the critical lack of surface-tension measurements in saltwater by making measurements over two years in the English Channel and complementary open-ocean work. Measured surface tension was used the calculate film coverage ($\Delta\sigma$) over the time series. Correlation analysis with various physical and biogeochemical variables was conducted to investigate the drivers of film coverage. Our weekly time series—from surface tension and surfactant activity measurements to chlorophyll-a, biomass, DOC, river discharge, wind speed, fatty-acid composition, and dissolved inorganic nitrogen—revealed strong seasonal cycles in biogeochemical processes, as expected for a temperate coastal environment. $\Delta\sigma$ exhibited pronounced seasonal variability, rising from ~1–2 mN m^{-1} in January–May 2020 to a summer peak of ~10 mN m^{-1}, declining to ~2–3 mN m^{-1} by November, and rebounding to ~4–5 mN m^{-1} in July–August 2021. We have shown that the sea surface microlayer (SML) in coastal waters is a highly dynamic, biologically driven interface whose surfactant film coverage reflects an interplay of phytoplankton production (with nutrient draw-down serving as an indicator of bloom progression), thermal forcing, phytoplankton production, and physical agitation. Building on the $\Delta\sigma$ seasonality reported by Schmidt and Schneider (2011) in the Baltic Sea, our key findings are:

First, phytoplankton biomass emerged as the single strongest predictor of film coverage ($r = +0.50$, $p = 0.0003$), suggesting that bloom-stage exudation of lipids, proteins, and polysaccharides forms the bulk of the surface-active matrix. Sea surface temperature was also linked with film coverage ($r = +0.32$, $p = 0.022$), not by directly generating films, but because it is associated with favorable conditions for phytoplankton growth.

Second, nitrate draw-down—reflecting active nutrient uptake during blooms—correlated negatively with film coverage ($r = –0.31$, $p = 0.013$), demonstrating that surfactant production intensifies precisely as inorganic nitrogen becomes depleted. In contrast, regenerated ammonium exhibited no significant relationship, indicating that only the primary uptake phase of nutrient cycling drives surfactant enrichment.

Third, physical and hydrological factors—river discharge, wind speed, pigment concentration, and bulk DOC—played subsidiary, modulating roles. Although terrestrial inputs and moderate winds can influence the timing and magnitude of film presence, their correlations with $\Delta\sigma$ were weak or non-significant, highlighting the primacy of in situ biological and temperature-mediated processes.

Finally, at an individual compound level, selected individual biogenic and anthropogenic fatty acids were not correlated with film coverage. Instead, $\Delta\sigma$ is thought to arise from a complex blend of amphiphiles—fatty acids, gel particles, and other exudates—supplied and modified by bloom senescence, grazing, and microbial cycling.

Taken together, these findings advance our mechanistic understanding of SML surfactant dynamics in coastal systems: film coverage is orchestrated by nitrate-limited phytoplankton blooms under warm, stratified conditions, with aggregate biomass as the most reliable proxy, while physical mixing and non-biological inputs act only as secondary modifiers. This synthesis not only fills a critical gap in the sparsely populated database of marine surfactant measurements but also provides a conceptual framework for predicting when and where biologically active surface films will arise—insights that are vital for modelling air–sea gas exchange, improving parameterizations in climate models, and assessing the biogeochemical role of the SML in future ocean scenarios.

Chapter 4: Surface Tension Dynamics in Oligotrophic Open-Ocean Waters (SO287–CONNECT)

4.1 Preface to the Chapter

This chapter investigates sea surface microlayer (SML) film coverage (Δσ) along the ~6000 km SO287–CONNECT transect across oligotrophic Atlantic waters (December 2021–January 2022). Surface tension measurements of unfiltered SML and underlying waters are examined across multiple Longhurst biogeochemical provinces to characterise spatial variability in surfactant film enrichment under nutrient-limited open-ocean conditions.

Surface tension is interpreted alongside nutrients, dissolved organic carbon, chlorophyll-a, phytoplankton abundance, fatty acids, wind speed, and sea surface temperature to evaluate controls on microlayer dynamics. In contrast to the seasonally dynamic English Channel, the CONNECT transect provides an open-ocean perspective for comparative assessment of surfactant film behaviour across distinct marine regimes.

4.2 Objectives

1. Quantify surface tension and enrichment factors in unfiltered SML and underlying waters across multiple Longhurst biogeochemical provinces.
2. Describe nutrient distributions and evaluate the degree of surface nutrient limitation relevant to SML processes.
3. Assess spatial patterns in dissolved organic carbon, chlorophyll-a, phytoplankton cell abundance, and selected fatty acids in relation to SML properties.
4. Examine the influence of physical forcing, including wind speed and sea surface temperature, on microlayer stability.

5. Compare open-ocean SML dynamics with those observed in the temperate coastal English Channel.

4.3. Methods

4.3.1 Sample locations

Surface microlayer (SML) samples were gathered during the SO287–CONNECT cruise on RV SONNE (11th December 2021 to 11th January 2022), which traversed from Las Palmas to Guayaquil via the Sargasso Sea (Figure 35). Daily SML sampling employed the Garrett screen—deployed either by shipboard crane or manually from a Zodiac boat (weather permitting)—to collect up to 12 L per site. Underlying water (ULW) was obtained via a pump intake 5 m below the surface. Following collection, samples were transferred into plastic bottles that had been cleaned between uses by rinsing with hot tap water, soaking in dilute hydrochloric acid (HCl), and rinsing three times with Milli-Q water. All samples were stored in insulated dark boxes throughout storage and transport to the laboratory to minimise photodegradation and microbial activity. Samples were collected by L. Brown, K. Weddell and D. Loades.

Figure 35: Cruise track (black line) and sampling stations (red dots) of the RV SONNE cruise SO287, covering the route between Las Palmas and Guayaquil.

Sampling stations along the SO287–CONNECT transect were assigned to Longhurst biogeochemical provinces based on their geographic coordinates, using the Longhurst (2007) classification scheme. A total of 39 stations were distributed across six provinces, encompassing both coastal (8 stations) and open-ocean (31 stations) environments. All provinces were classified as low or very low productivity, reflecting the predominantly oligotrophic conditions encountered throughout the cruise. These province assignments, along with associated station counts and sampling date ranges (Table 13), provide a spatial and environmental framework for interpreting surface microlayer properties and biogeochemical variability observed during the campaign.

Table 13: Distribution of CONNECT sampling stations across Longhurst biogeochemical provinces, relative productivity classifications, and sampling date ranges (SO287–CONNECT campaign, December 2021–January 2022). All provinces were classified as low or very low productivity, consistent with oligotrophic conditions along the transect.

Biogeochemical Province	Relative Productivity	Station Count	Start Date	End Date
Trades - N. Atlantic Tropical Gyral Province (WATR)	Very low	11	2021-12-12	2021-12-28
Westerlies - N. Atlantic Subtropical Gyral Province (NASE)	Very low	3	2021-12-24	2021-12-27
Trades - Caribbean Province	Low	4	2021-12-29	2022-01-02
Coastal - Central American Coastal Province	Middle	1	2022-01-05	2022-01-05
Trades - N. Pacific Equatorial Countercurrent Province (PEQD)	Very low	1	2022-01-06	2022-01-07
Coastal - Chile-Peru Current Coastal Province	Low	2	2022-01-07	2022-01-08

4.3.2 Surface Tension Measurements

Surface tension (ST) measurements were conducted using the Kibron EZ Plus tensiometer equipped with a platinum Wilhelmy plate, following the cleaning, calibration, and analytical procedures described in Chapter 3, Section 3.3.2**.** Instrument accuracy and precision were as specified previously. For the CONNECT campaign, unfiltered SML and ULW samples were frozen after collection and analysed at the University of York within two months. This contrasts with the coastal time-series (Chapter 3), where samples were analysed within 4 hours of collection at PML.

4.3.3 Ancillary Biogeochemical Measurements

Dissolved organic carbon (DOC), chlorophyll-a, phytoplankton cell counts, fatty acids, and nutrient concentrations were measured using the same analytical protocols described in Chapter 3, Section 3.3.4. Only campaign-specific analytical responsibilities differed:

DOC for CONNECT was analysed by Anja Engel.

Chlorophyll-a was determined by Rüdiger Röttgers (Hereon Institute).

Phytoplankton cell counts were conducted onboard and provided by Anja Engel.

Fatty acid analyses followed the protocol detailed in Weddell (2023).

Nitrate and phosphate concentrations were measured and provided by Hermann Bange (GEOMAR).

Full methodological details are provided in Chapter 3 and referenced studies

4.4 Results and Discussion

4.4.1 Surface-Microlayer Dynamics on the SO287–CONNECT Cruise

Unlike the English Channel campaign (PML campaign; see Section 3.4.5), fewer concurrent observations of biogeochemical variables in the SML are available for the CONNECT cruise. Nevertheless, synthesising these measurements with collocated physical data provides coherent biogeochemical patterns that influence SML composition and its role in air–sea exchange. These transect regions are characterized by oligotrophic surface waters—defined as waters with very low concentrations of bioavailable nutrients (typically nitrate $< 1\ \mu mol\ L^{-1}$ and phosphate $< 0.1\ \mu mol\ L^{-1}$) and low primary productivity (Falkowski et al. 1998; Moore et al. 2013; Fagan et al. 2022) compared to the tidally mixed, seasonally dynamic English Channel, yielding fundamentally different phytoplankton phenologies, carbon export pathways, and surface microlayer (SML) composition. We begin

by presenting surface tension and enrichment factors, then proceed through nutrient gradients, spatial biogeochemical patterns, microlayer composition, and physical forcing, before closing with a contrast between CONNECT and the English Channel.

4.4.2 Surface Tension and Enrichment Factors

Surface tension (ST) and surface tension enrichment factors (EF(ST)) measured across the SO287–CONNECT transect showed minimal variability and only modest tension depression relative to pure water (mean ST: 72.34 mN m^{-1}; range: 68.53–73.30 mN m^{-1}; mean EF(ST): 0.98; range: 0.94–0.99) (Figure 24-25). These values were tightly clustered near the baseline, indicating weak enrichment by surfactant-active substances and a relatively pristine microlayer in open-ocean settings. Given this narrow range, no correlation analyses between ST and environmental drivers were attempted. Instead, this section aims to describe spatial patterns in SML properties across the CONNECT transect and explore how physical and biogeochemical conditions shape microlayer dynamics in oligotrophic regimes.

4.4.3 Nutrient Gradients

Surface nutrient measurements (< 10 m) confirmed oligotrophic conditions, with mean nitrate and phosphate concentrations of 0.269 µmol L^{-1} and 0.051 µmol L^{-1}, respectively, well below thresholds typically associated with nutrient-rich regimes. As illustrated in Figure 36 (top panel), daily mean surface nitrate concentrations remained consistently below 1 µmol L^{-1} across most of the transect, often close to the detection limit, while phosphate was similarly depleted and rarely exceeded 0.1 µmol L^{-1} (Figure 36, bottom panel). While such low surface nutrient concentrations are expected in oligotrophic regions, their persistence highlights sustained nutrient limitation in the surface layer most relevant to SML processes. In contrast, the daily means for the entire water column (up to 5000 m) revealed substantially higher nutrient levels (nitrate: up to ~35 µmol L^{-1}; phosphate: up to ~2.5 µmol L^{-1}), reflecting strong vertical nutrient gradients typical of stratified gyre systems. This pronounced disparity between surface and subsurface layers highlights the nutrient

limitation experienced by surface microbial and phytoplankton communities, a hallmark of oligotrophic regimes. Even when considered on a surface-only scale, nutrient concentrations showed no systematic longitudinal trend, consistent with the minimal spatial variability observed in surface tension and EF(ST) across the CONNECT transect.

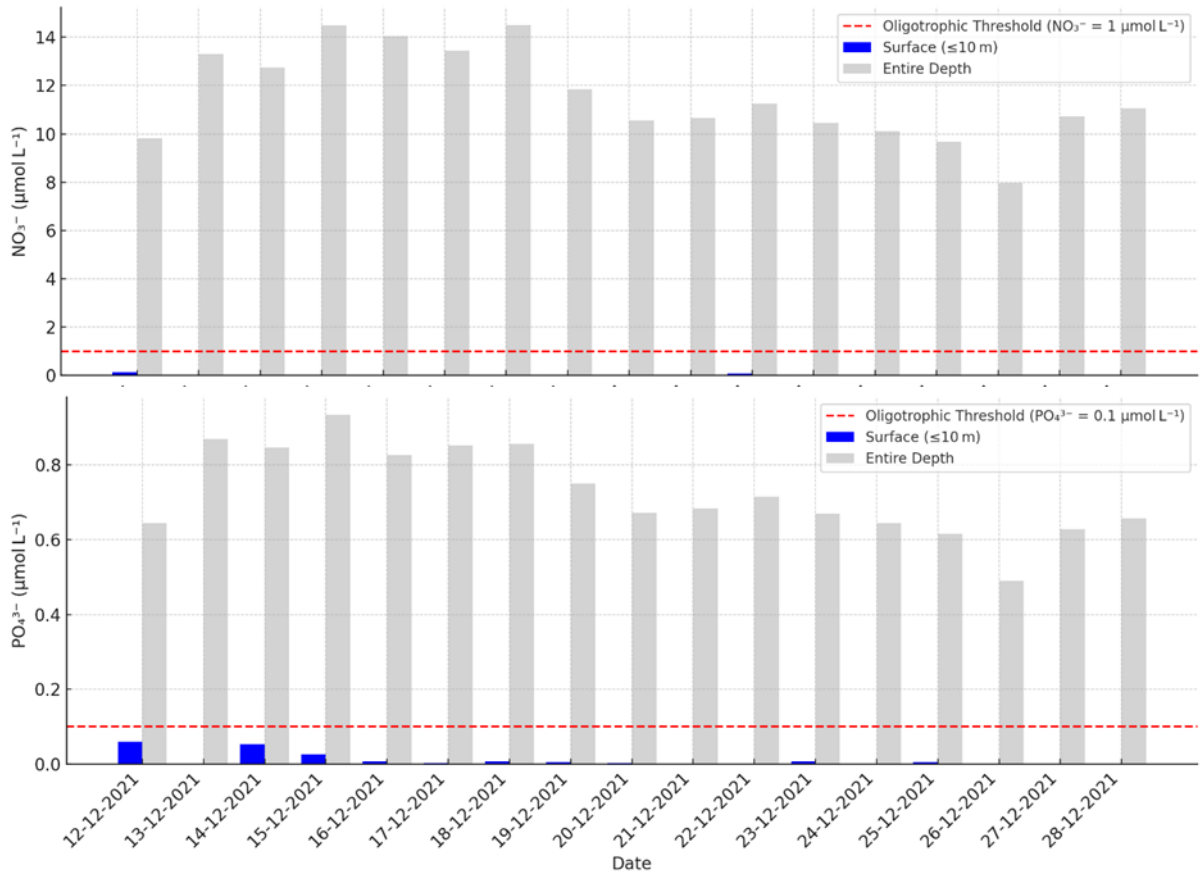

Figure 36: Daily mean nitrate (NO_3^-, top) and phosphate (PO_4^{3-}, bottom) concentrations along the SO287–CONNECT transect (12–28 Dec 2021). Grey bars show whole-water-column means (0–5000 m), and blue bars show surface values (≤ 10 m). Dashed red lines mark the oligotrophic thresholds for NO_3^- (1 µmol L^{-1}) and PO_4^{3-} (0.1 µmol L^{-1}), respectively.

4.4.4 Spatial Patterns (DOC/Chl-a/Cells)

To provide environmental context for interpreting SML properties, we examined dissolved organic carbon (DOC), chlorophyll-a, and phytoplankton cell counts along the SO287–CONNECT transect from 15° W (Las Palmas) to 80° W (Guayaquil) to highlight spatial trends (Figure 37).

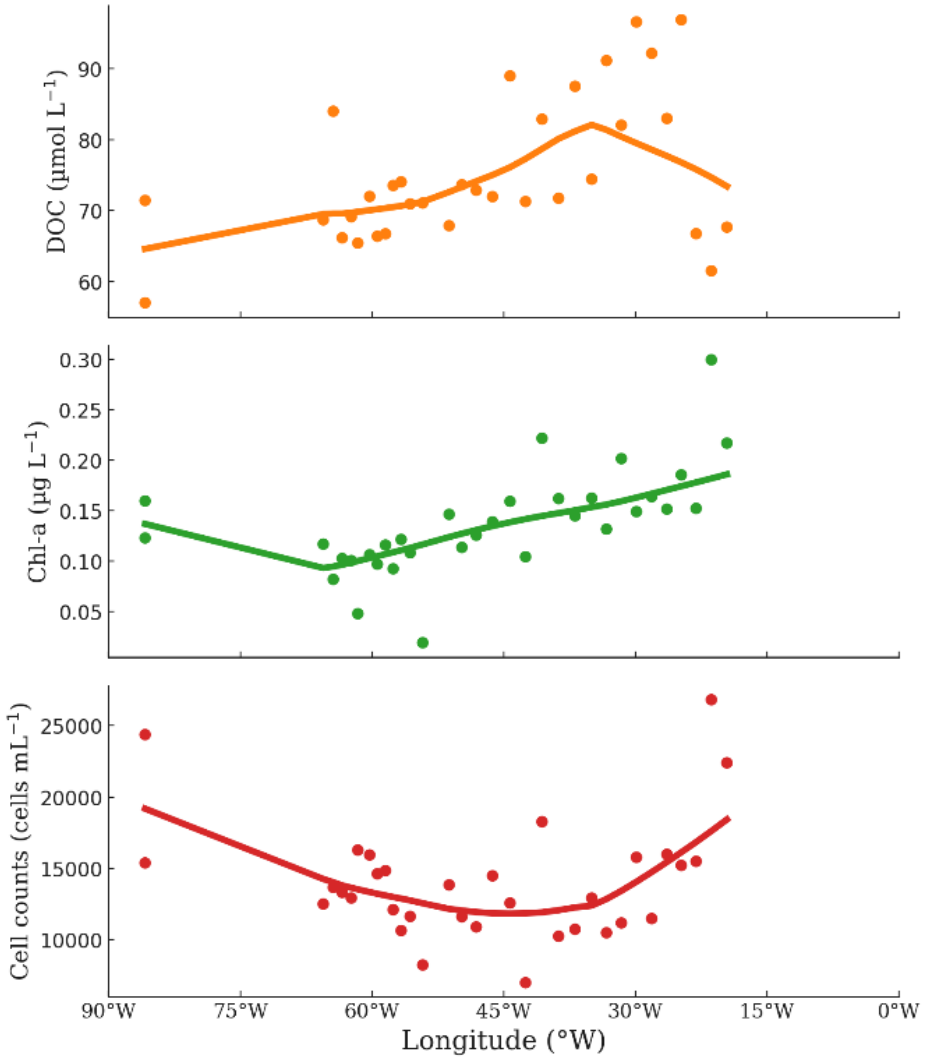

Figure 37: Spatial patterns of DOC (top), chlorophyll-a (middle), and phytoplankton cell counts (bottom) along the SO287–CONNECT transect. Dots show station means; lines indicate LOESS-smoothed trends.

This transect crosses the mid-Atlantic gyre (~45–55° W), a broad oligotrophic region that forms part of the North Atlantic Subtropical Gyre (Longhurst, 2007). This zone is characterized by persistently low chlorophyll-a concentrations (~0.08 µg L^{-1}) and reduced phytoplankton abundances (~9×10^3 cells mL^{-1}), consistent with strong stratification, nutrient limitation, and suppressed primary productivity typical of subtropical gyres. DOC concentrations were relatively stable across this region (~65–75 µmol L^{-1}), with occasional localized peaks but no sustained large-scale anomalies.

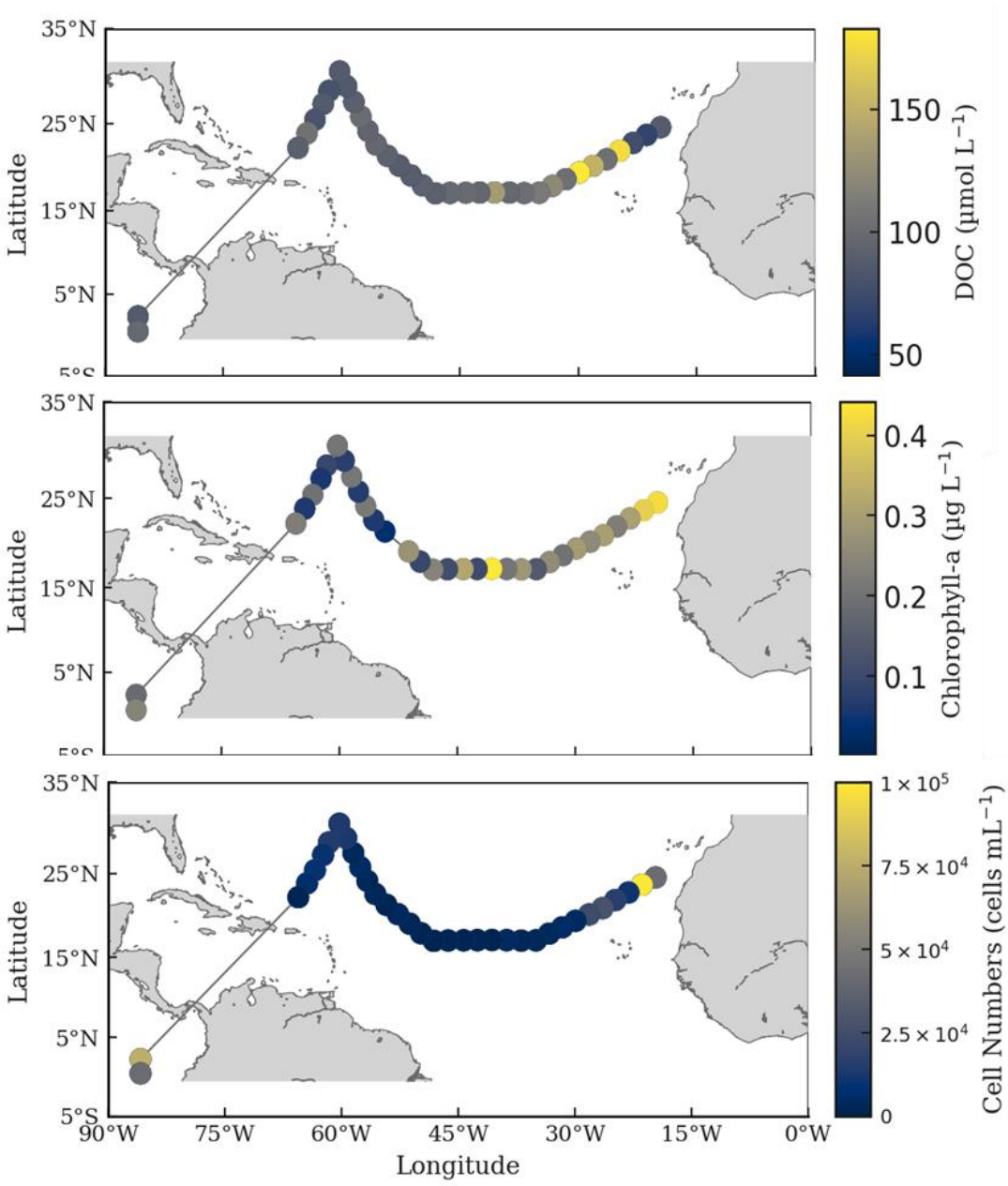

Figure 38: Spatial distributions of dissolved organic carbon (DOC), chlorophyll-a, and phytoplankton cell counts across the SO287–CONNECT transect. Colours represent concentration gradients at each station.

To link these longitudinal patterns back to geography, we mapped each station by latitude and longitude in Figure 38. At the eastern end of the transect (~15–25° W), chlorophyll-a concentrations increased slightly to ~0.18–0.20 µg L^{-1}, accompanied by higher phytoplankton cell counts (~2.5 × 10^4 cells mL^{-1}). DOC also showed a modest rise in this region, while surface tension values remained tightly clustered and showed no pronounced deviation from the low-variability background observed across the transect. These changes

may reflect enhanced biological activity near the eastern boundary, potentially influenced by physical processes such as nutrient entrainment or weak upwelling in the vicinity of the Canary Current system. By contrast, at the western end of the transect (~75–80° W), only minor increases in chlorophyll-a (~0.15–0.17 µg L^{-1}) and phytoplankton cell counts (~1.5 × 10^4 cells mL^{-1}) were observed. DOC concentrations remained within the range recorded across the mid-Atlantic gyre, and there was no strong evidence of pronounced biogeochemical enhancement in this region during the CONNECT cruise. Overall, only modest east–west biogeochemical gradients emerge under persistent oligotrophy.

4.4.5 Fatty Acids

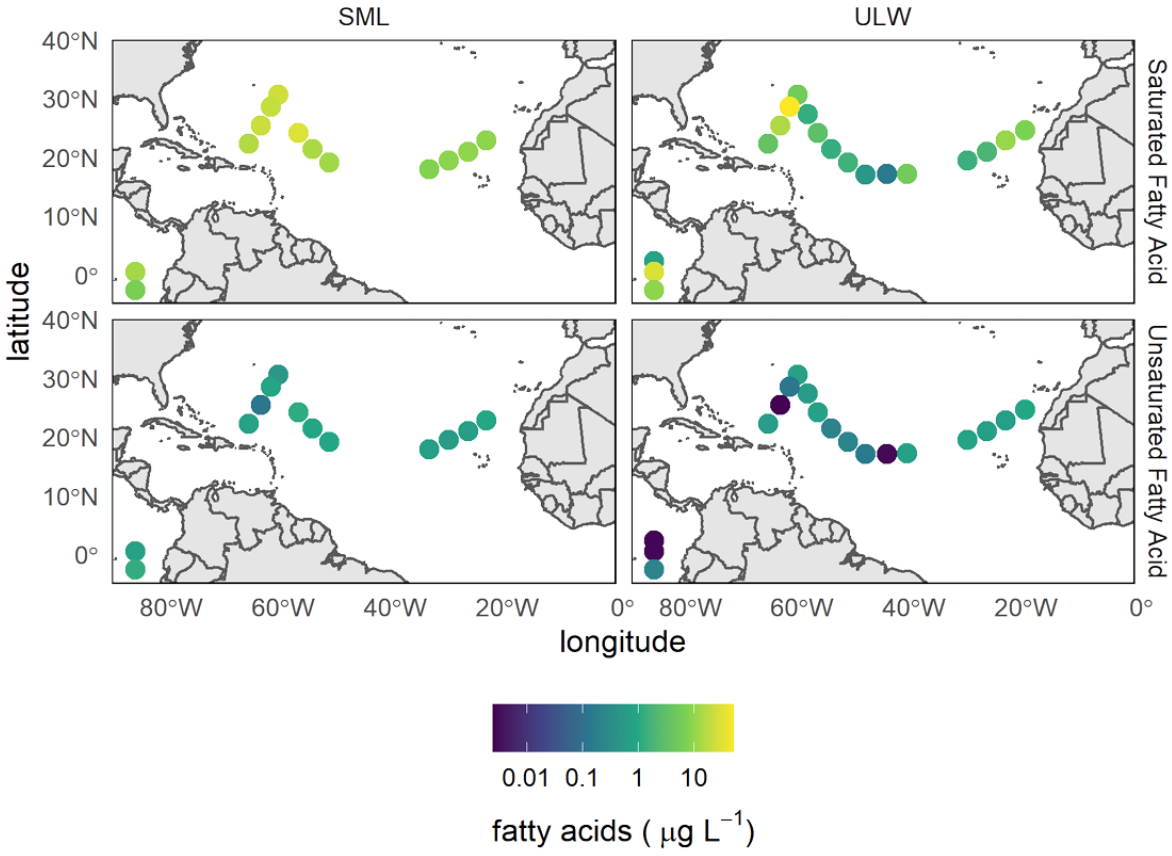

Figure 39: Concentrations of saturated and unsaturated fatty acids (µg L^{-1}) in the surface microlayer (SML) and underlying water (ULW) along the SO287–CONNECT transect.

Fatty acid analyses provided additional insights into microlayer composition (Figure 39). Mean total fatty acid concentrations in the SML (15.1 µg L^{-1}) were nearly double those of

the underlying water (ULW; 8.4 µg L^{-1}), indicating moderate microlayer enrichment. Saturated fatty acids dominated (SML: 14.4 µg L^{-1}; ULW: 8.1 µg L^{-1}), while unsaturated fatty acids, although minor in total mass (SML: 0.8 µg L^{-1}; ULW: 0.4 µg L^{-1}), exhibited higher enrichment factors (mean EF = 28.3; median = 2.7), reflecting their low background levels in the ULW. These findings confirm the presence of amphiphilic organic matter in the SML but suggest that fatty acids alone are unlikely to fully account for microlayer enrichment. The absence of simultaneous measurements of other classes of surfactant-active compounds (e.g., polysaccharides, proteins) precludes a complete assessment of their structural and functional roles in the surfactant film.

4.4.6 Physical Forcing (Wind & SST)

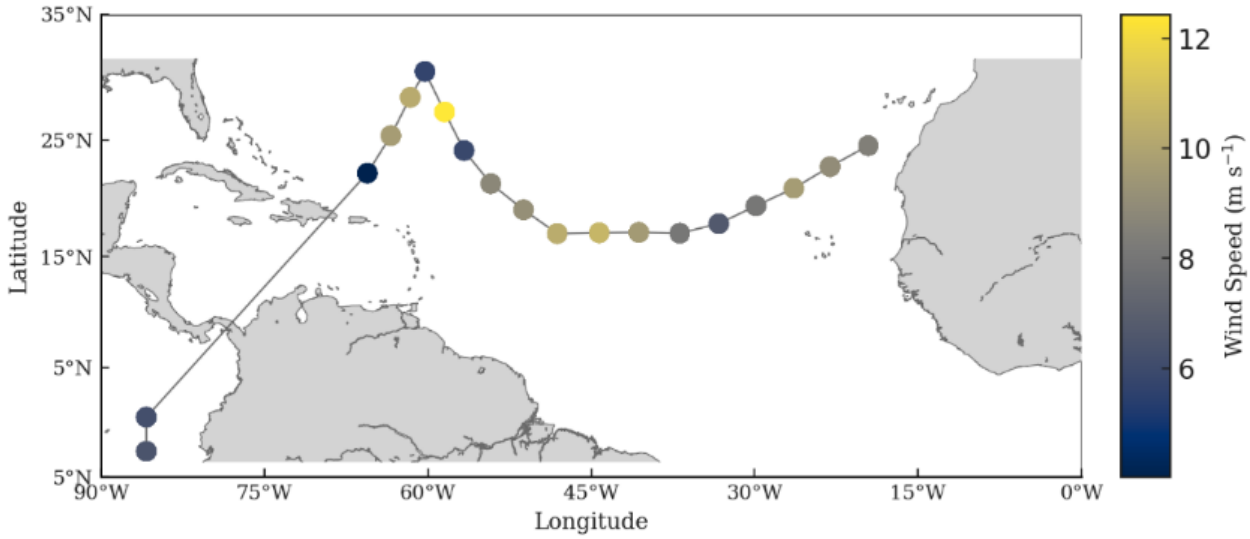

Figure 40: Wind speed (m s^{-1}) across the SO287–CONNECT transect, with colour gradients indicating variations at each station.

Wind speed along the SO287–CONNECT transect ranged from 4.03 m s^{-1} to a maximum of 12.44 m s^{-1}. Moderate winds prevailed in the early part of the transect, intensifying mid-cruise before subsiding towards the southern segment (Figure 40). Elevated turbulence in these high-wind areas likely deepens the mixed layer and disrupts the SML, potentially reducing the residence time of surfactants (Wurl et al., 2011; Cunliffe et al., 2013). However,

SML surface tension remained remarkably invariant across wind regimes. This suggests that wind forcing during CONNECT had limited measurable impact on microlayer enrichment.

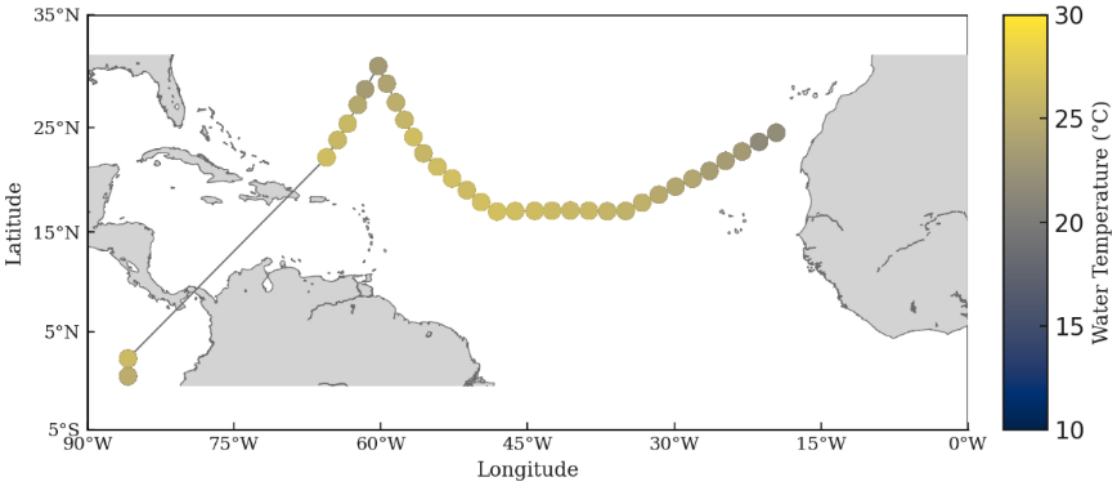

Figure 41: Sea surface temperature (°C) across the SO287–CONNECT transect, with colour gradients showing spatial variations at each station.

Sea surface temperature (SST) increased steadily from ~22 °C in the eastern Atlantic to a peak of ~26.5 °C in the mid-Atlantic, before declining to ~23 °C near the equatorial terminus (Figure 41). SST exerts dual influence on microlayer dynamics: physiologically, it regulates microbial and phytoplankton metabolic activity, potentially modulating surfactant exudation (Wurl et al., 2011); physically, it affects seawater viscosity and intrinsic surface tension. Light availability is a well-established control on phytoplankton production and extracellular organic matter release, and has been shown to influence the accumulation of biologically derived surface-active material in the SML through its coupling to stratification and mixed-layer depth. Although direct irradiance measurements were not available in this study, light is therefore expected to act as an indirect co-driver of surfactant enrichment along the transect.

4.4.7 CONNECT–Channel Comparison

As noted earlier in this chapter, fewer concurrent SML biogeochemical measurements were available for the CONNECT cruise than for the English Channel campaign; the comparison

below therefore focuses on contrasts that can be robustly supported by the available datasets. In the oligotrophic CONNECT region, surface nutrient scarcity and weak biogeochemical gradients—including only modest rises in chlorophyll-a, DOC, and fatty acids—proved insufficient to induce significant film enrichment. English Channel blooms drove SML surface tension depressions of >10 mN m^{-1} (EF > 1.3), whereas CONNECT transect values hovered near pure-water levels (mean ST 72.34 mN m^{-1}; EF ≈ 0.98). These contrasting outcomes reflect the dominant influence of trophic regime and mixing: nutrient-replete, seasonally dynamic coastal waters foster robust surfactant films, while stratified oligotrophy and physical disturbance in open-ocean gyres maintain a minimal, stable microlayer. Together, these findings underscore how nutrient availability and hydrodynamic forcing jointly govern the strength, variability, and persistence of surface-active films across marine settings, with implications for air–sea exchange processes.

Chapter 5: Conclusion, Future Study, and Recommendations

5.1 Conclusion

This thesis aimed to enhance our understanding of surfactant dynamics in marine surface microlayers (SML) through the investigation of surfactant stability under various storage conditions, and the quantification of surface tension (ST) and surfactant activity (SA) across diverse marine environments. Our analysis involved tensiometric and voltammetric methodologies, systematically applied to both coastal (English Channel) and oligotrophic open-ocean (CONNECT campaign) regimes.

We demonstrated that surfactant stability in stored SML samples is significantly influenced by storage temperature and preservation conditions, with deep-freezing at –80 °C better maintaining surfactant integrity (as measured by tensiometry) compared to refrigeration at 4 °C. Refrigerated samples showed substantial degradation relative to initial measurements (T_0), highlighting significant loss of surfactant activity. The established protocols successfully minimized alterations caused by microbial activity, photodegradation, and freeze–thaw cycles. These findings establish essential methodological benchmarks, addressing critical gaps in the literature concerning surfactant stability and storage-induced biases in marine microlayer analyses.

Field observations in the temperate coastal ocean revealed pronounced seasonal variability in surfactant film coverage ($\Delta\sigma$), closely aligned with phytoplankton biomass and sea-surface temperature (SST) fluctuations. Coastal waters displayed significantly broader $\Delta\sigma$ variability and higher surfactant enrichment factors (EF) relative to open-ocean settings, reflecting the influence of seasonal biological productivity in coastal waters compared to oligotrophic open-ocean regimes. A statistically significant positive relationship between phytoplankton biomass and film coverage ($r = 0.50$, $p = 0.001$) supported the dominance of biogenic surfactants, particularly under warmer spring and summer conditions. Nitrate

depletion was negatively correlated with surfactant enrichment ($r = –0.31$, $p = 0.013$), suggesting that enhanced surfactant concentrations coincide with phytoplankton-driven nutrient drawdown. These patterns highlight the intricate interplay between environmental forcing and biological surfactant dynamics.

Comparative analysis of tensiometric and voltammetric methodologies demonstrated their complementary nature. While tensiometry directly assessed surfactant-induced alterations in interfacial tension, voltammetry provided rapid and selective quantification of surfactants exhibiting similar adsorption properties to the TX-100 standard. Although voltammetric measurements offered practical advantages for rapid field assessment, tensiometry provided a more integrative characterization of surfactant coverage, highlighting the benefit of combining both methodologies.

Taken together, these outcomes provide critical insights for future air–sea gas-exchange models, emphasizing the importance of accurately representing SML dynamics, especially in regions influenced by phytoplankton blooms and nutrient cycling. Our comprehensive dataset significantly extends existing knowledge, refining current paradigms regarding surfactant enrichment processes and their spatial-temporal variability in marine ecosystems.

5.2 Recommendations

The findings presented in this thesis underline several key recommendations for methodological standardization and improved measurement reliability in marine surfactant studies:

1. Optimal Storage Protocols: Given the observed substantial degradation at 4°C, we strongly recommend deep-freezing at -80°C for the preservation of SML samples. Immediate freezing and at ultra-low temperature storage should be standard practice to ensure minimal surfactant loss.

2. Integrated Analytical Approaches: Employing complementary analytical techniques (tensiometry and voltammetry) provides robust, comprehensive characterization of surfactant dynamics. Future studies should consistently adopt such integrated methodologies to capture both bulk and specific surfactant behaviours.

3. Improved Temporal and Spatial Coverage: Long-term monitoring programs with regular sampling intervals are critical to understanding seasonal and interannual variability. Moreover, spatially diverse sampling across gradients from coastal to open ocean will refine understanding of terrestrial and anthropogenic impacts on marine surfactants.

4. Standardization of Analytical Calibration and Reporting: Uniform calibration standards and clear reporting of analytical protocols are essential. Establishing inter-laboratory calibration exercises could enhance reproducibility and comparability across global datasets.

5. Enhanced Methodological Innovation: Developing in situ tensiometry systems capable of operating aboard moving vessels will significantly improve real-time surfactant assessment and support more responsive environmental monitoring.

5.3 Future Study

While substantial progress has been made, further exploration into several promising areas remains essential:

- Molecular-Level Identification of Surfactants: Employing advanced analytical techniques, such as high-resolution mass spectrometry and nuclear magnetic resonance spectroscopy, can elucidate specific surfactant structures and their biogenic sources. Molecular-level identification will clarify mechanistic pathways linking phytoplankton biomass and nutrient dynamics with surfactant production.

- Climate Change Implications: Given the established linkage between SST, phytoplankton blooms, and surfactant enrichment, future research should explore surfactant dynamics under projected climate-change scenarios. Enhanced understanding of how warming ocean temperatures influence surfactant production, degradation, and air–sea interactions will be invaluable.
- Microbial Dynamics and Surfactant Production: Investigations focusing on microbial community structure and metabolic pathways can significantly improve understanding of microbial contributions to surfactant pools. Metagenomic and transcriptomic approaches offer promising avenues for this research.
- Global Modeling and Predictive Frameworks: Developing robust predictive models that incorporate surfactant dynamics into global biogeochemical and climate models is essential. High-resolution, process-based modeling approaches will significantly improve predictive capabilities for air–sea gas exchange under diverse marine conditions.
- Artificial Intelligence and Big Data Integration: Leveraging machine learning and artificial intelligence techniques to analyze large-scale datasets will aid in identifying complex patterns and interactions among multiple environmental variables. Such integrative approaches can enhance our understanding of surfactant dynamics at broader temporal and spatial scales.

In conclusion, the outcomes and recommendations of this thesis provide a foundation for advancing marine surfactant research through methodological refinement, interdisciplinary collaboration, and the application of innovative analytical techniques. Addressing the identified research gaps will support more accurate understanding and improved prediction of surfactant dynamics in marine ecosystems.

References

Abbott, S., 2017. Surfactant Science: Principles & Practice. Ipswich: DEStech Publications. (Also available at: https://www.stevenabbott.co.uk/practical-surfactants/)

ABP Marine Environmental Research Ltd., 2014. Mapping UK Shipping Density and Routed from AIS. The Marine Management Organisation, Newcastle, England.

Agogué, H., Casamayor, E.O., Bourrain, M., Obernosterer, I., Joux, F., Herndl, G.J. & Lebaron, P., 2004. Comparison of samplers for the biological characterization of the sea surface microlayer. Limnology and Oceanography: Methods, 2, pp.213–225.

Alexander, M.A., Blade, I., Newman, M., Lanzante, J.R., Lau, N.C. and Scott, J.D., 2000. The atmospheric bridge: Processes that influence sea surface temperature and ocean mixed layer depth variability in a coupled model. Journal of Climate, 15(16), pp.2205–2231. https://doi.org/10.1029/2000JC900074

Alpers, W. and Hühnerfuss, H. (1989) 'The damping of ocean waves by surface films: a new look at an old problem', Journal of Geophysical Research: Oceans, 94(C5), pp. 6251–6265. https://doi.org/10.1029/JC094iC05p06251

Amann, R.I., Ludwig, W. and Schleifer, K.H., 1995. Phylogenetic identification and in situ detection of individual microbial cells without cultivation. Microbiological Reviews, 59(1), pp.143–169.

Andersson, B. and Olofsson, G., 1988. [No title available]. Journal of the Chemical Society, Faraday Transactions 1, 84, pp.4087–4096.

Andren, A.W., Elzerman, A.W. and Armstrong, D.E., 1976. [No title available]. Journal of Great Lakes Research, 2, pp.101–110.

Asher, W.E. (1997) 'The sea-surface microlayer and its effect on global air-sea gas transfer', The sea surface and global change, pp. 251-286.

Astoreca, R., Rousseau, V. and Lancelot, C., 2009. Coloured dissolved organic matter (CDOM) in Southern North Sea waters: Optical characterization and possible origin. Estuarine, Coastal and Shelf Science, 85(4), pp.633–640.

Authelin, J.-R., et al. (2020). Freezing of biologicals revisited: A decade of progress. Journal of Pharmaceutical Sciences, 109(1), 31–44.

Atkins, P., 2014. Atkins' Physical Chemistry. 10th ed. Oxford: Oxford University Press.

Azam, F., 1998. Microbial control of oceanic carbon flux: the plot thickens. Science, 280(5364), pp.694–696.

Baker, A., 2002. Fluorescence properties of some farm wastes: implications for water quality monitoring. Water Research, 36(1), pp.189–195.

Barker, D.R. and Zeitlin, H. (1972) 'Metal‐ion concentrations in sea‐surface microlayer and size‐separated atmospheric aerosol samples in Hawaii', Journal of Geophysical Research, 77(27), pp. 5076-5086

Barthelmeß, T., Schütte, F. and Engel, A., 2021. Variability of the sea surface microlayer across a filament's edge and potential influences on gas exchange. Frontiers in Marine Science, 8, https://doi.org/10.3389/fmars.2021.718384.

Barthelmeß, J. & Engel, A. (2022). How biogenic polymers control surfactant dynamics in the surface microlayer: insights from a coastal Baltic Sea study. Biogeosciences, 19(24), 4965–4983. https://doi.org/10.5194/bg-19-4965-2022

Beaumont, N.J., Austen, M.C., Atkins, J.P., Burdon, D., Degraer, S., Dentinho, T.P., Derous, S., Holm, P., Horton, T., van Ierland, E., Marboe, A.H., Starkey, D.J.,

Townsend, M. and Zarzycki, T., 2007. Identification, definition and quantification of goods and services provided by marine biodiversity: Implications for the ecosystem approach. Marine Pollution Bulletin, 54, pp.253–265.

Behrenfeld, M.J., O'Malley, R.T., Siegel, D.A., McClain, C.R., Sarmiento, J.L., Feldman, G.C., Milligan, A.J., Falkowski, P.G., Letelier, R.M. and Boss, E.S., 2006. Climate-driven trends in contemporary ocean productivity. Nature, 444(7120), pp.752–755.

Bendure, R. L. (1971). Dynamic surface tension determination with the maximum bubble pressure method. Journal of Colloid and Interface Science, 35, 238–248.

Bolin, B., 1960. Tellus, 12, pp.274–281.

Broecker, W.S. and Peng, T.-H., 1974. Gas exchange rates between air and sea. Tellus, 26(1–2), pp.21–35. https://doi.org/10.3402/tellusa.v26i1-2.9733.

Brown, E., Colling, A., Park, D., Phillips, J., Rothery, D. and Wright, J., 1997. Seawater: Its composition, properties and behaviour. Butterworth-Heinemann, Oxford.

Brüggemann, M., Hayeck, N. and George, C. (2018) 'Interfacial photochemistry at the ocean surface is a global source of organic vapors and aerosols', Nature Communications, 9, p. 2101. https://doi.org/10.1038/s41467-018-04528-7.

Burrows, S.M., Easter, R.C., Liu, X., Ma, P.-L., Wang, H., Elliott, S.M., Singh, B., Zhang, K. and Rasch, P.J. (2022) 'OCEANFILMS (Organic Compounds from Ecosystems to Aerosols: Natural Films and Interfaces via Langmuir Molecular Surfactants) sea spray organic aerosol emissions – implementation in a global climate model and impacts on clouds', Atmospheric Chemistry and Physics, 22(8), pp. 5223–5252. https://doi.org/10.5194/acp-22-5223-2022

Carlson, C.A. (2002) 'Production and removal processes', Biogeochemistry of marine dissolved organic matter, pp. 91-151.

Carlson, C.A., Ducklow, H.W. and Sleeter, T.D. (1996) 'Stocks and dynamics of bacterioplankton in the northwestern Sargasso Sea', Deep Sea Research Part II: Topical Studies in Oceanography, 43(2-3), pp. 491-515.

Carlson, D.J. (1982) 'A field evaluation of plate and screen microlayer sampling techniques', Marine Chemistry, 11(3), pp. 189-208.

Carlson, D.J. (2013) 'The early diagenesis of organic matter: reaction at the air-sea interface', Organic Geochemistry MH Engel, SA Macko, pp. 255-268.

Carlson, D.J., 1983. Dissolved organic materials in surface microlayers: Temporal and spatial variability and relation to sea state. Limnology and Oceanography, 28(3), pp.415–431.

Carlson, D.J., 2013. The early diagenesis of organic matter: reaction at the air-sea interface. In: Engel, M.H. and Macko, S.A., eds. Organic Geochemistry. pp.255–268.

Carlucci, A.F., Craven, D.B. and Wolgast, D.M., 1991. Marine Biology, 108, pp.329–339.

Carpenter, L.J. and Nightingale, P.D., 2015. Chemistry and release of gases from the surface ocean. Chemical Reviews, 115(10), pp.4015–4034.

Castrejón-Godínez, M.L., Tovar-Sánchez, E., Valencia-Cuevas, L., Rosas-Ramírez, M.E., Rodríguez, A. and Mussali-Galante, P. (2021) ‘Glyphosate pollution treatment and microbial degradation alternatives, a review’, Microorganisms, 9(11), p. 2322. https://doi.org/10.3390/microorganisms9112322.

Chang, W.N., Heikes, B.G. and Lee, M.H., 2004. Ozone deposition to the sea surface: chemical enhancement and wind speed dependence, Atmospheric Environment, 38, pp.1053–1059.

Chang, T. & Zhao, G. (2021). Ice Inhibition for Cryopreservation: Materials, Strategies, and Challenges. Advanced Science, 8(5), 2002425.

Chen, W., Westerhoff, P., Leenheer, J.A. and Booksh, K. (2003) 'Fluorescence excitation− emission matrix regional integration to quantify spectra for dissolved organic matter', Environmental science & technology, 37(24), pp. 5701-5710.

Cincinelli, A., Stortini, A.M., Perugini, M., Checchini, L. and Lepri, L. (2001) 'Organic pollutants in sea-surface microlayer and aerosol in the coastal environment of Leghorn- (Tyrrhenian Sea)', Marine Chemistry, 76(1), pp. 77-98

Clesceri, L.S., 1998. Standard Methods for the Examination of Water and Wastewater, 20th edn. American Public Health Association, Washington D.C.

Clifford, D., Donaldson, D.J., Brigante, M., D'Anna, B. and George, C., 2008. Environmental Science and Technology, 42, pp.1138–1143.

Compiano, A., Romano, J., Garabetian, F., Laborde, P. and de la Giraudièrea, I., 1993. Marine Chemistry, 42, pp.237–251.

Ćosović, B. and Vojvodic, V., 1982. Limnology and Oceanography, 27, pp.361–369.

Ćosović, B. and Vojvodić, V., 1998. Voltammetric analysis of surface-active substances in seawater. Electroanalysis, 10(6), pp.429–434.

Croot, P.L., Passow, U., Assmy, P., Jansen, S. and Strass, V.H. (2007) 'Surface active substances in the upper water column during a Southern Ocean Iron Fertilization Experiment (EIFEX)', Geophysical research letters, 34(3).

Ciuraru, R., Fine, L., van Pinxteren, M., D'Anna, B., Herrmann, H. and George, C., 2015. Photosensitized production of functionalized and unsaturated organic compounds at the air–sea interface. Scientific Reports, 5, p.12741. https://doi.org/10.1038/srep12741

Cunliffe, M. and Murrell, J.C., 2009. The sea-surface microlayer is a gelatinous biofilm. The ISME Journal, 3(9), p.1001

Cunliffe, M., Engel, A., Frka, S., Gašparović, B., Guitart, C., Murrell, J.C., Salter, M., Stolle, C., Upstill-Goddard, R. and Wurl, O. (2013) 'Sea surface microlayers: A unified physicochemical and biological perspective of the air–ocean interface', Progress in Oceanography, 109, pp. 104-116.

Cunliffe, M., Harrison, E., Salter, M., Schafer, H., Upstill-Goddard, R.C. and Murrell, J.C., 2009. Aquatic Microbial Ecology, 57, pp.69–77.

Cochran, R.E., Laskina, O., Jayarathne, T., Laskin, A., Laskin, J., Lin, P., Sultana, C., Lee, C., Moore, K.A., Cappa, C.D., Bertram, T.H., Prather, K.A., Grassian, V.H. and Stone, E.A. (2016) 'Molecular diversity of sea spray aerosol particles: Impact of ocean biology on particle composition and hygroscopicity', Environmental Science & Technology, 50, pp. 2477–2486. https://doi.org/10.1021/acs.est.5b04136

Dettre, R.H. & Johnson, R.E. (1966). Contact angle measurements with the Wilhelmy plate. Journal of Colloid and Interface Science, 21, 367–377.

Dittmar, T., Koch, B., Hertkorn, N. and Kattner, G., 2008. Limnology and Oceanography: Methods, 6, pp.230–235.

Donelan, M.A., Drennan, W.M., Saltzmann, E.S. and Wanninkhof, R. (Eds.), 2002. Gas Transfer at Water Surfaces. American Geophysical Union, Washington D.C.

Doney, S.C., Ruckelshaus, M., Duffy, J.E., Barry, J.P., Chan, F., English, C.A., Galindo, H.M., Grebmeier, J.M., Hollowed, A.B., Knowlton, N., Polovina, J., Rabalais, N.N., Sydeman, W.J. and Talley, L.D., 2012. Climate change impacts on marine ecosystems. Annual Review of Marine Science, 4, pp.11–37. https://doi.org/10.1146/annurev-marine-041911-111611

Du Noüy, P.L., 1925. Journal of General Physiology, 7, pp.625–632.

Engel A, Bange HW, Cunliffe M, Burrows SM, Friedrichs G, Galgani L, Herrmann H, Hertkorn N, Johnson M, Liss PS, Quinn PK, Schartau M, Soloviev A, Stolle C, Upstill-Goddard RC, van Pinxteren M, Zäncker B (2017) The Ocean's vital skin: toward an integrated understanding of the sea surface microlayer. Front Mar Sci 4:165. https://doi.org/10.3389/fmars.2017.00165

Environment Agency, 2018. Water Body: GB104026066630. Available at: http://environment.data.gov.uk/catchment-planning/WaterBody/GB104026066630 [Accessed May 2018].

Environment Agency, 2018. Water Body: GB104026066640. Available at: http://environment.data.gov.uk/catchment-planning/WaterBody/GB104026066640 [Accessed May 2018].

Environment Agency, 2018. Water Body: GB104026066650. Available at: http://environment.data.gov.uk/catchment-planning/WaterBody/GB104026066650 [Accessed May 2018].

Environment Agency, 2018. Water Body: GB104026072780. Available at: http://environment.data.gov.uk/catchment-planning/WaterBody/GB104026072780 [Accessed May 2018].

Environment Agency, 2018. Water Body: GB104026072790. Available at: http://environment.data.gov.uk/catchment-planning/WaterBody/GB104026072790 [Accessed May 2018].

Environment Agency, 2018. Water Body: GB104026077770. Available at: http://environment.data.gov.uk/catchment-planning/WaterBody/GB104026077770 [Accessed May 2018].

Environment Agency, 2018. Water Body: GB104026077780. Available at: http://environment.data.gov.uk/catchment-planning/WaterBody/GB104026077780 [Accessed May 2018].

Estep, K.W., Maki, J.S., Danos, S.C. and Remsen, C.C., 1985. Freshwater Biology, 15, pp.15–19.

Falkowska, L. and Piekarek-Jankowska, H., 1999. ICES Journal of Marine Science, 56, pp.153–160.

Flickr, 2018. [Dr. Slippers Flickr Photo Set]. Available at: https://www.flickr.com/photos/drslippers/sets/72157602458120713/ (Accessed: May 2018).

Frew, N. M., Goldman, J. C., Dennett, M. R., Johnson, A. S., 1990. Impact of phytoplankton-generated surfactants on air–sea gas exchange. Journal of Geophysical Research 95, 3337–3352.

Frew, N.M., 1997. The role of organic films in air–sea gas exchange. In: P.S. Liss and R.A. Duce, eds. The Sea Surface and Global Change. Cambridge: Cambridge University Press, pp. 121–172.

Frka, S., Kozarac, Z. and Ćosović, B. (2009) 'Characterization and seasonal variations of surface-active substances in the natural sea surface micro-layers of the coastal Middle Adriatic stations', Estuarine, coastal and shelf science, 85(4), pp. 555-564.

Gade, M., Hühnerfuss, H. and Korenowski, G.M. (Eds.), 2006. Marine Surface Films: Chemical Characteristics, Influence on Air-Sea Interactions and Remote Sensing. Springer-Verlag, Berlin.

Gantt, B., Meskhidze, N. and Carlton, A.G., 2010. Atmospheric Chemistry and Physics, 10, pp.7415–7423.

Ganzeveld, L., Helmig, D., Fairall, C.W., Hare, J. and Pozzer, A., 2009. Global Biogeochemical Cycles, 23, DOI: 10.1029/2008GB003301.

Gao, Q., Leck, C., Rauschenberg, C. and Matrai, P.A., 2012. On the chemical dynamics of extracellular polysaccharides in the high Arctic surface microlayer. Ocean Science, 8(4), pp.401–418.

Garland, J.A., Elzerman, A.W. and Penkett, S.A., 1980. Journal of Geophysical Research: Oceans and Atmospheres, 85, pp.7488–7492.

Garrett, W.D., 1965. Limnology and Oceanography, 10, pp.602–605.

Găsparović, B. and Ćosović, B., 2001. Marine Chemistry, 75, pp.301–313.

Goldacre, R.J., 1949. [No title available]. Journal of Animal Ecology, 18, pp.36–39.

Hamilton, B., Dean, C., Kurata, N., Vella, K., Soloviev, A., Tartar, A., Shivji, M., Perrie, W. and Lehner, S., 2014. Proceedings of the 2014 IEEE International Geoscience & Remote Sensing Symposium and 35th Canadian Symposium on Remote Sensing. IEEE Xplore.

Hamilton, E.I. and Clifton, R.J., 1979. Techniques for sampling the air‐sea interface for estuarine and coastal waters. Limnology and Oceanography, 24(1), pp.188‐193.

Hansell, D.A. and Carlson, C.A. (2014) Biogeochemistry of marine dissolved organic matter. Academic Press.

Hansell, D.A., Carlson, C.A., Repeta, D.J. and Schlitzer, R. (2009) 'Dissolved organic matter in the ocean: A controversy stimulates new insights', Oceanography, 22(4), pp. 202–211.

Hansell, D.A., 2013. Recalcitrant dissolved organic carbon fractions. Annual Review of Marine Science, 5, pp.421–445.

Hardy, J.T., Crecelius, E.A., Antrim, L.D., Kiesser, S.L., Broadhurst, V.L., Boehm, P.D., Steinhauer, W.G. and Coogan, T.H. (1990) 'Aquatic surface microlayer contamination in Chesapeake Bay', Marine Chemistry, 28(4), pp. 333-351.

Harkins, W.D. and Jordan, H.F., 1930. Journal of the American Chemical Society, 52, pp.1751–1772.

Harkins, W.D., Brown, F.E. and Davies, E.C.H., 1917. Journal of the American Chemical Society, 39, pp.354–364.

Harvey, G.W. and Burzell, L.A., 1972. A simple microlayer method for small samples. Limnology and Oceanography, 17(1), pp.156–157.

Harvey, G.W., 1966. Limnology and Oceanography, 11, pp.608–613.

Hatcher, R.F. and Parker, B.C., 1974. Limnology and Oceanography, 19, pp.162–165.

Hayase, S., Yabushita, A., Kawasaki, M., Enami, S., Hoffmann, M.R. and Colussi, A.J., 2010. Journal of Physical Chemistry, 114, pp.6016–6021.

Heydarizadeh, P., Poirier, I., Loizeau, D., Ulmann, L., Mimouni, V., Schoefs, B. and Bertrand, M. (2013) Marine Drugs, 11, pp. 3425–3471.

Henson, S., Beaulieu, C., Ilyina, T., Sarmiento, J.L., Dunne, J.P., Bopp, L., Séférian, R., Lima, I.D., Romanou, A. and Slater, R.D. (2017) 'Rapid emergence of climate change in environmental drivers of marine ecosystems', Nature Communications, 8, 14682. https://doi.org/10.1038/ncomms14682

Horrocks, L.A., Candy, B., Nightingale, T.J., Saunders, R.W., O'Carroll, A., Harris, A.R., 2003. Journal of Geophysical Research, 108, DOI: 10.1029/2002JC001503.

Hunter, K.A. and Liss, P.S., 1982. Organic sea surface films. In: E.K. Duursma and R. Dawson, eds. Marine Organic Chemistry. Amsterdam: Elsevier, pp.259–298

Hunter, K.A., 1975. Chemistry of the sea surface microlayer. In: P.S. Liss and R.A. Duce (eds.) Chemical Oceanography. Cambridge University Press, Cambridge, pp. 287–319.

Hunter, K.A., 1997. Chemistry of the sea-surface microlayer. In: P.S. Liss and R.A. Duce (eds.) The Sea Surface and Global Change. Cambridge University Press, Cambridge, pp. 287–319.

Hunt, C.J., 2017. Cryopreservation: vitrification and controlled rate cooling. Cryopreservation and Freeze-Drying Protocols. Springer, New York, NY. Available at: https://link.springer.com/protocol/10.1007/978-1-4939-6921-0_5

Ignatiades, L., 1987. Marine Ecology Progress Series, 39, pp.207–208.

IPCC (2019) IPCC Special Report on the Ocean and Cryosphere in a Changing Climate. Pörtner, H.-O., Roberts, D.C., Masson-Delmotte, V., Zhai, P., Tignor, M., Poloczanska, E., Mintenbeck, K., Alegría, A., Nicolai, M., Okem, A., Petzold, J.,

Rama, B. and Weyer, N.M. (eds.). Cambridge University Press, Cambridge, UK and New York, NY, USA, 755 pp. https://doi.org/10.1017/9781009157964

Korshin, G.V., Li, C.-W. and Benjamin, M.M. (1997) 'Monitoring the properties of natural organic matter through UV spectroscopy: a consistent theory', Water Research, 31(7), pp. 1787-1795.

Kowalczuk, P., Tilstone, G.H., Zabłocka, M., Röttgers, R. and Thomas, R. (2013) 'Composition of dissolved organic matter along an Atlantic Meridional Transect from fluorescence spectroscopy and Parallel Factor Analysis', Marine Chemistry, 157, pp. 170-184.

Kujawinski, E.B. (2011) ‘The impact of microbial metabolism on marine dissolved organic matter’, Annual Review of Marine Science, 3, pp. 567–599. https://doi.org/10.1146/annurev-marine-120308-081003

Kiørboe, T. & Hansen, J.L.S. (1993). Phytoplankton aggregate formation: observations of patterns and mechanisms of cell sticking and the significance of exopolymeric material . Journal of Plankton Research, 15, 993–1018.

Kushkevych, I., et al. (2021). Distribution of Sulfate-Reducing Bacteria in the Environment: Cryopreservation Techniques and Their Potential Storage Application. Processes, 9(10), 1843.

Kurata, N., Vella, K., Hamilton, B., Shivji, M., Soloviev, A., Matt, S., Tartar, A. and Perrie, W., 2016. Surfactant-associated bacteria in the near-surface layer of the ocean. Scientific Reports, 6, DOI: 10.1038/srep19123.

Kuznetsova, M. and Lee, C., 2001. Enhanced extracellular enzymatic peptide hydrolysis in the sea-surface microlayer. Marine Chemistry, 73, pp.319–332.

Kuznetsova, M., Lee, C. & Aller, J. (2005). Characterization of the proteinaceous matter in marine aerosols. Marine Chemistry, 96(3–4), 229–242.

Kou H., Li W., Zhang X., Xu N., Zhang X., Shao J., Ma J., Deng Y. (2019). Temperature-dependent coefficient of surface tension prediction model without arbitrary parameters. *Fluid Phase Equilibria*, 497, 201–214

Laha, S., Tansel, B. and Ussawarujikulchai, A., 2009. Journal of Environmental Management, 90(1), pp.95–100.

Laidler, K.J., 1987. Chemical Kinetics. 3rd ed. New York: Harper & Row.

Lapham, G.S., Dowling, D.R. & Schultz, W.W. (1999). In situ force-balance tensiometry. Springer Verlag, 27.

Large, W.G., McWilliams, J.C. and Doney, S.C. (1994). Ocean vertical mixing: A review and a model with a nonlocal boundary layer parameterization. Reviews of Geophysics, 32(4), 363–403.

Lee, C. and Wakeham, S.G., 1988. Organic matter in seawater: biogeochemical processes. In: J.P. Riley, ed. Chemical Oceanography, vol. 9. San Diego, CA: Academic Press, pp.1–49

Li, W.K.W. (2002). Primary production of prochlorophytes, cyanobacteria, and eukaryotic ultraphytoplankton: Measurements from flow cytometry. *Limnology and Oceanography*, 47(1), 203–213.

Liss, P.S. and Martinelli, F.N., 1978. The effect of oil films on the transfer of oxygen and water vapour across an air–water interface. Thalassia Jugoslavica, 14(1/2), pp.215–220.

Liss, P.S. and Merlivat, L. (1986) Air–sea gas exchange rates: introduction and synthesis. In: Buat-Ménard, P. (ed.) The Role of Air–Sea Exchange in Geochemical Cycling. NATO ASI Series (Series C: Mathematical and Physical Sciences), vol 185. Dordrecht: Springer, pp. 113–127. https://doi.org/10.1007/978-94-009-4738-2_5

Liss, P.S. and Slater, P.G., 1974. Flux of gases across the air–sea interface. Nature, 247(5438), pp.181–184.

Liss, P.S., 1975. Chemistry of the sea surface microlayer. Chemical Oceanography, 2, pp.193–243.

Liss, P.S., Liss, P.S. and Duce, R.A. (2005) 'The sea surface and global change', in The sea surface and global change Cambridge University Press, pp. 121-172.

MacIntyre, F., 1968. Journal of Physical Chemistry, 72, pp.589–592.

Marañón, E., Holligan, P.M., Barciela, R., González, N., Mouriño, B., Pazó, M.J. and Varela, M. (2001). Patterns of phytoplankton size structure and productivity in contrasting open-ocean environments. Marine Ecology Progress Series, 216, 43–56.

Marguš, M., Morales-Reyes, I., Bura-Nakić, E., Batina, N. and Cigleneč, I., 2015. Continental Shelf Research, 109, pp.24–34.

Martino, M., Lézé, B., Baker, A.R. and Liss, P.S., 2012. Geophysical Research Letters, 39, DOI: 10.1029/2011GL050282.

Mazurek, Z.A., Pogorzelski, J.S. and Boniewicz-Szmyt, K. (2008) 'Evolution of natural sea surface film structure as a tool for organic matter dynamics tracing', Journal of Marine Systems, 74, pp. S52-S64.

McKnight, D.M., Boyer, E.W., Westerhoff, P.K., Doran, P.T., Kulbe, T. and Andersen, D.T. (2001) 'Spectrofluorometric characterization of dissolved organic matter for indication of precursor organic material and aromaticity', Limnology and Oceanography, 46(1), pp. 38-48.

McLeish, W. and Putland, G.E., 1975. Journal of Physical Oceanography, 5, pp.516–518.

Meskhidze, N., Xu, J., Gantt, B., Zhang, Y., Nenes, A., Ghan, S.J., Liu, X., Easter, R. and Zaveri, R., 2011. Atmospheric Chemistry and Physics, 11, pp.11689–11705.

MILAN Data, unpublished work.

Momzikoff, A., Brinis, A., Dallot, S., Gondry, G., Saliot, A. and Lebaron, P., 2004. Field study of the chemical characterization of the upper ocean surface using various samplers. Limnology and Oceanography: Methods, 2, pp.374–386.

Modini, R.L., Russell, L.M., Deane, G.B. and Stokes, M.D. (2013) ‘Effect of soluble surfactant on bubble persistence and bubble-produced aerosol particles’, Journal of Geophysical Research: Atmospheres, 118(3), pp. 1388–1400. https://doi.org/10.1002/jgrd.50186

Mumford, S.A. and Phillips, J.W.C., 1950. [No title available]. Journal of the Chemical Society, 0, pp.75–84.

Mühlroth, A., Li, K., Røkke, G., Winge, P., Olsen, Y., Hohmann-Marriott, M.F., Vadstein, O. and Bones, A.M. (2013) 'Pathways of lipid metabolism in marine algae, co-expression network, bottlenecks and candidate genes for enhanced production of EPA and DHA in species of Chromista', Marine Drugs, 11, pp. 4662–4697. https://doi.org/10.3390/md11114662

Murray, K.A. and Gibson, M.I. (2022) 'Chemical approaches to cryopreservation', Nature Reviews Chemistry, 6, pp. 579–593. https://doi.org/10.1038/s41570-022-00407-4.

Mungall, E.L., Abbatt, J.P.D., Wentzell, J.J.B., Lee, A.K.Y., Thomas, J.L., Blais, M., Gosselin, M., Miller, L.A., Papakyriakou, T., Willis, M.D., Liggio, J., 2017. Proceedings of the National Academy of Sciences (PNAS), 114, pp.6203–6208.

Myklestad, S., Djurhuus, R., Mohus, A., 1982. Determination of exo-(β-1,3)-dglucanase activity in some planktonic diatoms. Journal of Experimental Marine Biology and Ecology 56, 205–211.

Nayar, K.G., Panchanathan, D., McKinley, G.H. and Lienhard V, J.H., 2014. Journal of Physical and Chemical Reference Data, 43, https://doi.org/10.1063/1.4899037.

Nightingale, P.D., 2009. Surface Ocean–Lower Atmosphere Processes. In: Quéré, C.L. and Saltzmann, E.S. (Eds.), American Geophysical Union, Washington D.C., Vol. 187, Chapter 6, pp.69–97.

Nightingale, P.D., Liss, P.S. and Schlosser, P. (2000) 'Measurements of air–sea gas transfer during an open ocean algal bloom', Geophysical Research Letters, 27(14), pp. 2117–2120. https://doi.org/10.1029/2000GL011541

O'Dowd, C., Facchini, M., Cavalli, F., Ceburnis, D., Mircea, M., Decesari, S., Fuzzi, S., Yoon, Y.J. and Putaud, J.P. (2004) 'Biogenically driven organic contribution to marine aerosol', Nature, 431, pp. 676–680. https://doi.org/10.1038/nature02959

Passow, U. (2002). Transparent exopolymer particles (TEP) in aquatic environments. Progress in Oceanography, 55(3–4), 287–333.

Passow, U. and Alldredge, A.L. (1999) 'Do transparent exopolymer particles (TEP) inhibit grazing by the euphausiid Euphausia pacifica?', Journal of Plankton Research, 21(11), pp. 2203–2217. https://doi.org/10.1093/plankt/21.11.2203

Pallas, N.R. & Pethica, B.A. (1983). Wilhelmy plate studies of water. Colloids and Surfaces, 6, 221–227.

Pingree, R.D. and Griffiths, D.K., 1978. Tidal fronts on the shelf seas around the British Isles. Journal of Geophysical Research: Oceans and Atmospheres, 83, pp.4615–4622.

Pollard, J.M., Shi, A.J. and Göklen, K.E. (2006) 'Solubility and partitioning behavior of surfactants and additives used in bioprocesses', Journal of Chemical & Engineering Data, 51(1), pp. 230-236.

Pereira, R., Schneider-Zapp, K. and Upstill-Goddard, R.C. (2016) 'Surfactant control of gas transfer velocity along an offshore coastal transect: results from a laboratory gas exchange tank', Biogeosciences, 13(13), p. 3981.

Richards, T.W. and Coombs, L.B., 1915. [No title available]. Journal of the American Chemical Society, 37, pp.1656–1676.

Sabbaghzadeh, B., Upstill-Goddard, R.C., Beale, R., Pereira, R. and Nightingale, P.D., 2017. The Atlantic Ocean surface microlayer from 50° N to 50° S is ubiquitously enriched in surfactants at wind speeds up to 13 m s^{-1}. Geophysical Research Letters, 44(6), pp.2852–2858.

Saiz-Lopez, A., Plane, J.M.C., Baker, A.R., Carpenter, L.J., von Glasow, R., Martin, J.C.F., McFiggans, F. and Saunders, R.W., 2012. Chemical Reviews, 112, pp.1773–1804.

Sakugawa, H., Handa, N., Ohta, K., 1985. Isolation and characterization of low molecular weight carbohydrates dissolved in seawater. Marine Chemistry 17, 341–362.

Saliot, A. (1981) 'Natural Hydrocarbons in Sea Water Alain Saliot', Elsevier Oceanography Series, 31, pp. 327-374.

Salter, M., 2010. PhD Thesis. University of Newcastle upon Tyne.

Salter, M.E., Upstill-Goddard, R.C., Nightingale, P.D., Archer, S.D., Blomquist, B., Ho, D.T., Huebert, B., Schlosser, P. and Yang, M., 2011. Journal of Geophysical Research, 116, DOI: 10.1029/2011JC007023.

Sareen, N., Schwier, A.N., Lathem, T.I., Nenes, A. and McNeil, V.F., 2012. Proceedings of the National Academy of Sciences (PNAS), 11, pp.2723–2728.

Saunders, P.M., 1967. Journal of Atmospheric Sciences, 24, pp.269–273.

Schmidt, R. and Schneider, B., 2011. Marine Chemistry, 126, pp.56–62.

Sims, R.P., Bell, T.G., Uncles, R.J., Torres, R., Widdicombe, S. and Tait, K. (2022). Tidal mixing of estuarine and coastal waters in the western English Channel controls spatial and temporal variability in seawater CO_2. Biogeosciences, 19, 1657–1674. https://doi.org/10.5194/bg-19-1657-2022

Sherwen, T., Evans, M.J., Carpenter, L.J., Andrews, S.J., Lidster, R.T., Dix, B., Koenig, T.K., Sinreich, R., Ortega, I., Volkamer, R., Saiz-Lopez, A., Prados-Roman, C., Mahajan, A.S. and Ordóñez, C., 2016. Atmospheric Chemistry and Physics, 16, pp.1161–1186.

Soloviev, A. and Lukas, R., 2014. The Near-Surface Layer of the Ocean. 2nd ed. Springer Netherlands, Heidelberg.

Stortini, A.M., Martellini, T., Del Bubba, M., Lepri, L., Capodaglio, G. and Cincinelli, A., 2009. [No title available]. Microchemical Journal, 92, pp.37–43.

The University of York, 2013. Landscape Management Plan 2013/18. Available at: https://www.york.ac.uk/admin/estates/operations/grounds/landscape_management_plan.pdf [Accessed May 2018].

Tilstone, G.H., Airs, R.L., Martinez-Vicente, V., Widdicombe, C. and Llewellyn, C., 2010. Limnology and Oceanography, 55, pp.1835–1850.

Tsai, W.t. and Liu, K.K. (2003) 'An assessment of the effect of sea surface surfactant on global atmosphere‐ocean CO2 flux', Journal of Geophysical Research: Oceans (1978‐2012), 108(C4), pp. 24-1-24-16.

Tseng, R.S., Viechnicki, J.T., Skop, R.A. and Brown, J.W., 1992. Journal of Geophysical Research: Oceans, 97, pp.5201–5206.

Turner, A. and Rawling, M.C. (2000) 'The behaviour of di-(2-ethylhexyl) phthalate in estuaries', Marine Chemistry, 68(3), pp. 203-217

Turney, D.E. and Banerjee, S., 2013. Air–water gas transfer and near-surface motions. Journal of Fluid Mechanics, 733, pp.588–624. https://doi.org/10.1017/jfm.2013.435

Turney, D. E., Smith, W. C., and Banerjee, S. (2005). A measure of near-surface fluid motions that predicts air-water gas transfer in a wide range of conditions. Geophys. Res. Lett. 32, 1–4. doi: 10.1029/2004GL021671

Underwood, G.J.C., Dumbrell, A.J., McGenity, T.J., McKew, B.A. and Whitby, C. (2022) 'The microbiome of coastal sediments', in Stal, L.J. and Cretoiu, M.S. (eds) The Marine Microbiome. The Microbiomes of Humans, Animals, Plants, and the Environment, vol. 3. Cham: Springer, pp. [insert page range if known]. https://doi.org/10.1007/978-3-030-90383-1_12

V. Zutic, B. Cosovic, E. Marcenko, N. Bihari, F. Krsinic, Marine Chem., 1981, 6, 505-520.

van Pinxteren, M., Barthel, S., Fomba, K.W., Müller, K., von Tümpling, W. and Herrmann, H., 2017. Elementa: Science of the Anthropocene, 35, DOI: https://doi.org/10.1525/elementa.225.

Vargaftik, N.B., Volkov, B.N. and Voljak, L.D., 1983. Journal of Physical and Chemical Reference Data, 12, pp.817–829.

Vargo, T.G., Hook, D.J., Gardella, J.A., Eberhardt, M.A., Meyer, A.E. and Baier, R.E., 1991. Applied Spectroscopy, 45, pp.448–456.

Vojvodić, V. and Ćosović, B., 1996. Fractionation of surface active substances on XAD-8 resin: Adriatic Sea samples and phytoplankton culture media. Marine Chemistry, 54, pp.119–133.

Wanninkhof, R. (1992) 'Relationship between wind speed and gas exchange over the ocean', Journal of Geophysical Research: Oceans, 97(C5), pp. 7373–7382. https://doi.org/10.1029/92JC00188

Weddell, K. (2023) Links between oceanic ozone uptake and ocean biology, pp. 1–92.

Williams, P.M., Carlucci, A.F., Henrichs, S.M., Van Vleet, E.S., Horrigan, S.G., Reid, F.M.H. and Robertson, K.J. (1986) 'Chemical and microbiological studies of sea-surface films in the southern Gulf of California and off the west coast of Baja California', Marine Chemistry, 19(1), pp. 17-98.

Wiggert, J.D., Wishner, K.F., Seibert, D.L., Wheeler, P.A., Fryxell, G.A., Flagg, C.N. and Hitchcock, G.L. (2005). Linking the ocean nitrogen and carbon cycles: Response of the northern Arabian Sea to monsoon forcing. Deep Sea Research Part II, 52(14–15), 3151–3176.

Wong, G.T.F., 1991. Reviews in Aquatic Sciences, 4, pp.45–73.

World Wildlife Fund, 2018. UK Rivers Map. Available at: https://www.wwf.org.uk/uk-rivers-map [Accessed May 2018].

Wurl, O. and Holmes, M., 2008. Marine Chemistry, 110, pp.89–97.

Wurl, O. and Obbard, J.P. (2004) 'A review of pollutants in the sea-surface microlayer (SML): a unique habitat for marine organisms', Marine pollution bulletin, 48(11), pp. 1016- 1030

Wurl, O., Ekau, W., Landing, W.M. and Zappa, C.J., 2017. Elementa: Science of the Anthropocene, 5, DOI: http://doi.org/10.1525/elementa.228.

Wurl, O., Wurl, E., Miller, L., Johnson, K. and Vagle, S. (2011b) 'Formation and global distribution of sea-surface microlayers', Biogeosciences, 8(1), pp. 121-135

Xie, J., Ekpo, M.D., Xiao, J., Zhao, H., Bai, X., Liang, Y., Zhao, G., Liu, D. and Tan, S. (2022) 'Principles and protocols for post-cryopreservation quality evaluation of stem cells in novel biomedicine', Frontiers in Pharmacology, 13, Article 907943. https://doi.org/10.3389/fphar.2022.907943.

Zhengbin, Z., Weijun, C., Liansheng, L., Chunying, L. and Feizhou, C., 2003. Sci. China, Ser. B, 46, pp.339–351.

Zhou, S., Gonzalez, L., Leithead, A., Finewax, Z., Thalman, R., Vlasenko, A., Vagle, S., Miller, L.A., Li, S.M., Bureekul, S., Furutani, H., Uematsu, M., Volkamer, R. and Abbatt, J., 2014. Atmospheric Chemistry and Physics, 14, pp.1371–1384.

Zhu, B., Zhao, X. and Gu, T., 1988. [No title available]. Journal of the Chemical Society, Faraday Transactions 1, 84, pp.3951–3960.

Zuti´c, V. B., ˇ Cosovi´c, E., Marˇcenko, E., Bihari, N., 1981. Surfactant production ´ by marine phytoplankton. Marine Chemistry 10, 505–520.